SLIDER CRANK MECHANISM FOR WAVE ENERGY CONVERSION (WEC): AN EXPERIMENTAL STUDY

A thesis presented to the faculty of the Graduate School of Western Carolina University in partial fulfillment of the requirements for the degree of Master of Science in Technology

By

Andrew Carlton Fowler

Advisor: Dr. Sudhir Kaul
School of Engineering & Technology

Committee Members:

Dr. Bora Karayaka, School of Engineering & Technology
Dr. Wes Stone, School of Engineering & Technology

July 2018

Table of Contents

List of Tables

List of Figures

ABSTRACT

SLIDER CRANK MECHANISM FOR WAVE ENERGY CONVERSION (WEC): AN EXPERIMENTAL STUDY

Andrew Fowler

Western Carolina University (July 2018)

Advisor: Dr. Sudhir Kaul

As more and more sources of renewable energy are being actively explored, there is a need for finding efficient means of converting energy into usable forms. Wave energy is one significant source of renewable energy that harnesses the movement of ocean waves to create energy. One of the possible means of tapping wave energy is the conversion of wave motion into rotational motion by using a wave energy conversion (WEC) mechanism. Currently, there are numerous methods that are being used to convert wave energy into electrical power, the slider crank mechanism is one such method. The slider crank power take-off (PTO) uses a buoy, riding on the waves, to drive a plunger that is connected to the crank shaft through a connecting rod. The goal of this study is to experimentally evaluate the working of the slider crank mechanism by using a wave generator on the flow table as the excitation source. The aim of the experimental evaluation is to comprehend the influence of variables such as wave type, wave generator, buoy geometry, etc. A high-speed camera is used to calculate the rotational speed of the crank and an accelerometer is used to gather acceleration of the plunger. A kinematic model of the slider crank is used to calculate the torque at the crank shaft. The

influence of multiple variables has been evaluated by performing a full factorial analysis and using the speed and torque of the crank shaft as the two output variables. Results indicate that the buoy geometry plays a critical role in the speed and torque characteristics of the crank shaft. The flywheel of the wave generator is also seen to be an important variable that directly governs the speed and torque characteristics of the crank shaft. The combination effect of the flywheel and buoy geometry is also observed to be influential. It is observed that out of the thirty-two configurations that have been tested during this study, many configurations result in an intermittent motion of the crank shaft. This implies that a control strategy would be required in a wave energy conversion system that uses the slider crank mechanism to ensure continuous motion for energy generation.

CHAPTER 1. INTRODUCTION

Renewable sources of energy are being increasingly sought to complement the use of fossil fuels. While the use of solar and wind energy is widespread, the use of ocean/wave energy is still being explored. Wave energy is available in abundance since approximately 70% of earth is covered by oceans. Therefore, finding efficient means of harnessing ocean energy could lead to another significant source of renewable energy.

1.1 Overview

Wave energy conversion (WEC) is the process of converting the mechanical energy of oceanic waves into electric energy. Compressing air in a sealed chamber to turn a turbine is typically how this conversion of energy is currently done. However, as WEC is growing, new and different methods of converting this energy are being actively examined by researchers.

WEC, along with other green energy devices, has the potential of satisfying a significant portion of the world's energy needs. However, finding a suitable device with an appropriate design to efficiently produce a large amount of energy is challenging. One device that has shown positive results in simulations is the slider-crank mechanism for WEC. [1]

The main purpose of this thesis is to build and test a prototype of a slider-crank design to determine the key characteristics of such a system. A wave table is used for the purpose of generating waves in a controlled manner. The main questions that this thesis aims to answer are as follows:

1. Can the slider-crank mechanism be successfully used for wave energy conversion and does the mechanism show results that are comparable to the simulations?
2. What is the appropriate size of various components that would be suitable for the wave table while maximizing energy conversion?
3. Which wave characteristics are the most significant on the energy produced?

1.2 Scope

This thesis will investigate several parameters that significantly affect the output from the slider-crank after the buoy is excited by the waves generated by the wave table. This study also intends to optimize and determine the significance of several different variables such as the wave amplitude, the wave frequency, different buoy shapes, and different ratios between the offset of the flywheel setting and the length of the connecting rod.

The different amplitude and frequency settings of the waves have been acquired from the wave generator attached to the downstream side of the wave table. The output variables that are measured, directly or indirectly, are the speed and torque of the output shaft of the slider-crank mechanism. The speed of the output shaft is acquired from a vision acquisition system through LabView. An accelerometer is attached to the buoy to indirectly compute the dynamic force, and eventually obtain the torque of the output shaft by using the dynamic model of the slider-crank mechanism.

This setup has allowed a reasonably accurate data collection, however, there are several limitations. While the wave generator can change the frequency and amplitude of the waves, the amplitude cannot be changed while the waves are being generated. This limits the scope of the test as compared to actual oceanic waves. However, the test set up

is expected to provide some insight into the design variables and their influence on the output variables.

1.3 Outline

This thesis has been divided into separate chapters. These chapters include an introduction, literature review, experimental design setup, methodology, experimental results, and conclusions along with a scope for future research. The literature review will discuss some previous designs of WEC that have been used by researchers. The experimental design will provide an elaborate description of the test set up and data collection. The methodology section will cover the setup of the system and how it works. The use of the measured variables to calculate the output variables will also be discussed. The resulting data is provided in the experimental results along with necessary discussion. Finally, the conclusions will sum up the findings and discuss possible experimentation that could be performed in the future.

1.4 Key Terms

A brief description of some of the key terms that have been used in this document is provided in this section:

- Wave Table: A test bench composed of a reservoir that holds water and a couple of pumps to pump the water into a glass container on top. These pumps create a flow of water, which is essential to create the waves required as an input for experimentation.
- Wave Generator: An electric motor attached to a flywheel with several different bolt holes and varying distances from the center of the flywheel. This unit is

contained in the wave table and allows the flow of water to be sinusoidal at varying frequencies and amplitudes.

- Accelerometer: An instrument commonly used for measuring acceleration. For this thesis, a three-axis accelerometer was used even though only one axis was of particular interest.
- VibraScout 6D: This is a software program that is used in conjunction with the accelerometer to collect acceleration data through a laptop connected to the accelerometer.
- Reservoir: A large tub that holds water for the wave table as the water gets circulated by the pumps.
- Upstream: The portion of the wave table that contains the porous beach and the head gate.
- Downstream: The portion of the wave table that contains the wave generator.
- LabView: A software program with graphical user interface that can be used for data collection.
- MATLAB: A software program that provides a numerical computational environment and a programming language that can be used for matrix calculations.

CHAPTER 2. LITERATURE REVIEW

This chapter provides a brief background on wave energy conversion and discusses some of the literature that has been referenced for this study. Some contextual information relevant to wave energy conversion is also presented in this chapter.

2.1 Background

The demand for different forms of energy keeps growing as the availability of fossil fuels continues to decline. This has stimulated interest in investigating multiple forms of renewable energy, and many forms of renewable energy are being studied to augment the supply of energy while mitigating environmental effects. A few of those forms are termed together as Green Energy. The definition for Green Energy is as follows: “Energy that can be produced in a way that protects the natural environment, for example using wind, water, or the sun” [2].

Over the last century, different devices have been used to harness sources of energy. These include solar panels, wind turbines, and wave energy converters (WECs). So far, the focus has primarily been on harnessing solar and wind energy, however, the last decade has seen a surge in different devices that have been studied to harness the energy produced from the ocean in the form of waves.

2.2 History of Wave Energy Conversion (WEC)

For the last few centuries, people have been trying to harness the energy of ocean waves. The oceans provide three primary sources of energy: waves, ocean thermal

energy, and tidal power [3]. Out of the three, the primary focus has been on the waves and tidal power. The main means of harnessing waves or tides is through the use of wave energy convertors, or WECs.

One of the earliest patents for this technology was filed in France in 1799. This effort began the investigation into this new device. However, Yoshio Masuda could be considered the father of modern wave energy technology with his studies in Japan since the 1940s. He developed one of the first oscillating water column (OWC) wave energy converter, however, the tests performed on his design were not very successful [4]. These early experiments led to the creation of several other different WECs that are being investigated currently by researchers.

2.3 Wave Energy Conversion

The motivation for investigating the use of wave energy can be described by paraphrasing Ozkop & Altas: “Over 70% of Earth's surface is covered by oceans, which are the world's largest solar collectors. Moreover, the oceans are the biggest untapped energy sources on Earth. The power density of wave energy is much higher than that of wind or solar energy. Depending on the sea surface, weather conditions, the shore structure and the location on Earth, the magnitude and periodic characteristic of waves may vary. Besides, waves show different characteristics from season to season, day to night, day to day, even hour to hour during the same day. Wave energy converters can produce power up to 90% of the time according to design and application methodologies, whereas wind and solar power systems produce 20–30% of the time.” [5]

The different forms of wave energy converters can be classified according to their location, the type of energy conversion mechanics used, and according to their end use. The location is important because it states how far the device is from the shore, either close to shore or farther away, leading to deep-water devices. The different energy conversion techniques are primarily mechanical, hydraulic, pneumatic, or electrical, with pneumatic being the most widely used. The main uses for these WECs include water pumping and desalination of water, but recently the focus of investigation has been shifting more towards the generation of electricity [4].

2.4 Types of Wave Energy Convertors

There is a wide variety of WECs, but they all use one general principle for energy extraction. The basic design of most WECs uses a variety of different mechanisms to convert the vertical linear motion produced by waves into a rotational motion which can be used by a generator to produce power. There are a few devices which use linear generators to convert the linear motion into electricity, however, those devices lead to a variety of different problems that are discussed in the literature [5].

The types of devices most related to the topic of this thesis are the turbine-based devices, and buoy-based mechanisms. These two devices can offer some insight into the problems which naturally occur with WEC such as invariability of the waves.

2.4.1 Turbine-Based Devices

One of the most common green energy devices that is being currently used is a water powered turbine. Hydroelectric dams are widely prevalent all over the world A water powered turbine converts the flow of water into electricity. However, as technology

has been advancing, several other uses of turbines have been investigated to help with the production of electricity.

One of the primary types of WECs is the Oscillating Water Column or OWC. OWCs are placed so that they are partially submerged. They are typically located close to the shore, usually with a concrete base. There are two main types of OWC. The first type uses water turbines like the hydro-electric dam. The movement of the waves turns a water turbine which turns a generator. However, in the second and more commonly used device, air is compressed by the waves and is forced up through the turbine, which then turns to create energy, as shown in Figure 1 [4].

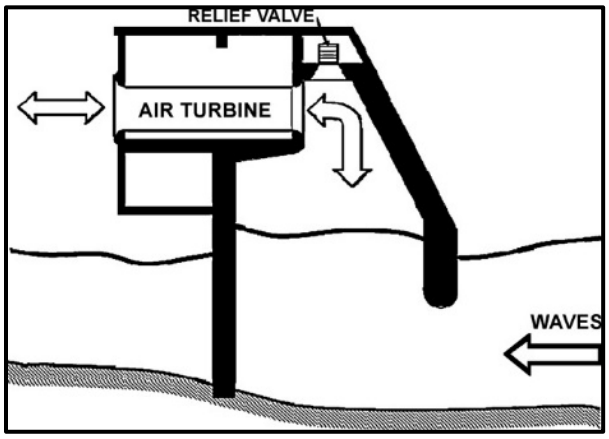

Figure 2-1 Oscillating Water Column [4].

2.4.2 Buoy-Based Devices

The use of a slider-crank mechanism is a relatively new idea for WEC and there are not many devices that can be directly used to help with the design of such a mechanism for wave energy conversion. There are a few devices that closely relate to the device chosen for this thesis and have been influential in the design developed.

Another wave energy conversion mechanism involves the oscillating water body. These devices are typically deployed in the deep water offshore and are either floating or completely submerged. There are several types of this device but they all share a similar

design. Energy is harnessed from the displacement between a stable body and a floating body. The stable body can either be anchored to the ocean floor or float separate from the other floating body [4], an example is shown in Figure 2.

Figure 2-2 Example - deep-sea buoy [4].

2.5 Problems with Current WEC Methods

As with all modern technologies in their early stages of development, there are quite a few challenges that are associated with the use of wave energy. Significant problems occur due to the nature of the waves from which the energy has to be

recovered. The ocean waves are highly variable in nature and demonstrate a significant amount of day-to-day variation in their magnitude, frequency, and the general nature. This poses a challenge when the energy is converted to any kind of rotational motion or anything that would need to be adjusted according to the changing variables. Also, the device would have to be fixed to work for any one location, as wave conditions are different according to distance from the equator. The device would also need to be able to survive in extreme environmental conditions [4].

2.5.1 Invariability in Waves

The two most critical variables in WEC are amplitude and frequency. These two variables are related to the height and length of the waves. While there are always some waves in the ocean at a given time, the amplitude and frequency of the waves are constantly changing. One main problem associated with collecting energy from ocean waves is the variability between the waves. Studies on OWCs and oscillating bodies have shown that in order for a device to be efficient, it needs to match the frequency of the waves themselves. In an optimal environment these frequencies should ideally be near-resonance [4].

Another issue with OWCs and WECs in general, is the effect of the other hydrodynamic forces that are acting on the buoy. For a mathematical model of the OWC and many other WECs, several assumptions must be made in order to develop a governing model that represents the kinematics and dynamics of the entire system. The first major assumption that is often used is that the system primarily needs to withstand heave forces (up and down) and no surge or sway forces. However, for experimental work or the working WEC, these other forces must be taken into consideration. Some of

the current research has investigated models of WECs that focus on implementing a six-degree of freedom model to determine the influence of these forces on system dynamics [6]. Another assumption that must be made is to limit the heave force to only have irregularities in a certain range [6]. This is because waves can be highly irregular depending on several reasons which can range anywhere from time of day to the weather conditions. For initial studies, this assumption is fine, however, these limitations must be kept in mind so that the solutions that are developed don't just account for ideal conditions.

2.6 Optimization of WEC Devices

Several studies have attempted to investigate optimization of WEC devices. For instance, "it has been proved that the individual components of a WEC system, such as types of wave energy converter and generator motion, control methods and power electronic converter, have a close relationship with each other and that no single component can be optimized without considering the others" [5]. As mentioned before, there are many factors that influence the energy that can be produced from WEC. Some of the factors should be investigated to enhance the performance of a WEC, particularly as the designed device is moved from an experimental environment to the actual test site in the ocean. This is because "the wave energy converters using relative motion for capturing power are much more complicated. The resonance periods between the two motion modes are very different. In this case, the maximal capture power may happen somewhere between these two resonance periods. Linear PTO damping optimization can provide a good analysis for the wave energy converter to see how much power is possible to convert, regardless of the real type of the PTO. The optimized linear PTO damping

coefficient can give the assessment of the maximal capture power for the device" [7]. Another variable that should be investigated is the damping of the system. This can be used to ensure that wave energy can be extracted even under irregular wave patterns. Most wave patterns consist of a mixture of larger and smaller waves which can disrupt the system and prevent energy from being harvested.

2.7 WEC Models

A wave energy converter can be extensively studied by using a theoretical model and by performing extensive testing in a wave basin or wave flume. The primary modeling technique can be very similar to the hydrodynamic models used for ships traveling in the ocean. Some of the modeling limitations include inability to account for losses due to viscous effects, and inability to model large wave oscillations. Such effects are known to be important for off-shore structures. In order to account for some of these modeling limitations, tests are carried out by using scaled models (1:80 to 1:10) in a wave basin after the model is used to finalize main parts of the geometry of the designed device [4].

Two examples of these devices are called a single-body heaving buoy and a two-body heaving system. The first device basically works by having one part of the mechanism attached sturdy while the other part, the buoy, is left to float up and down. The other system works similarly but instead of one part being attached to the oceanic floor or something else, the force instead comes from the relative motion between them [4].

2.8 Chosen Techniques

The technique that has been chosen for wave energy conversion for this thesis is the slider-crank mechanism. This mechanism consists of a buoy, a connecting rod, and a crankshaft. The buoy is at the water level in a semi-submerged condition and should have half the density of water so that it will be able to float while remaining half submerged. The buoy is connected to the crankshaft via a connecting rod. The crankshaft changes the linear motion of the buoy into rotational motion. The rotational speed of the crankshaft and the torque of the shaft are two important variables for energy generation and need to be measured. The output motion must be rotational instead of linear so that it can provide input to a generator for producing power.

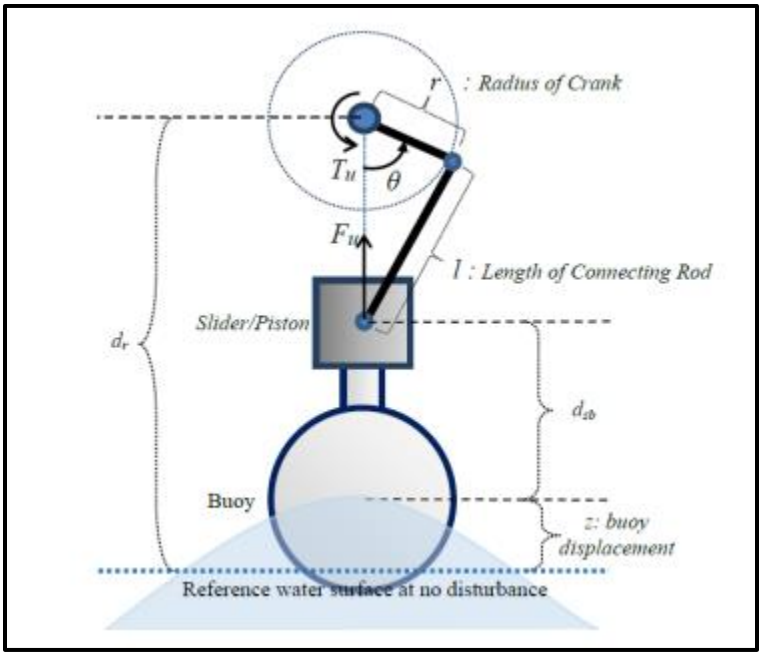

Figure 2-3 Slider-crank mechanism [8].

Figure 3 shows the basic layout of the slider-crank mechanism that has been used for this thesis. Two of the critical variables of the mechanism, the radius of the crank (r), and the length of the connecting rod (l), are illustrated in Figure 3 [8].

2.8.1 Simulations and Results

The continuous rotation at the power take-off of the crankshaft is important in a slider crank mechanism. Since a generator is expected to be directly coupled to the power take-off of the crankshaft, any discontinuity in the motion of the crankshaft will reduce the efficiency of the power generation [1]. However, it can be significantly challenging to provide continuous motion. As a result, it may be necessary to use a dynamic control that helps the system in achieving continuous motion. In other words, the buoy provides the initial motion of the mechanism and the electrical control system would enable the system to maintain continuous rotation [1]. From a previously conducted study [1], a buoy size and shape, and a ratio for the length (l) of the connecting rod to the crank (r) were picked. An r/l ratio of 0.4 to 0.6 was chosen for this thesis, as recommended in the reference literature [1].

2.8.2 Design Optimization

For most of the theoretical studies, excitation force and buoy velocity are assumed to be in phase. This is an assumption that must be made for simple simulations, however, it is a very hard assumption to make happen. For this condition to be true, the buoy would need to be designed so that it captures all the linear motion possible and does not get submerged at any time. In the reference studies [9], it has been found that once the mechanism reaches a certain point, the buoy cannot exhibit any more upward motion and instead gets submerged in water. More research needs to be done into the size and shape of the buoy to allow for an optimal energy recovery from the buoy's movement.

In the future, a weighted flywheel could be investigated to help with continuous motion of the flywheel, as ideally desired from the slider crank mechanism. Previous use

of slider crank mechanisms includes one-cylinder engines which rely on the mechanical advantage of a weighted flywheel to help create continuous motion from the linear movement of a piston. In this case, the buoy would create the initial movement which would transfer energy to the flywheel. This energy is then released by the flywheel through its momentum.

Another limitation of the idealized simulation is that it only considers regular sinusoidal wave patterns. It may be noted that there are a few studies in the literature that use irregular waves. This is not the case with oceanic waves most of the time. For instance, a rule-based control methodology for a slider-crank WEC has been investigated that enables it to work under irregular wave conditions [9]. In such a system, knowledge of the half-wave period is needed to ensure that the generator rotates in resonance with the wave excitation force, thereby providing a relatively high efficiency of energy extraction.

This thesis mainly investigates the influence of different variables such as the buoy design, the slider crank mechanism ratio, wave amplitude, wave frequency, etc. experimentally. With a slider crank that is optimally designed for specific wave conditions and a controller that can be used to adjust for irregularities, the system investigated in this thesis could be able to adapt to actual oceanic circumstances, as suggested in the relevant literature [9].

CHAPTER 3. MODEL AND EXPERIMENTAL SETUP

This chapter presents details of the experimental setup that has been used for data collection for this study. The kinematic model that has been used for indirectly calculating the output variables from the data collected is also discussed in this chapter.

3.1 Wave Table and Wave Generator

For the experimental work carried out for this study, a wave table and a wave generator have been used to provide the input waves. The wave table was procured from Hydraulic Design and Products Company (part number 664847) and the wave generator was procured from Engineering Laboratory Design (B-16 Hydraulic Demonstration Channel). The wave table that has been used for all data collection is shown in Figure 3.1. The wave table consists of a large reservoir as the base. This reservoir is used to contain the water needed to create the waves for the wave energy conversion mechanism to ride on. This reservoir is attached to another tank on top. The other tank consists of acrylic sides and bottom and an open top. The water is pumped between the bottom reservoir and the top tank via two pumps. Also, two valves are connected to the pumps, these valves can be used to keep water from draining back into the reservoir whenever the pumps are turned off. The mechanism used to obtain the energy from the waves is placed in the middle of the table with a porous beach located on the upstream side of the table. This porous beach is used to try to remove some of the reflecting waves going back towards the wave generator. Across the top tank from the pumps is the wave generator mechanism. This mechanism consists of an electric motor, a flywheel, a connecting rod, an acrylic paddle, and an acrylic blocker piece, a schematic of this mechanism can be

seen in Figure 3.2. To form the waves, the motor is attached to the flywheel. The flywheel is a short cylinder with several different holes drilled at different distances from the center and one center hole where the motor is attached. These different holes are all individually tapped so it can be attached to the wave paddle. The different distances of the holes are used to allow for different amplitudes and frequencies of the waves produced by the wave generator.

Figure 3-1 Wave Table and Generator.

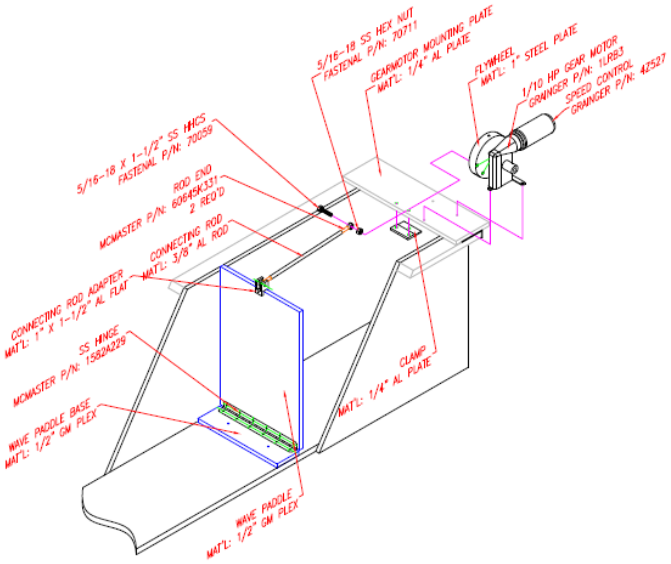

Figure 3-2 Wave Generator Mechanism

3.2 Wave Energy Conversion

The wave energy conversion mechanism that has been designed and manufactured for this study can be divided into a few different components. These individual components are as follows: a removeable tower to mount the mechanism above the table, the slider that reciprocates with the wave, a connecting rod and a crank mechanism. The slider is directly connected to a buoy, as shown in a picture of the slider-crank mechanism used for wave energy conversion in Figure 3.3.

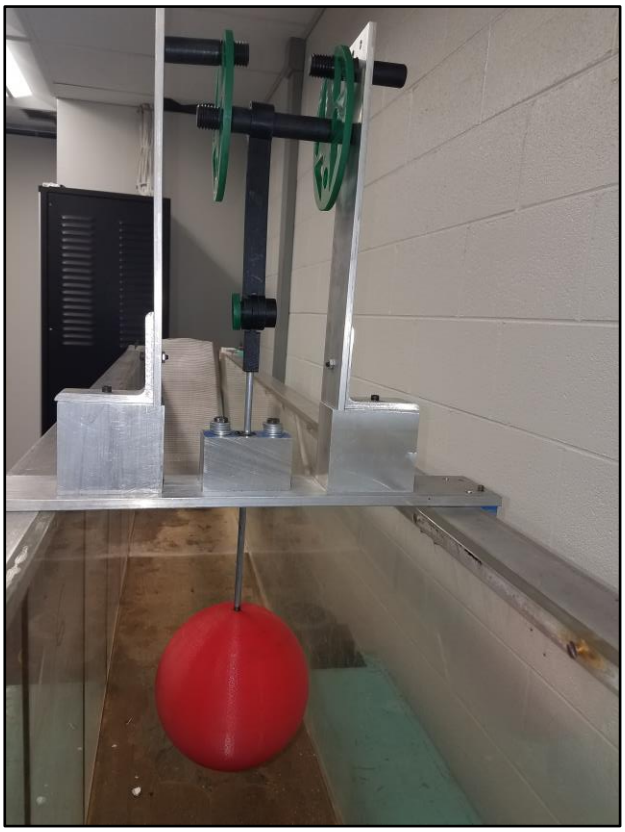

Figure 3-3 Slider-Crank Mechanism – Picture.

3.2.1 Aluminum Tower

The tower has been made from aluminum with a mounting design that can be easily assembled and disassembled. The tower has been designed to be removable to allow for easier adjustment and storage. The removability comes from the two side pieces that screw on and act as clamps on the two sides of the wave tank. The tower also features a guide hole that acts as a sleeve for the connecting rod of the slider-crank mechanism to slide through. This guide hole has been dimensioned so as to allow for an optimal range of travel of the connecting rod and buoy. The last important part of the tower are the holes on either side at the top. These holes are where the slider-crank mechanism rides in the tower. These holes also must be carefully dimensioned in order to

allow for the mechanism to rotate as required. All the bearing joints are greased to minimize friction resulting from relative motion.

3.2.2 Slider-Crank Mechanism

The primary part of this experiment is the slider-crank mechanism. This mechanism is composed of different parts with the main aim of designing and manufacturing parts in order to minimize the weight of the mechanism. The mechanism consists of two flywheels, attachment links, a steel connecting rod, and two plastic rods. The parts of the mechanism are shown in Figure 3.4. The two flywheels have been manufactured with a combination of through holes, this has been done to accommodate different spacing from the center of the flywheel or the rotating axis. A selection of the spacing allows to adjust the crank radius as needed. The ratio between the crank radius and the length of the connecting rod ranges from 0.4 to 0.6, as recommended in the reference literature. The connecting rod is attached to the crank through a pin joint, attached on the crank pin at a pre-selected offset from the rotating axis of the crank. It is six inches in length from one pin joint to the other. The other side of the connecting rod is a small connector which is used to attach the rod by a pin joint. The connecting rod slides up and down through the aluminum tower, which only allows the vertical movement of the buoy, not the horizontal. Figure 3.4 shows an exploded view of all of the components of the slider-crank mechanism. A picture of the assembled mechanism is shown in Figure 3.3. A screen shot of the solid model is provided in Figure 3.5.

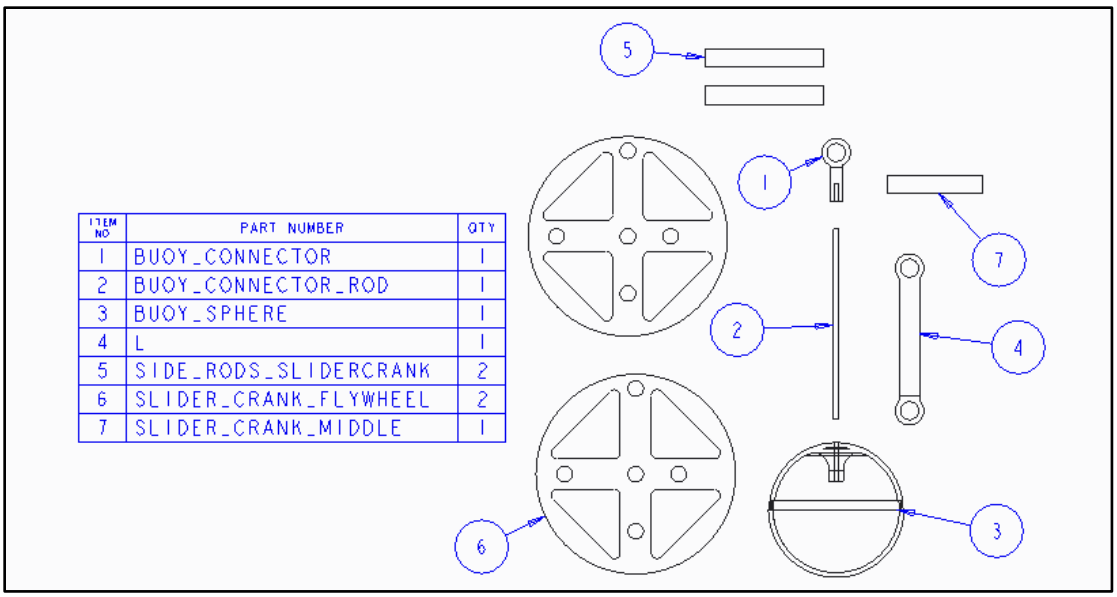

Figure 3-4 Exploded View - Mechanism.

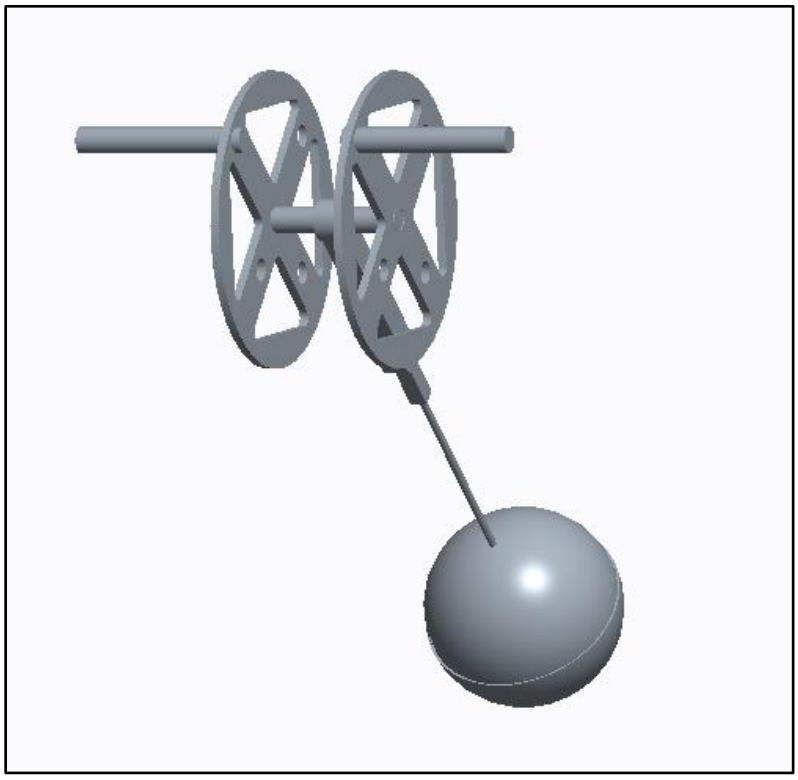

Figure 3-5 Mechanism Model.

3.2.3 Buoy

At the very bottom of the mechanism, the buoy is directly connected to the mechanism and floats on the surface of water of the wave table. The buoy drives the mechanism by riding on the waves produced by the wave generator. There are several different buoys that have been used for the experiment with different draft heights. Different draft heights are used because the different shapes of the buoy respond differently to the waves, as discussed in the literature. This will be discussed further in Chapter 4. Different buoy shapes lead to specific differences between vertical motion and horizontal motion of the buoy.

3.3 Data Collection

The two outputs that are sought from the experimental setup in this study are the speed of the crank measured as revolutions per minute (RPM) and the torque at the crank. These two outputs are critical for any power generation system that would be integrated with the wave energy conversion system. A non-contact vision-based system has been used to measure the RPM while the torque has been indirectly computed from the kinematic model after measuring the acceleration of the slider connected to the buoy. A flow chart of the data collection system is shown in Figure 3.6.

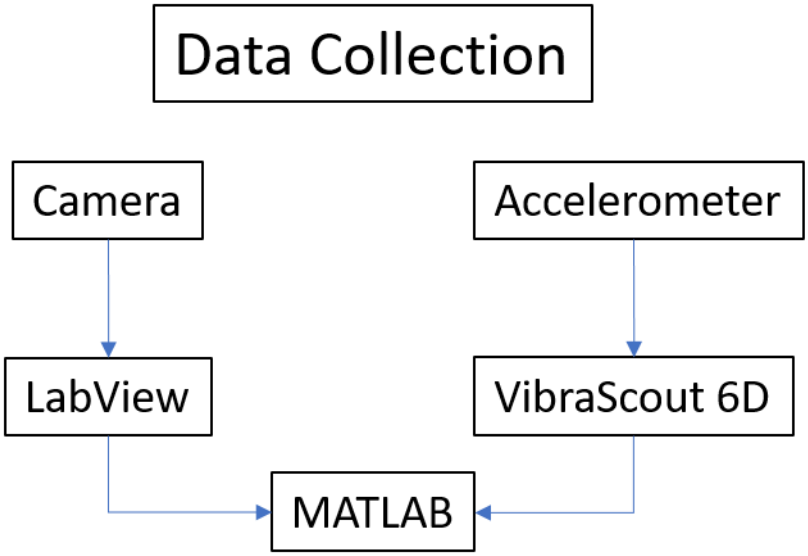

Figure 3-6 Data Collection Flow Chart.

The camera used for measuring the speed of the system was a normal webcam with a framerate of 30 FPS. The camera was attached to a tripod and boosted up a little using several small blocks. The camera was focused so that the wheel it was tracking was in the middle of its field of view. To get rid of any extra circles which LabView picked up, a black sheet was also hung behind the mechanism. This gave the camera a solid black background, which made it easier for it to track the movement of the white circle.

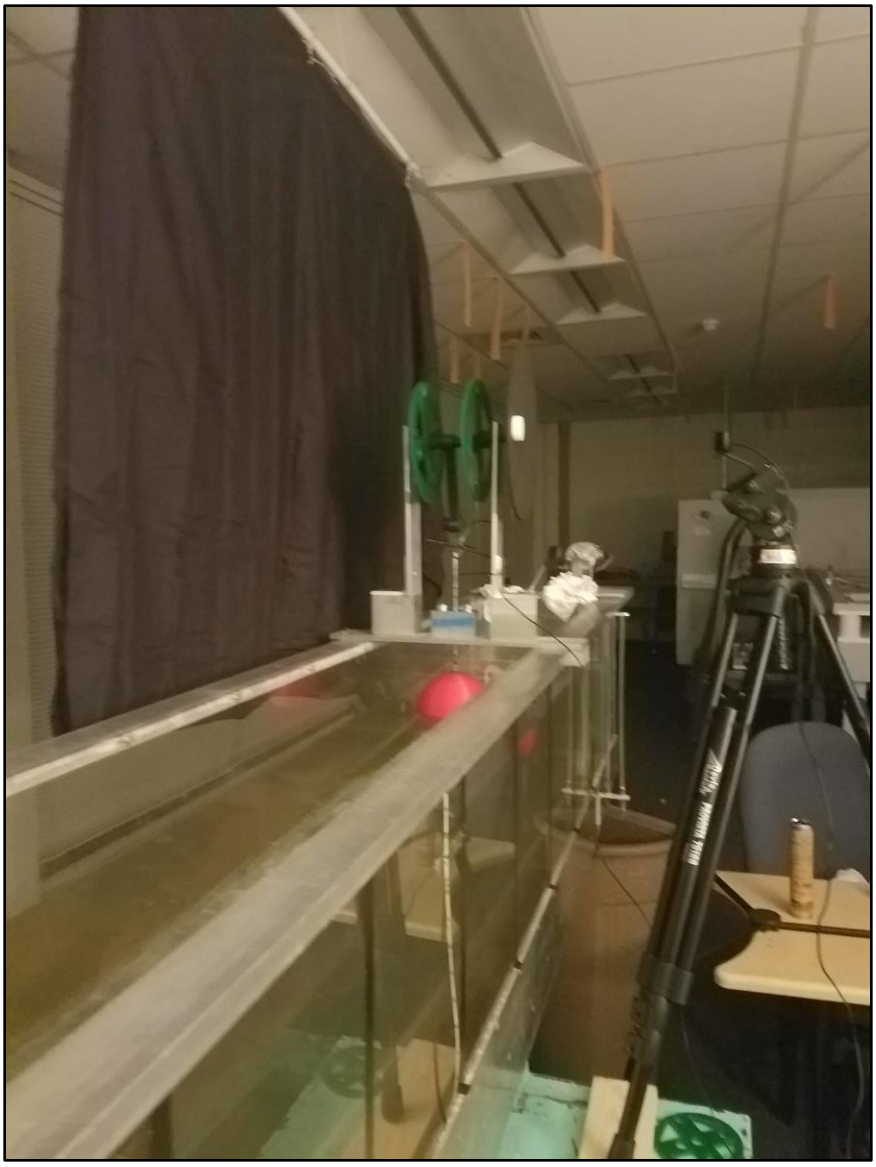

Figure 3-7 Data Collection – Camera Setup.

The accelerometer used to measure the torque output of the system was a wired DYTRAN 7546A USB tri-axial accelerometer. The accelerometer measured acceleration in all three axes x, y, and z. The accelerometer was positioned so that the x-axis was in line with the vertical movement of the buoy.

Figure 3-8 Accelerometer.

3.3.1 LabView Code

The LabView code used for data collection from the camera is shown in Figure 3.9.

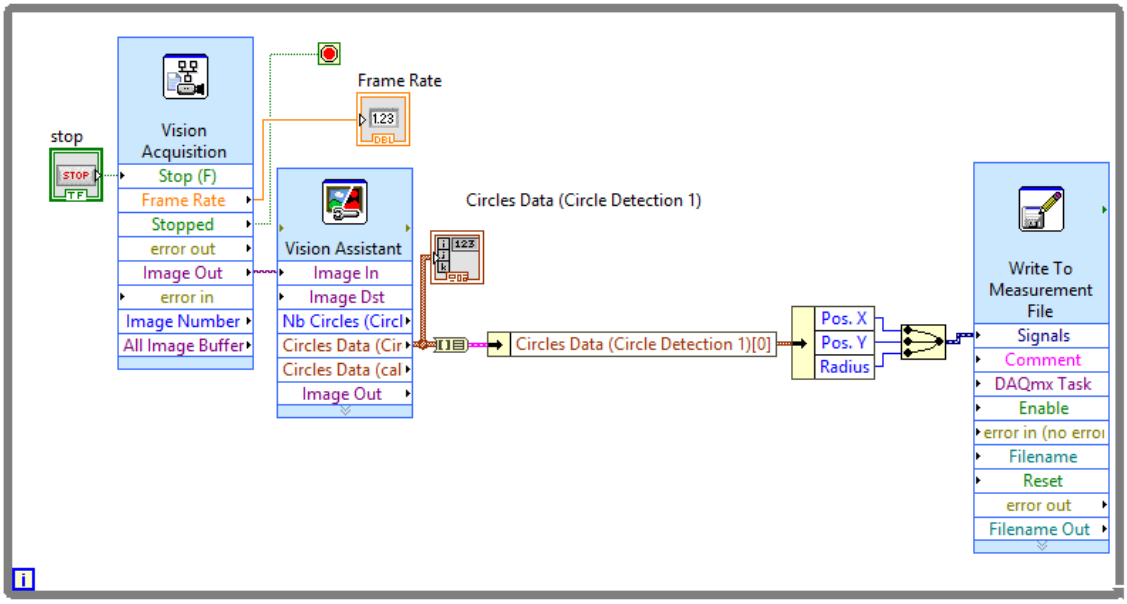

Figure 3-9 LabView Block Diagram.

Figure 3.9 depicts the block diagram for the LabView program that has been used for data collection. An image is brought in using a webcam at around 15 frames per second.

These images are then processed in the vision assistant function, as shown in the detailed sequential block diagram in Figure 3.10.

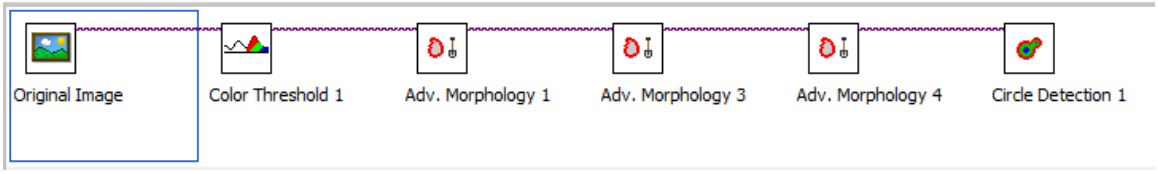

Figure 3-10 LabView Vision Assistant Function.

Vision assistant has several smaller sub-functions which have been used to find the rotating disk and track it. The first sub-function used is the color threshold, its purpose is to help the camera distinguish the white disk from its black background. It converts the white disk to a red circle which the program can easily track. Next, because of light reflections and other issues, advance morphology must be used to get rid of any little odd shapes that the camera is picking up. Advance morphology has several functions that can be further used. The first one is used to remove small objects, this removes any small light reflections that the camera picks up from the processed images. Next, remove large objects is another function that does the same. A function that helps in completing the circle is also used. Lastly, a circle detector function is used to track the circle as it completes every rotation. This sequence can be seen in the diagram in Figure 3.10.

The output from the vision assistant yields the x and y positions of the disk. This position data along with the time data given by the while loop that the program is encased in is then exported to a MS Excel file by the xlswrite function.

3.3.2 Instrumentation

For this thesis, an accelerometer and camera have been used to capture the acceleration and rotational speed respectively. The accelerometer was attached to the

connecting rod of the mechanism and therefore provided the vertical acceleration of the linkage connected to the buoy. This data is used in the kinematic model described in the next section to calculate the torque of the crank. The camera has been used in conjunction with the LabView code described in the previous section to track the rotational motion of the crank, the position data along with the time data has been used to track the speed of the crank.

3.4 Kinematic Model

To calculate the maximum torque produced by the system, a kinematic model of the slider-crank mechanism has been used. A visual representation of the kinematic model can be seen in Figure 3.11. All the equations relevant to the model will be presented in the subsequent section.

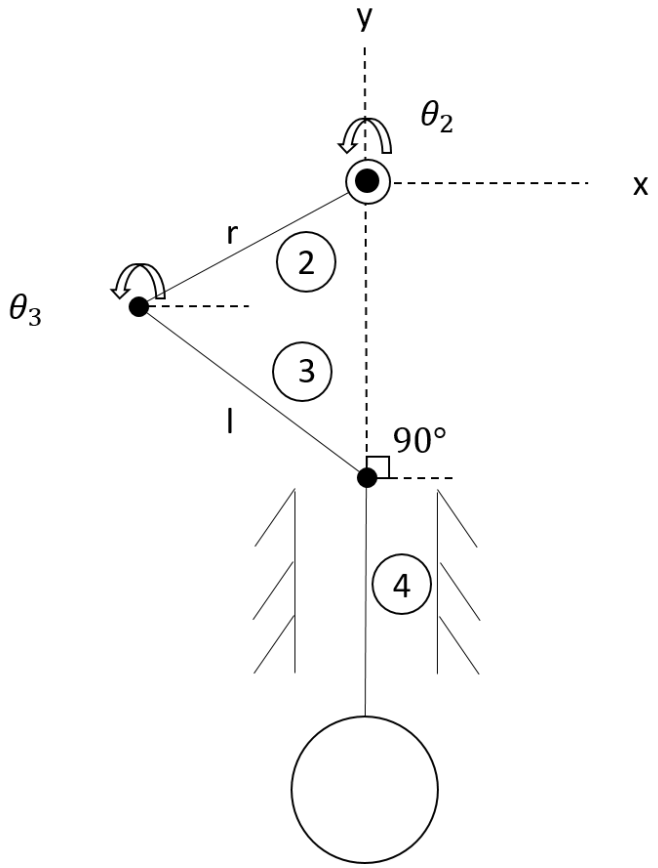

Figure 3-11 Kinematic model – Slider-crank.

3.5 Modeling Equations

A set of equations has been derived to calculate the torque at the crank shaft resulting from the buoy motion that is excited by the wave. Eq. 3.1 is the vector loop equation for the model in Figure 3.11:

$$re^{j\theta_2} + le^{j\theta_3} + ye^{j90} = 0 \tag{3.1}$$

In Eq. 3.1, θ_2 and θ_3 are the angles of the crank and the connecting rod respectively, both angles are measured with respect to the x-axis, as shown in Figure 3.11. Also, r is the crank radius and l is the length of the connecting rod, y is the variable length of the rod connected to the buoy.

3.5.1 Position Variables

From the vector loop equation in Eq. 3.1, the position variables are computed by using the real and imaginary components of the vector loop equation. These variables give the position of the mechanism all based on the varying crank angle:

$$\theta_3 = \cos^{-1}\left(\frac{-r\cos\theta_2}{l}\right) \tag{3.2}$$

$$y = -r\sin\theta_2 - l\sin\theta_3 \tag{3.3}$$

Eq. 3.2 and Eq. 3.3 can be used to solve for θ_3 and y for varying values of θ_2.

3.5.2 Velocity Variables

The differentiation of the vector loop equation yields the velocity equations, providing the angular velocity of the crank and the velocity of the rod connected to the buoy:

$$\omega_3 = \frac{-r\omega_2\sin\theta_2}{l\sin\theta_3} \tag{3.4}$$

$$\dot{y} = -r\omega_2\cos\theta_2 - l\omega_3\cos\theta_3 \tag{3.5}$$

In Eq. 3.4 and Eq. 3.5, ω_3 is the angular velocity of the connecting rod and $\dot{y}$ is the velocity of the rod connected to the buoy. It may be noted that ω_2 is the angular velocity of the crank that is directly computed from the camera system discussed in the previous sections.

3.5.3 Acceleration Equation

To find the acceleration of the components in the mechanism, the vector loop equation is differentiated twice to obtain the governing equation:

$$jr\alpha_2 e^{j\theta_2} - r\omega_2^2 e^{j\theta_2} + jl\alpha_3 e^{j\theta_3} - lw_3^2 e^{j\theta_3} + j\ddot{y} \tag{3.6}$$

In Eq. 3.6, α_2 and α_3 are angular accelerations of the crank and the connecting rod respectively, $\ddot{y}$ is the acceleration of the rod connected to the buoy. For steady state operation, the angular acceleration of the crank can be assumed to be zero.

3.5.3.1 Acceleration Variables

From the acceleration equation in Eq. 3.6, the real and imaginary components are used to calculate the angular acceleration of the connecting rod and the acceleration of the rod connected to the buoy as follows:

$$\alpha_3 = \frac{-r\alpha_2 \sin\theta_2 - r\omega_2^2 \cos\theta_2 - l\omega_3^2 \cos\theta_3}{l \sin\theta_3} \tag{3.7}$$

$$\ddot{y} = -r\alpha_2 \cos\theta_2 + r\omega_2^2 \sin\theta_2 - l\alpha_3 \cos\theta_3 + l\omega_3^2 \sin\theta_3 \tag{3.8}$$

3.5.4 Free Body Diagram

In Figure 3.12, the free body diagram of the slider-crank mechanism is shown. The free body diagram is used to compile the equations for the dynamic model that is needed to compute the torque at the crank. The free body diagram shows each link and the forces acting on each link, these forces include external forces as well as constraint forces resulting from the pin joints at several locations of the mechanism. In Figure 3.12, G_2 and G_3 are the centers of mass of the crank and the connecting rod respectively. Also, R_{12}, R_{23}, R_{32} and R_{43} are position vectors.

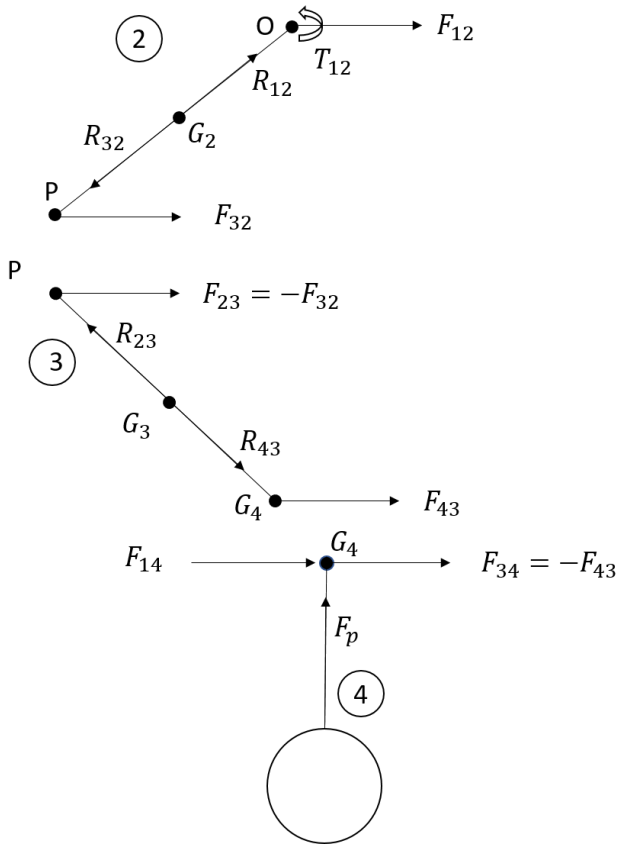

Figure 3-12 Free Body Diagram – Slider-crank Mechanism.

3.5.5 Dynamic Model

The dynamic model compiled from the equations of motion resulting from the free body diagram shown in Figure 3.12 is shown in Eq. 3.9:

$$\begin{bmatrix} 1 & 0 & 1 & 0 & 0 & 0 & 0 & 0 \\ 0 & 1 & 0 & 1 & 0 & 0 & 0 & 0 \\ -R_{12y} & R_{12x} & -R_{32y} & R_{32x} & 0 & 0 & 0 & 1 \\ 0 & 0 & -1 & 0 & 1 & 0 & 0 & 0 \\ 0 & 0 & 0 & -1 & 0 & 1 & 0 & 0 \\ 0 & 0 & R_{23y} & -R_{23x} & -R_{43y} & R_{43x} & 0 & 0 \\ 0 & 0 & 0 & 0 & -1 & 0 & 1 & 0 \\ 0 & 0 & 0 & 0 & 0 & -1 & \mu & 0 \end{bmatrix} \begin{bmatrix} F_{12x} \\ F_{12y} \\ F_{32x} \\ F_{32y} \\ F_{43x} \\ F_{43y} \\ F_{14x} \\ T_{12} \end{bmatrix} = \begin{bmatrix} m_2 a_{G2x} \\ m_2 a_{G2y} \\ I_{G2}\alpha_2 \\ m_3 a_{G3x} \\ m_3 a_{G3y} \\ I_{G3}\alpha_3 \\ m_4 a_{G4x} \\ m_4 a_{G4y} - F_p \end{bmatrix} \quad (3.9)$$

In Eq. 3.9, T_{12} is the torque at the crank that has been calculated indirectly from the model, a_{G2} and a_{G3} are the accelerations at the centers of mass of the crank and connecting rod respectively. Also, m_2, m_3, m_4 are the masses of the crank, connecting rod

and the buoy rod respectively. I_{G2} and I_{G3} is the mass moment of inertia of the crank and the connecting rod about the z-axis respectively.

The dynamic model in Eq. 3.9 has been used to calculate the torque produced from the system at the crank by substituting all the variables and measured input into the equations. A MATLAB program has been written for carrying out these calculations.

3.6 Conclusions

This chapter presented the kinematic and dynamic model of the slider crank mechanism that has been used in conjunction with data collection to calculate the output torque and rotational speed of the crank. The experimental design and data collection method that has been used in this study has also been presented in this chapter. The next chapter will present the detailed results and an analysis of the results.

CHAPTER 4. RESULTS

This chapter presents the post-processed results from the wave energy conversion experiment. These results include the analysis carried out from the kinematic model as well as results analyzed through a Design of Experiments (DOE) study in order to identify critical variables influencing the output of the wave energy conversion mechanism.

4.1 Data Analysis

To analyze the data acquired from the wave energy conversion mechanism, two MATLAB programs have been written, these programs are provided in Appendix A. The first program has been used to calculate the speed of the crank from the measurements done through the high-speed camera. The second program has been used to calculate the torque at the crank by using the kinematic model of the slider crank discussed in Chapter 3. The purpose of the two programs is to find the torque and speed of the crankshaft for each configuration. These two parameters are critical in the use of the wave energy conversion mechanism for power generation.

4.1.1 Speed and Torque Calculation

The first MATLAB program has been written to calculate the speed of the crankshaft in revolutions per minute (rpm). This has been done by bringing in the location and time data from the LabView code and using in-built MATLAB functions to calculate speed, as can be seen from the program in Appendix A. The program provides a plot which shows the speed of the mechanism at every increment of time. However, instead of using the entire time history, the maximum speed has been calculated and used

for further analysis. This has been done to avoid any outliers that may have been recorded during data collection. A total of 32 configurations was tested for this study. As an example, results from two of these configurations are discussed here in detail. The results from the remaining configurations are shown in Appendix B. Figure 4-1 and Figure 4-2 show an example of the position and speed calculated from one of the configurations (Test 10) during data collection.

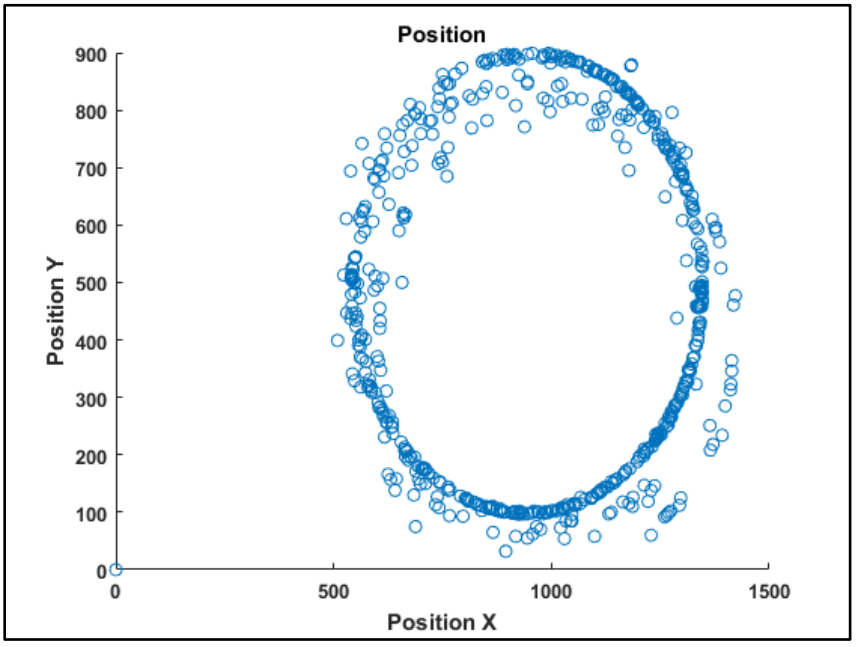

Figure 4-1 Position Plot – Test 10.

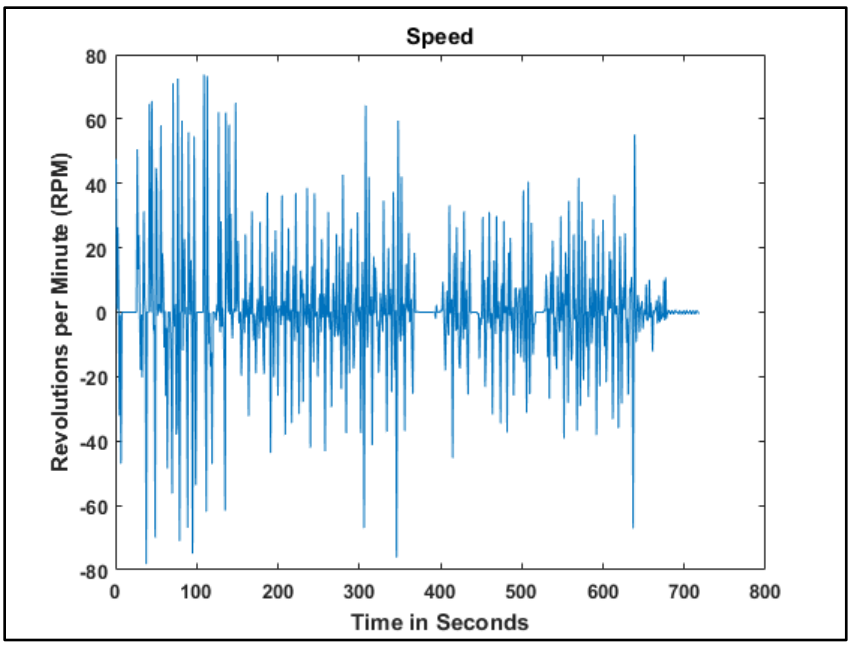

Figure 4-2 Speed (RPM) Plot – Test 10.

Figure 4-1 is from Test 10 and shows a complete revolution of the mechanism that was repeated continuously a few times, with nearly full revolutions of the mechanism for the entire duration of the test. The crank did not stay in its steady state for too long. The maximum rotational speed from this test was one of the highest out of all the configurations that were tested.

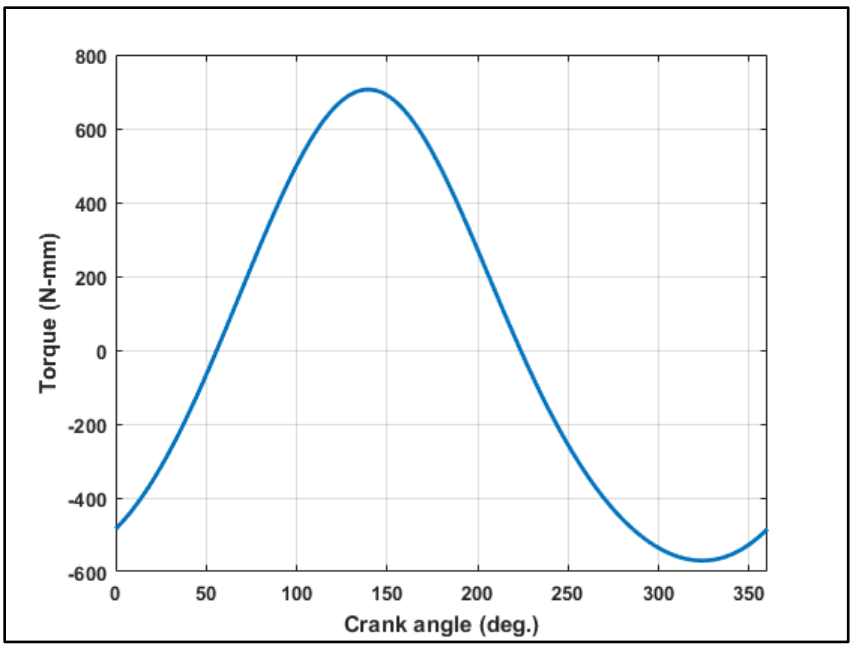

Figure 4-3 Torque Plot – Test 10.

The maximum torque from Test 10 was 705.6 N-mm, as shown from the torque plot in Figure 4-3. Figure 4-3 shows the torque profile for one complete revolution of the mechanism, calculated at steady state. It should be noted that the torque curve is not produced from direct measurements but are instead calculated by using the kinematic model that uses the acceleration results discussed in data collection.

The second configuration that is shown in this section is for Test 22. As can be seen from Figure 4-4, the crank was not able to complete a full revolution for this configuration. This can be observed by a small portion of the circle in Figure 4-4. For Test 22, the maximum rotational speed of the crank was calculated to be 9.17 rpm, as can be seen from the plot in Figure 4-5. As can be seen from a comparison of the plots from the two configurations, the configurations that result in a full revolution of the crank with continuous rotation also demonstrate a higher variance in speed, this can be clearly seen by comparing Figure 4-2 with Figure 4-5. It may be noted that there is some error in the

recording of the camera that directly affects the speed calculation. This error may be resulting from the camera picking up random white circles from the reflections of the background.

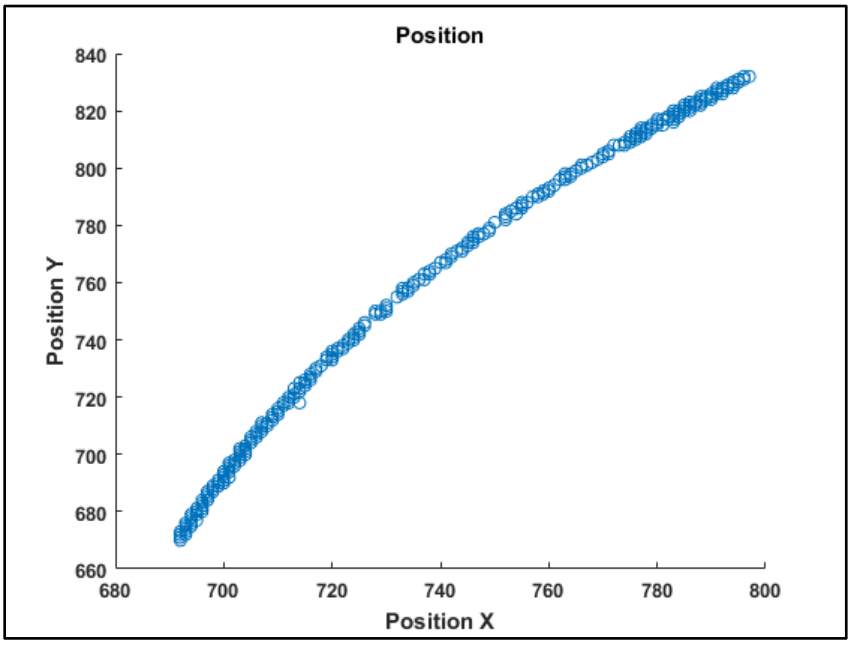

Figure 4-4 Position Plot – Test 22.

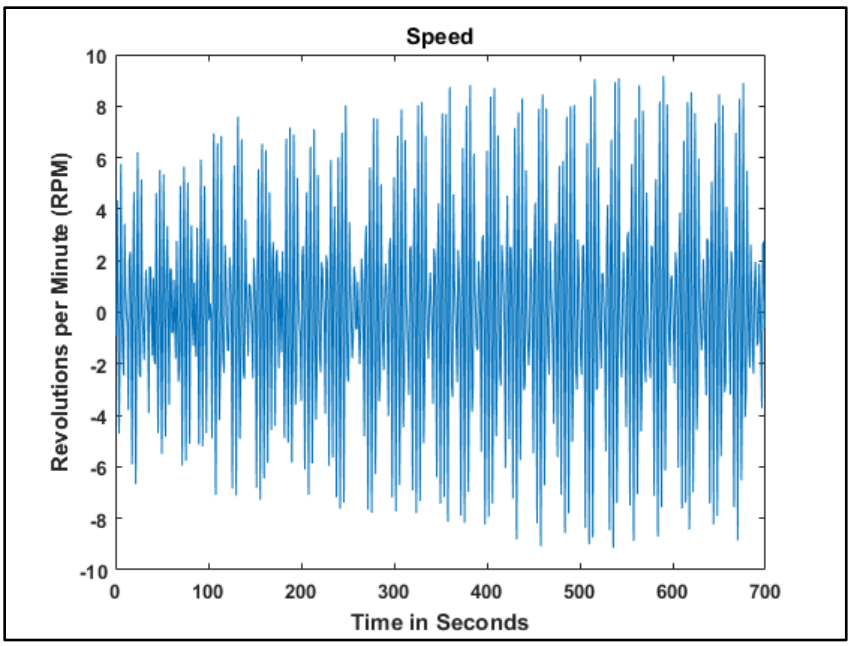

Figure 4-5 Speed (RPM) Plot – Test 22.

The torque result for Test 22 is shown in Figure 4-6. The maximum torque for this configuration is 1227 N-mm, as seen from the result in Figure 4-6. This configuration demonstrated one of the highest torque levels, however this configuration also resulted in a relatively lower speed of the crank.

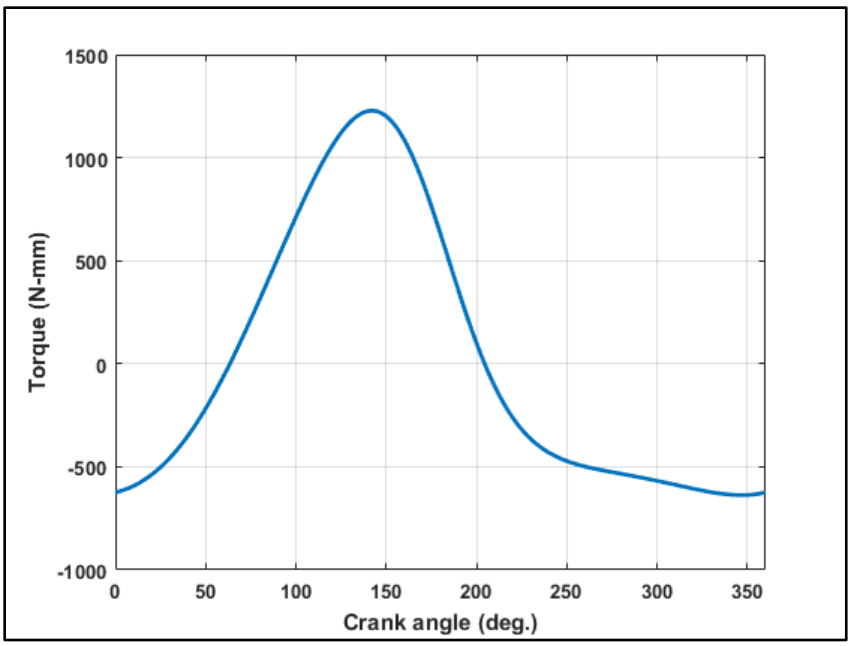

Figure 4-6 Torque Plot – Test 22.

From the results presented in this section and the remaining results for other configurations in Appendix B, it can be seen that torque and speed at the crank are inversely related, implying that as the speed increases the torque decreases. This is a reasonable result since the power input to the wave energy conversion mechanism is maintained at the same level regardless of the configuration that is being used. Therefore, an increase in torque should correspond with a decrease in speed and vice versa. This relationship also appears to be directly related to the size of the flywheel and the setting that is being used. The smaller flywheel and flywheel setting appear to result in a higher speed and lower torque, while the larger flywheel and flywheel setting seem to yield the opposite results. This will be investigated further in the next section.

In order to investigate the power output at the crank shaft, the RMS (root mean square) values of torque and speed have been used, this will be discussed further in the next section.

4.2 Design of Experiment Study

A Design of Experiment (DOE) has been used to analyze the results in order to attribute the output to specific variables since 32 configurations were tested for this study with varying settings of different variables. The different variables that have been used to test the wave generation mechanism include multiple amplitudes and frequencies of the wave input (via different wave generator settings), different buoy sizes and shapes, different flywheel sizes, and different flywheel settings. The DOE study has been used to formulate a matrix consisting of different combinations of these factors. The DOE has then been used to calculate the effect size in order to identify a specific variable or a combination of variables that is critical for the output of the test. Torque and speed have been used as the two outputs. Various effects have been plotted in this section.

For each test configuration, a series of values associated with the mechanism and the output are either measured or calculated, these values can be seen in Table 4-1. The mass and inertia were obtained from measured values, while the maximum speed is calculated from the post-processed data, and torque and acceleration are calculated from the kinematic model. The nomenclature of different combinations can be seen in the second column of Table 4-1 using the following logic: the buoy type is identified by RF (spherical buoy) or GF (spheroid buoy), the flywheel is identified by F1 (smaller flywheel) or F2 (larger flywheel), the flywheel settings are identified by S1 or S2 or S3 or S4 to indicate the four possible options, the generator setting is identified by WG4 or WG5 and directly relates to the values on the wave generator potentiometer. The main purpose of establishing a nomenclature is to easily identify different configurations from the test matrix.

Test	Symbolic Description	r (in)	l (in)	w2 (RPM)	Accel (m/s^2)	Torque (Nm)	m2 (g)	m3 (g)	m4 (g)	Ia2 (lb*in^2)	Ia3 (lb*in^2)
1	GF_F1_S1_WG4	1	6	19.1254	1.96288	0.2531	159	20.2	356	1.1583282	0.0104837
2	GF_F1_S1_WG5	1	6	29.9304	2.86742	0.3703	159	20.2	356	1.1583282	0.0104837
3	GF_F1_S2_WG4	1.5	6	3.4755	2.86742	0.5896	159	20.2	356	1.5675294	0.0104837
4	GF_F1_S2_WG5	1.5	6	28.4809	5.07634	1.0484	159	20.2	356	1.5675294	0.0104837
5	GF_F1_S3_WG4	1.75	6	1.6023	5.07634	1.259	159	20.2	356	1.8443964	0.0104837
6	GF_F1_S3_WG5	1.75	6	6.3937	2.18142	0.5415	159	20.2	356	1.8443964	0.0104837
7	GF_F1_S4_WG4	2	6	5.8835	2.34214	0.6883	159	20.2	356	2.1265560	0.0104837
8	GF_F1_S4_WG5	2	6	8.3534	3.3339	0.9801	159	20.2	356	2.1265560	0.0104837
9	RF_F1_S1_WG4	1	6	7.7436	1.86488	0.2732	159	20.2	405	1.1583282	0.0104837
10	RF_F1_S1_WG5	1	6	29.8432	4.8088	0.7056	159	20.2	405	1.1583282	0.0104837
11	RF_F1_S2_WG4	1.5	6	4.1146	1.95504	0.4574	159	20.2	405	1.5675294	0.0104837
12	RF_F1_S2_WG5	1.5	6	5.2343	1.76492	0.413	159	20.2	405	1.5675294	0.0104837
13	RF_F1_S3_WG4	1.75	6	28.1283	1.96386	0.5638	159	20.2	405	1.8443964	0.0104837
14	RF_F1_S3_WG5	1.75	6	21.3383	2.05304	0.5849	159	20.2	405	1.8443964	0.0104837
15	RF_F1_S4_WG4	2	6	17.5228	1.95896	0.6607	159	20.2	405	2.1265560	0.0104837
16	RF_F1_S4_WG5	2	6	48.0452	2.37644	0.8418	159	20.2	405	2.1265560	0.0104837
17	RF_F2_S1_WG4	1.8	6	27.2731	1.67182	0.4987	337	20.2	405	8.8102009	0.0104837
18	RF_F2_S1_WG5	1.8	6	25.0593	4.54824	1.3378	337	20.2	405	8.8102009	0.0104837
19	RF_F2_S2_WG4	2.4	6	21.1313	2.18142	0.949	337	20.2	405	10.6053060	0.0104837
20	RF_F2_S2_WG5	2.4	6	9.4648	1.84528	0.7897	337	20.2	405	10.6053060	0.0104837
21	RF_F2_S3_WG4	3	6	0	2.94986	1.7411	337	20.2	405	13.0110190	0.0104837
22	RF_F2_S3_WG5	3	6	9.1698	2.06088	1.2277	337	20.2	405	13.0110190	0.0104837
23	RF_F2_S4_WG4	3.6	6	0	2.05892	1.6571	337	20.2	405	15.8563280	0.0104837
24	RF_F2_S4_WG5	3.6	6	2.9243	1.9668	1.5864	337	20.2	405	15.8563280	0.0104837
25	GF_F2_S1_WG4	1.8	6	8.3107	1.96484	0.5055	337	20.2	356	8.8102009	0.0104837
26	GF_F2_S1_WG5	1.8	6	1.8623	2.70572	0.695	337	20.2	356	8.8102009	0.0104837
27	GF_F2_S2_WG4	2.4	6	4.4836	2.05598	0.7702	337	20.2	356	10.6053060	0.0104837
28	GF_F2_S2_WG5	2.4	6	9.5973	5.04694	1.8923	337	20.2	356	10.6053060	0.0104837
29	GF_F2_S3_WG4	3	6	0	1.87272	0.9715	337	20.2	356	13.0110190	0.0104837
30	GF_F2_S3_WG5	3	6	2.9126	3.55244	1.8439	337	20.2	356	13.0110190	0.0104837
31	GF_F2_S4_WG4	3.6	6	0	1.86488	1.3192	337	20.2	356	15.8563280	0.0104837
32	GF_F2_S4_WG5	3.6	6	1.8589	1.9619	1.389	337	20.2	356	15.8563280	0.0104837

Table 4-1 Test Matrix – All configurations.

4.2.1 Full factorial analysis

A full factorial analysis has been performed to identify the specific influence of each variable or a combination of variables on the speed and torque of the crankshaft. A 2^4 analysis is performed with two levels (-1 and +1) of each variable: buoy type (A), flywheel size (B), flywheel setting (C), and wave generator setting (D). The two levels of the buoy are defined as the spheroid buoy (-1) and the spherical buoy (+1), the two levels of the flywheel size are defined as the smaller diameter flywheel (-1) and the larger diameter flywheel (+1), the two levels of the flywheel setting are the lower setting (-1) and the higher setting (+1), and the two levels of the wave generator are defined as the setting 'four' on the potentiometer (-1) and the setting 'six' on the potentiometer (+1). The analysis has been limited to four variables in order to avoid a fractional factorial analysis that may lead to confounding, making it difficult to identify the effect size. During the testing of the mechanism, four flywheel settings were used. For the purpose of the design of the full factorial analysis, the two outermost settings were used. These settings are the smallest setting on the flywheels, and the largest settings. The full factorial designs are shown in Table 4-2 and Table 4-3 with speed (RPM) and torque as output variables respectively. The last column of both tables provides the output from the corresponding configuration in Table 4-1. The effect for each variable or a combination of variables is shown in the penultimate rows of the two tables. The coefficients for the regression equation are listed in the last row of each column. After the columns with each variable (A, B, C, D), the full factorial formulation accounts for all combinations of the variables (AB, AC, AD, BC, BD, CD) with two variables, all combinations with three variables (ABC, ABD, ACD, BCD), and all variables together (ABCD).

DOE Speed (RPM)																							
	I	Buoy	Flywheel Size	Flywheel Setting	Wave Generator																		RPM
		A	B	C	D	AB	AC	AD	BC	BD	CD	ABC	ABD	ACD	BCD	ABCD							
	1	-1	-1	-1	-1	1	1	1	1	1	1	-1	-1	-1	-1	1							4.11
	1	1	-1	-1	-1	-1	-1	-1	1	1	1	1	1	1	-1	-1							3.48
	1	-1	1	-1	-1	-1	1	1	-1	-1	1	-1	1	-1	1	-1							21.13
	1	1	1	-1	-1	1	-1	-1	-1	-1	1	-1	-1	1	1	1							4.48
	1	-1	-1	1	-1	1	-1	1	-1	1	-1	1	-1	1	1	-1							28.13
	1	1	-1	1	-1	-1	1	-1	1	1	-1	-1	1	-1	1	1							1.60
	1	-1	1	1	-1	-1	-1	1	-1	-1	-1	-1	1	1	-1	1							0.00
	1	1	1	1	-1	1	1	-1	1	-1	-1	1	-1	-1	-1	-1							0.00
	1	-1	-1	-1	1	1	-1	-1	1	-1	-1	-1	1	1	1	-1							5.23
	1	1	-1	-1	1	-1	1	1	1	-1	-1	1	-1	-1	1	1							28.48
	1	-1	1	-1	1	-1	-1	-1	-1	1	-1	1	-1	1	-1	1							9.46
	1	1	1	-1	1	1	-1	1	-1	1	-1	-1	1	-1	-1	-1							9.60
	1	-1	-1	1	1	-1	-1	-1	-1	-1	1	1	1	-1	-1	1							21.34
	1	1	-1	1	1	-1	1	1	-1	-1	1	-1	-1	1	-1	-1							6.39
	1	-1	1	1	1	-1	-1	-1	1	1	1	-1	-1	-1	1	-1							9.17
	1	1	1	1	1	1	1	1	1	1	1	1	1	1	1	1							2.91
	155.53	-41.64	-42.01	-16.44	29.66	-3.91	-53.82	45.99	-48.75	-18.60	-9.49	74.34	-24.94	-35.34	46.76	-10.73							
Effects	77.76	-5.20	-5.2510625	-2.0546625	3.7070125	-0.4887	-6.7275	5.74876	-6.094	-2.32	-1.1861	9.29	-3.12	-4.42	5.84	-1.34							
Coeffs	38.88	-2.60	-2.63	-1.03	1.85	-0.24	-3.36	2.87	-3.05	-1.16	-0.59	4.65	-1.56	-2.21	2.92	-0.67							

Table 4-2 Full Factorial 2^4 Analysis – Speed.

DOE Torque (N-mm)																									
	I	Buoy	Flywheel	Flywheel Setting	Wave Generator																			Torque
		A	B	C	D	AB	AC	AD	BC	BD	CD	ABC	ABD	ACD	BCD	ABCD								
	1	-1	-1	-1	-1	1	1	1	1	1	1	-1	-1	-1	-1	1								457.4
	1	1	-1	-1	-1	-1	-1	-1	1	1	1	1	1	1	-1	-1								589.6
	1	-1	1	-1	-1	-1	1	1	-1	-1	1	1	1	-1	1	-1								949
	1	1	1	-1	-1	1	-1	-1	-1	-1	1	-1	-1	1	1	1								770.2
	1	-1	-1	1	-1	1	-1	1	-1	1	-1	1	-1	1	1	-1								563.8
	1	1	-1	1	-1	-1	1	-1	1	-1	-1	-1	1	-1	-1	1								1259
	1	-1	1	1	-1	-1	-1	1	-1	1	-1	-1	1	-1	1	-1								1741.1
	1	1	1	1	-1	1	1	-1	1	-1	-1	1	-1	1	-1	1								971.5
	1	-1	-1	-1	1	1	-1	1	-1	1	-1	-1	1	1	1	-1								413
	1	1	-1	-1	1	-1	1	-1	1	-1	-1	1	-1	-1	1	1								1048.4
	1	-1	1	-1	1	-1	-1	1	-1	1	-1	1	-1	1	-1	1								1845.28
	1	1	1	-1	1	1	1	-1	-1	1	-1	-1	1	-1	-1	1								1892.3
	1	-1	-1	1	1	1	-1	1	-1	-1	1	1	1	-1	-1	1								584.9
	1	1	-1	1	1	-1	1	-1	-1	-1	1	-1	-1	1	-1	1								541.5
	1	-1	1	1	1	-1	-1	1	-1	1	1	-1	-1	-1	1	-1								1227.7
	1	1	1	1	1	1	1	1	1	1	1	1	1	1	1	1								1843.9
	16698.58	1134.22	5783.38	768.22	2095.38	-1704.58	-137.42	1376.22	-113.38	2659.38	-2770.18	94.18	1847.02	-81.82	-548.58	2401.78								
Effects	8349.29	141.78	722.9225	96.0275	261.92	-213.07	-17.18	172.03	-14.173	332.423	-346.27	11.8	230.88	-10.2	-68.57	300.22								
Coeffs	4174.65	70.89	361.46	48.01	130.96	-106.54	-8.59	86.01	-7.09	166.21	-173.14	5.89	115.44	-5.11	-34.29	150.11								

Table 4-3 Full Factorial 2^4 Analysis – Torque.

4.2.2 Full factorial results

In order to identify the variables that may be influential in the outcome of the full factorial experiment, the effects for the four variables as well as the combined effects of these variables are plotted in a Normal Probability Plot. In the Normal Probability plot, the points on the straight line or close to the line are not significantly influential in the outcome whereas points that are significantly away from the straight line may be substantially influential. The farther the point from the straight line, the more influential it is for the outcome. The two Normal Probability Plots are shown in Figure 4-7 and Figure 4-8 for all the effects from the two full factorial results. From Figure 4-7, the most influential factors for the crank speed are found to be as follows: buoy, flywheel size, flywheel setting, and the wave generator setting. From Figure 4-8, the flywheel size and the flywheel setting are found to be most influential.

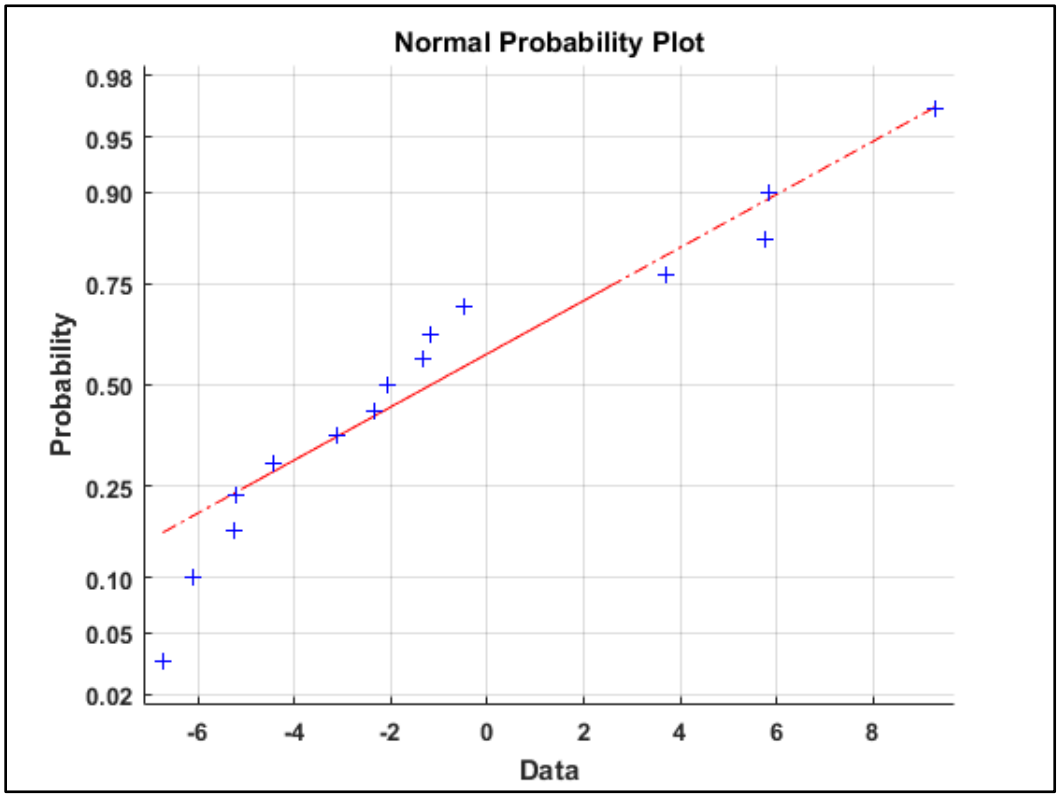

Figure 4-7 Normal Probability Plot – Speed.

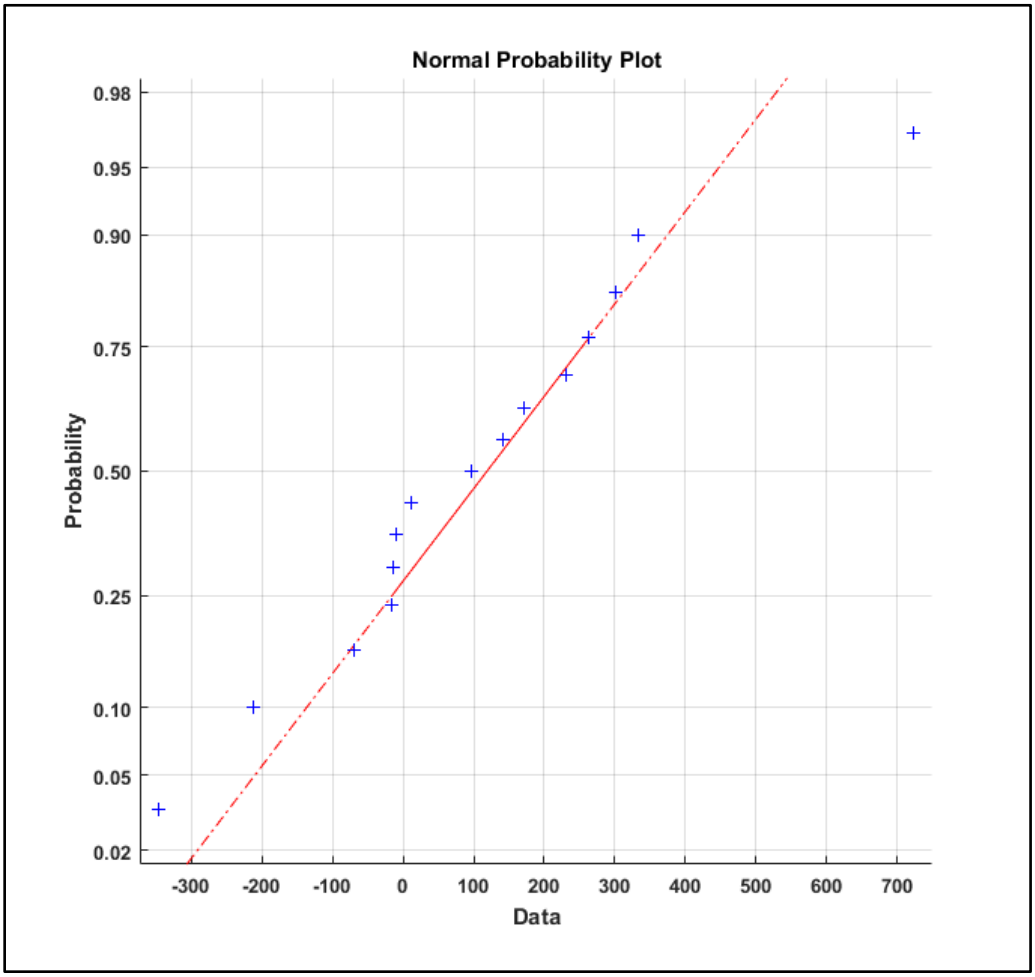

Figure 4-8 Normal Probability Plot – Torque.

It is acknowledged that the Normal Probability Plot is a visual method and is not quantitative and precise. However, it is commonly used in full factorial analysis for an experiment that does not involve a replicated test output.

For the results in Table 4-2 and Table 4-3, the influence of the significant variables identified in the Normal Probability Plots is further investigated through effect plots for each variable or a combination of variables for each output – speed or torque. The x-axis of each effect plot is scaled to be between -1 and +1 whereas the y-axis has been maintained at the same scale to easily compare the results from the plots. The

influence of flywheel size, flywheel type, and the wave generator on the speed of the crank is shown in Figures 4-9, 4-10, and 4-11.

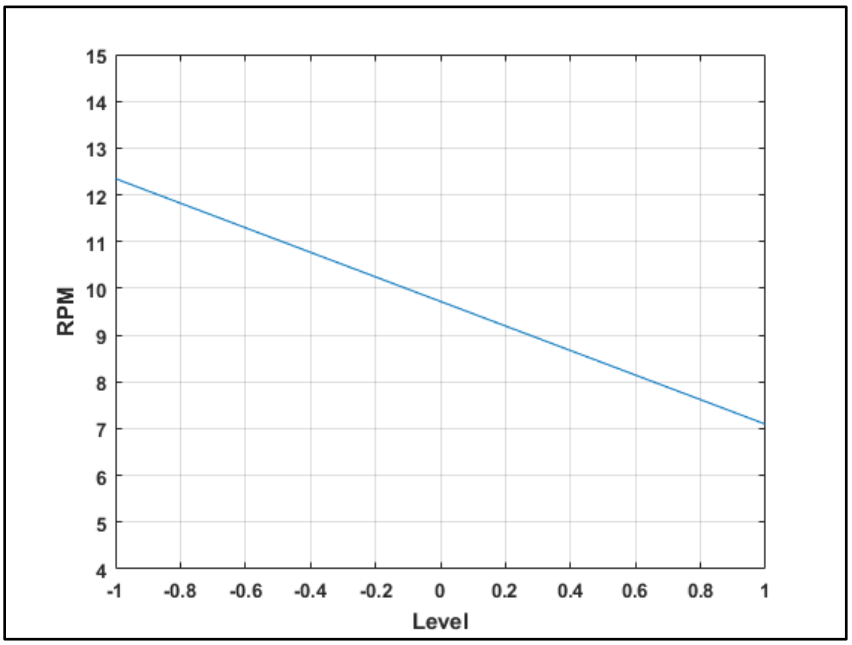

Figure 4-9 Flywheel Size Effect – Speed.

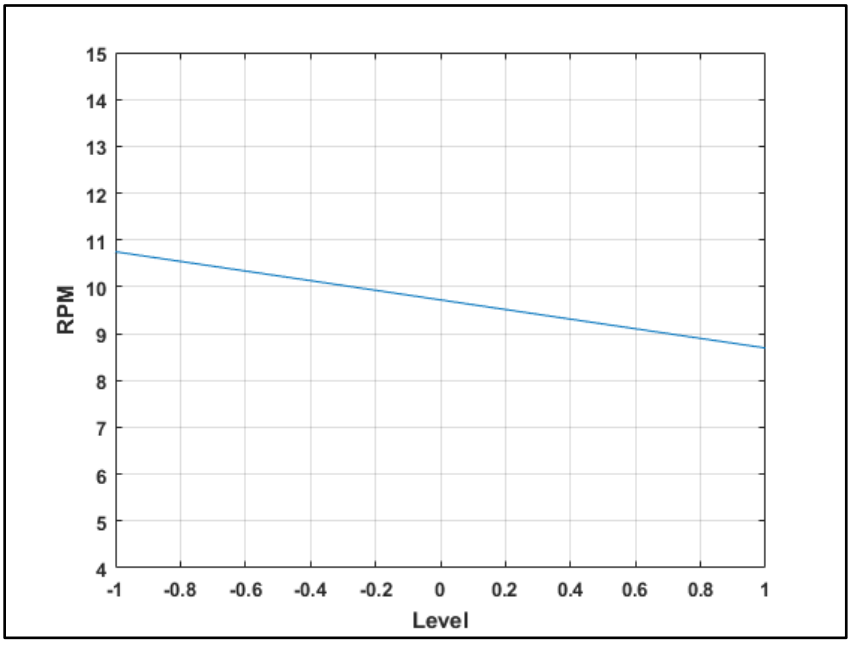

Figure 4-10 Flywheel Setting Effect – Speed.

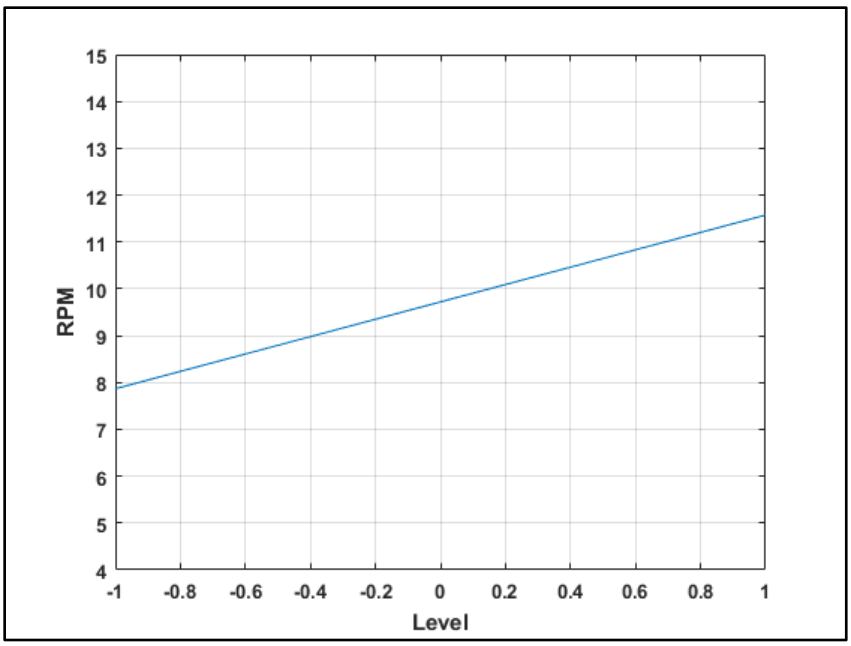

Figure 4-11 Wave Generator Effect – Speed.

It can be seen from Figure 4-9 and Figure 4-10 that the speed reduces as the flywheel size goes from -1 to +1 and as the flywheel setting goes from -1 to +1. However, the wave generator setting demonstrates an opposite influence, the crank speed increases as the setting goes from -1 to +1. The buoy is also seen to have a significant influence on the speed of the crank, this will be shown in the combined effect plots. Overall, it can be stated that the buoy and the flywheel are the most significant variables for the speed of the crank.

Some combination effects are also found to be influential from the Normal Probability Plot, these combination effect plots can be seen in Figures 4-12 to 4-16. For the combined effect of the buoy and flywheel size shown in Figure 4-12, it can be seen that the higher flywheel size (+1) and the shorter (spheroid) buoy (-1) result in the highest speed. However, the smaller flywheel and the taller (spherical) buoy also result in a

relatively high speed. The other two combinations result in a significantly lower speed, as can be seen from the plot in Figure 4-12.

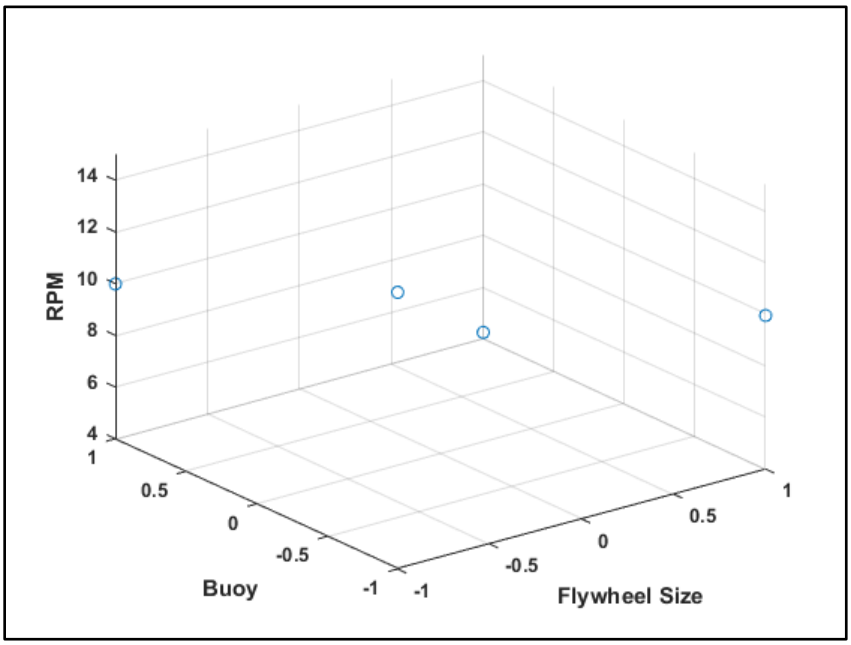

Figure 4-12 Buoy and Flywheel Size Combined Effect – Speed.

For the combined effect of the buoy and flywheel setting, it can be seen from Figure 4-13 that the higher flywheel setting (+1) and the shorter buoy (-1) result in the highest speed. All other configurations results in a relatively lower speed, as seen in Figure 4-13.

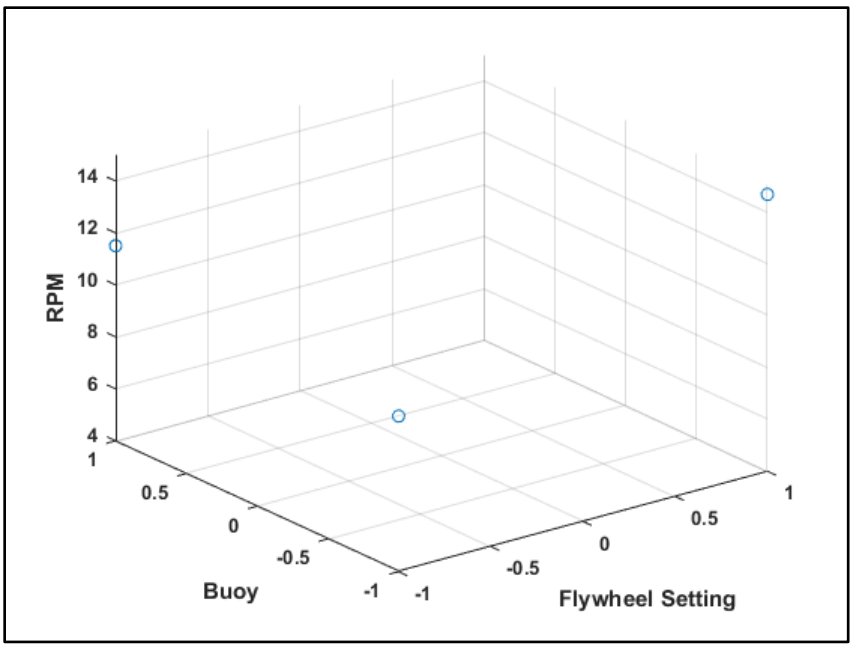

Figure 4-13 Buoy and Flywheel Setting Combined Effect – Speed.

The next highest combined effect for speed is due to the higher flywheel setting in conjunction with the smaller flywheel, as seen in Figure 4-14. The larger flywheel with the lower flywheel setting also shows a relatively high speed. The other two combinations result in a relatively lower speed, as seen in Figure 4-14.

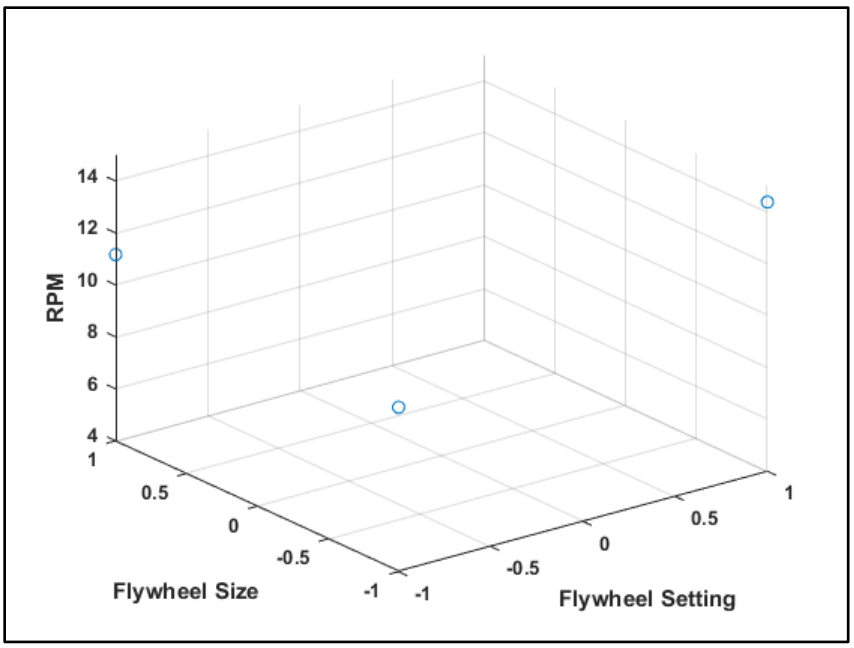

Figure 4-14 Flywheel Size and Flywheel Setting Combined Effect – Speed.

Even though the wave generator effect itself is not significant, it can be seen from Figure 4-15 and Figure 4-16 that the higher wave generator setting results in an increase in speed with the flywheel setting and buoy size. The lower wave generator setting has a significant influence only when it is combined with the shorter buoy. The other combinations have a very limited influence on the crank speed, as seen from the results in Figure 4-15 and Figure 4-16.

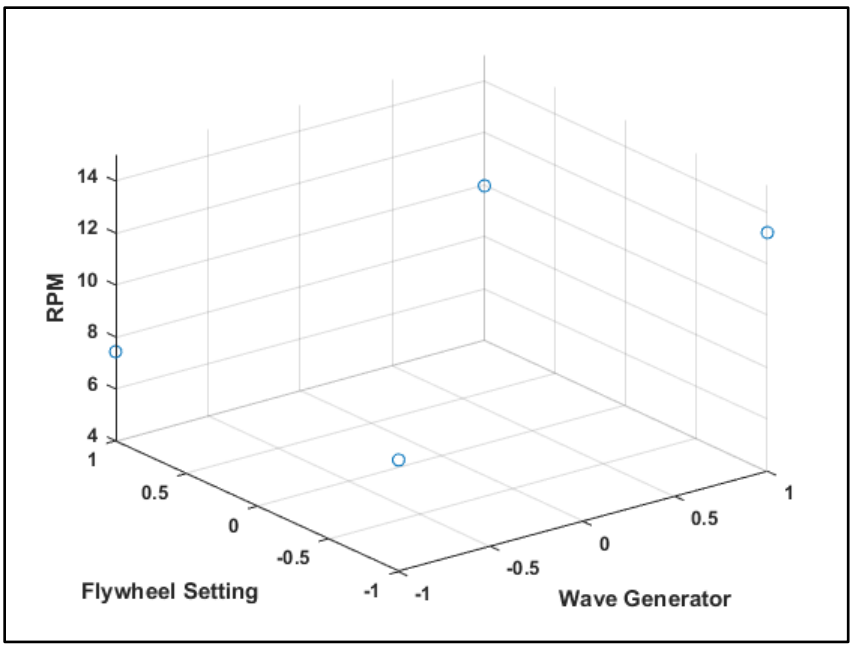

Figure 4-15 Flywheel Setting and Wave Generator Combined Effect – Speed.

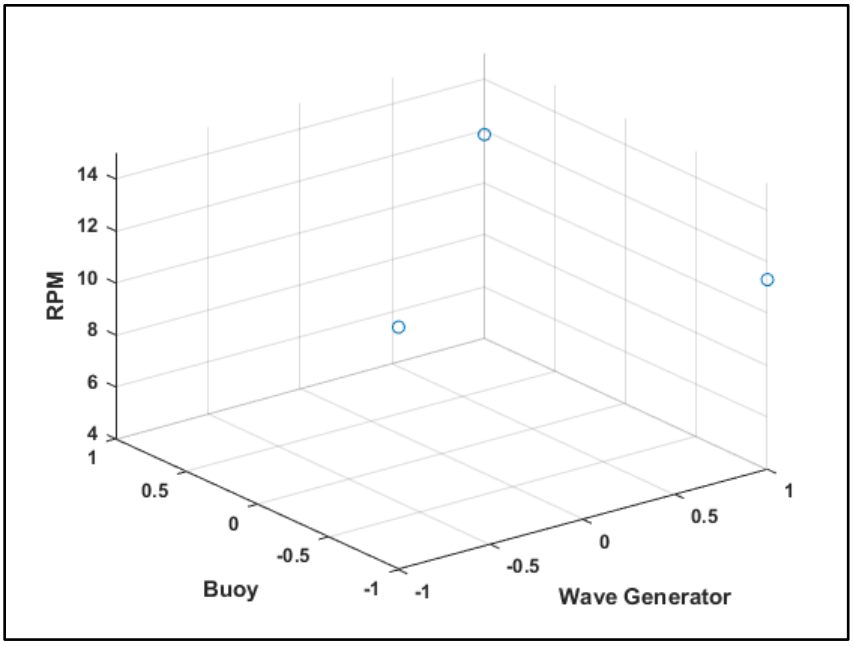

Figure 4-16 Buoy and Wave Generator Combined Effect – Speed.

From the analysis of torque results from Table 4-3, the only two variables that are found to be significant are the flywheel size and the flywheel setting. The effects for these two variables are plotted in Figure 4-17 and Figure 4-18.

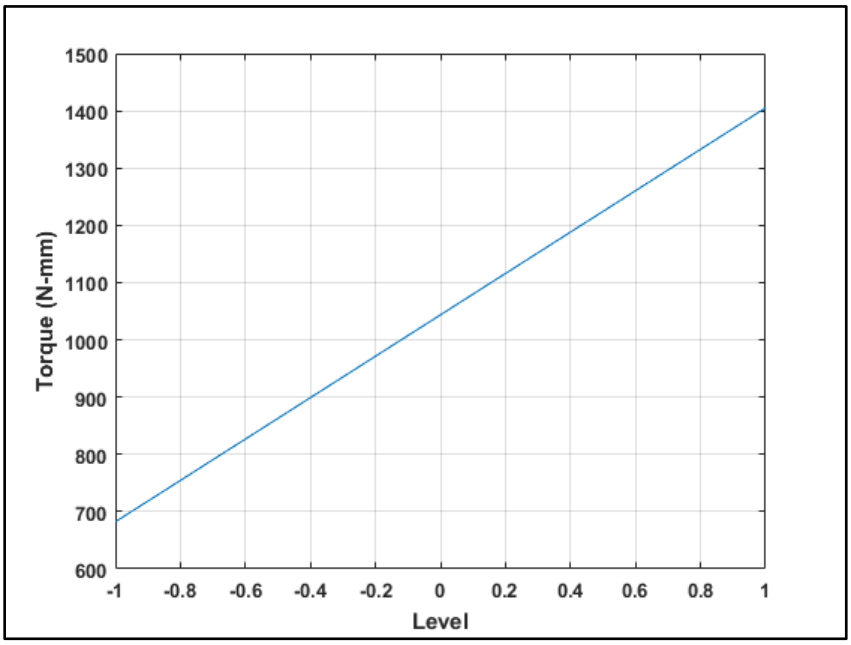

Figure 4-17 Flywheel Size Effect – Torque.

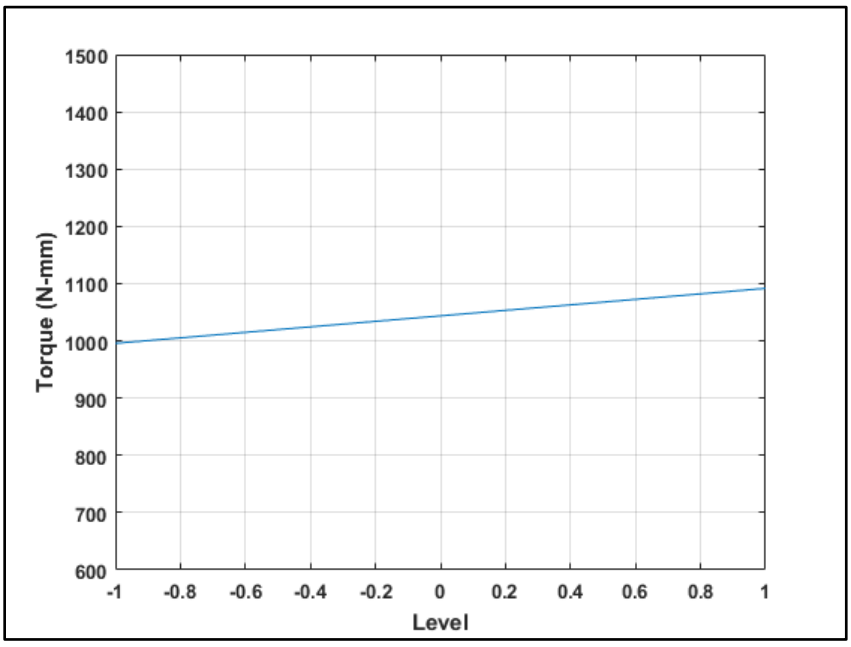

Figure 4-18 Flywheel Setting Effect – Torque.

The flywheel size seems to be more significant than the flywheel setting, as can be seen from a comparison of the slope of Figure 4-17 and Figure 4-18. For both variables, changing the level from -1 to +1 results in an increase in torque. It can be concluded from the analysis results that the most significant variable is the flywheel size for both speed and torque. The larger flywheel results in higher torque while the smaller flywheel results in higher speed.

The combined effects for torque are plotted in Figures 4-19 to 4-22. Even though the individual effect of the buoy has not been found to be significant for torque, it is seen that the combined effect of the buoy with other variables is still significant.

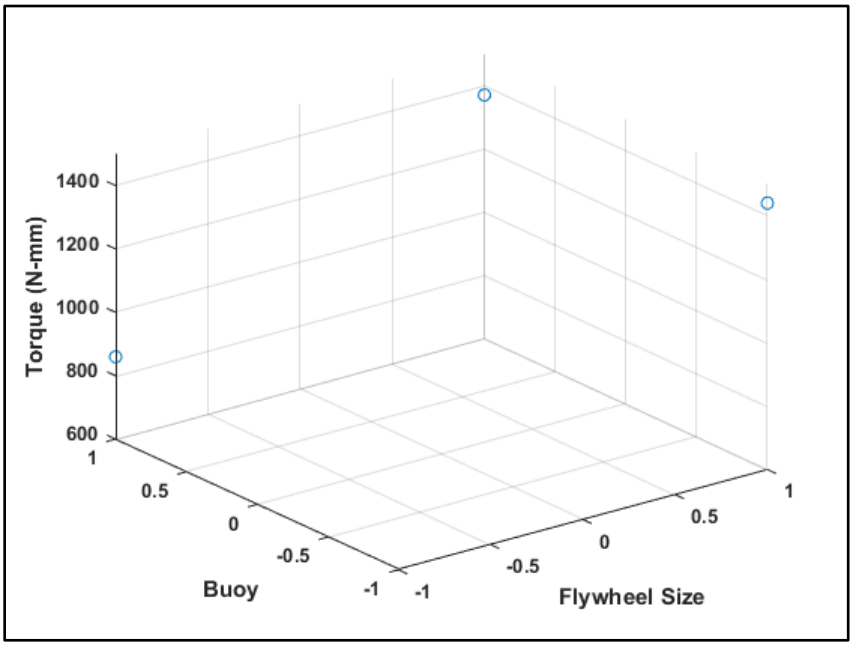

Figure 4-19 Buoy and Flywheel Size Combined Effect – Torque.

As seen from the individual effect plots, the larger flywheel is seen to be significant regardless of the other variables. This can also be seen from Figure 4-19, where the larger flywheel (+1) is seen to yield higher torque particularly in conjunction with the shorter buoy (-1).

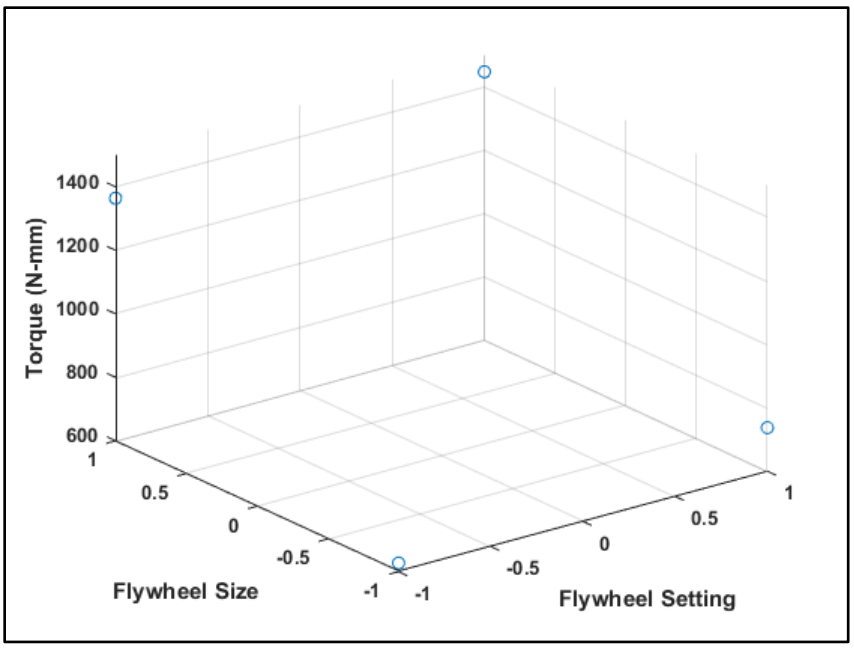

Figure 4-20 Flywheel Size and Setting Combined Effect – Torque.

The influence of the larger flywheel size (+1) can also be seen in Figure 4-20, where the torque is highest for the larger flywheel size in conjunction with the higher flywheel setting.

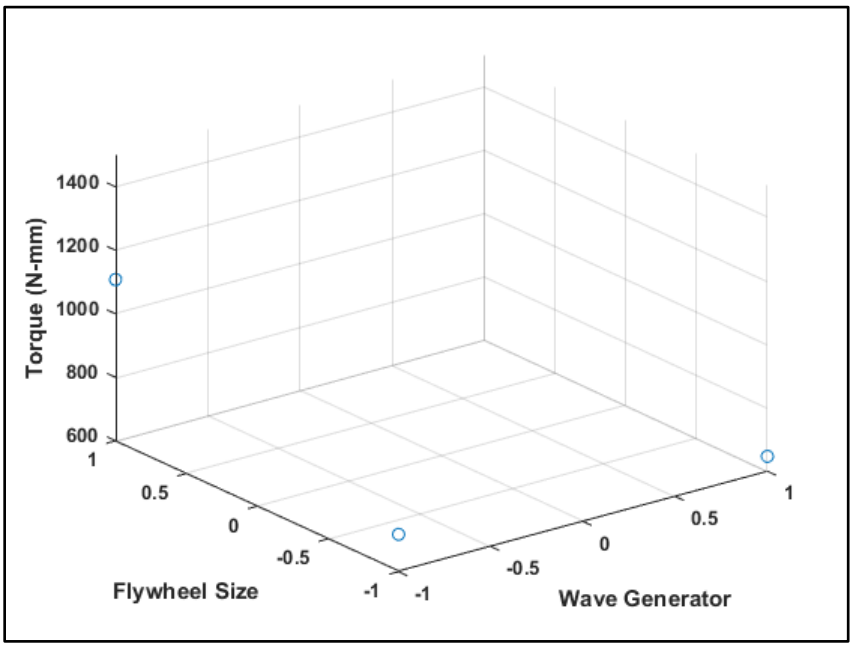

Figure 4-21 Flywheel Size and Wave Generator Combined Effect – Torque.

The wave generator setting is seen to have a negative influence on the torque, this can be seen from the combined effect plot in Figure 4-21. The lower setting of the wave generator (-1) is seen to significantly reduce the torque even for a larger flywheel size (+1). However, the higher setting of the wave generator results in a high torque with the larger flywheel size, as can be seen in Figure 4-21.

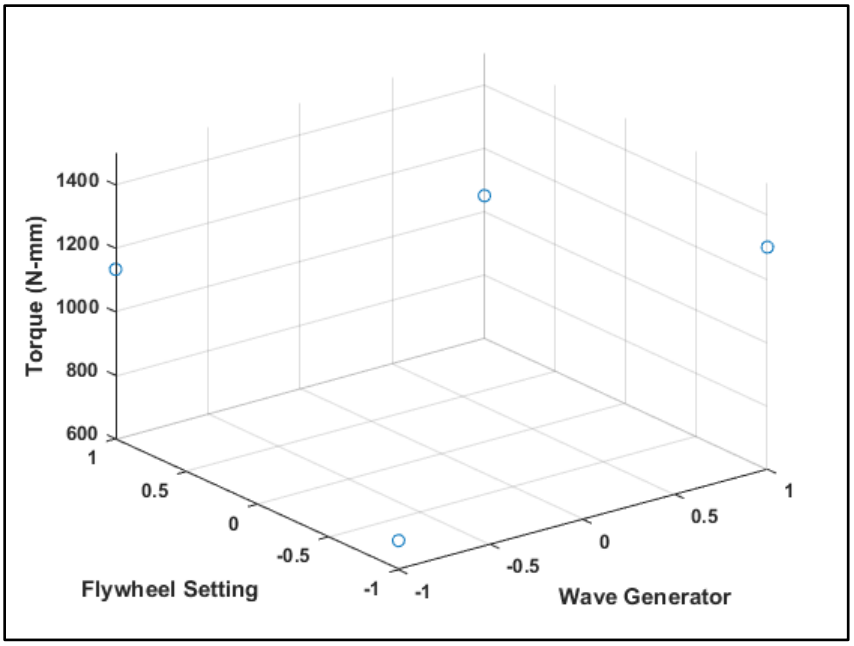

Figure 4-22 Flywheel Setting and Wave Generator Combined Effect – Torque.

The combined influence of the flywheel setting, and the wave generator setting is relatively lower, as can be seen from the results in Figure 4-22. If both variables are at a low setting, the torque is seen to be particularly low.

The root mean square (RMS) of torque and speed characteristics has also been used to calculate the power output of the crankshaft. Figures 4-23, 4-24, and 4-25 demonstrate the influence of the buoy, the flywheel, and the flywheel setting on the power output.

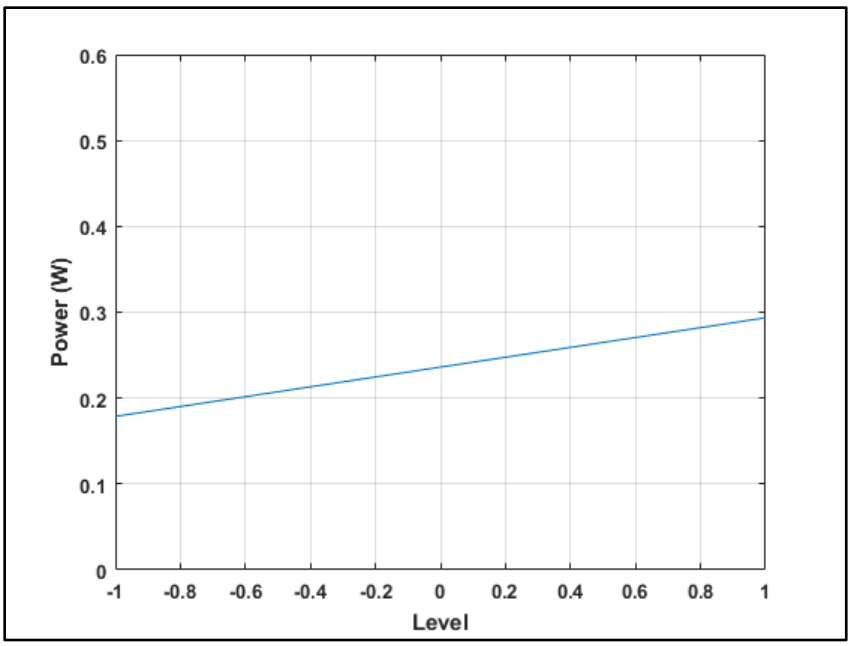

Figure 4-23 Buoy Effect – Power.

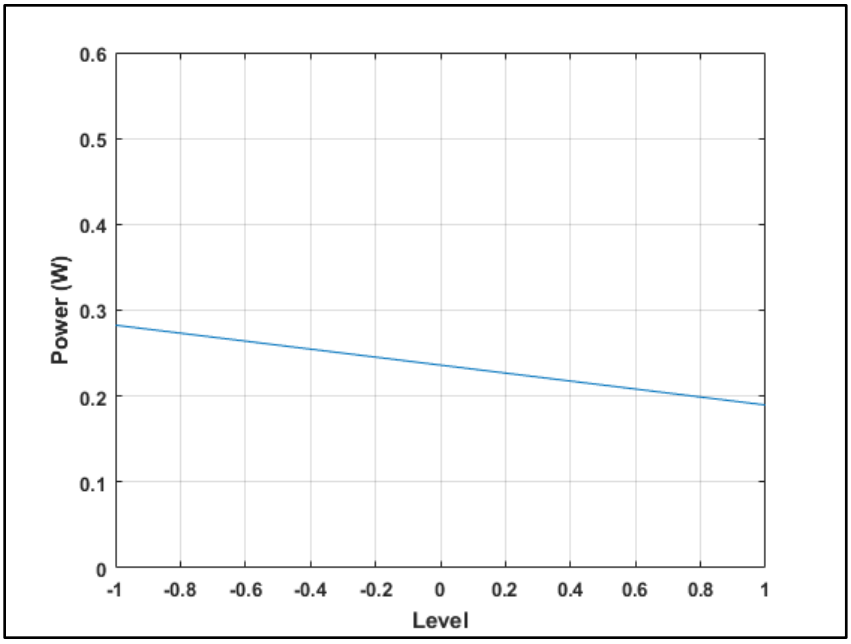

Figure 4-24 Flywheel Size Effect – Power.

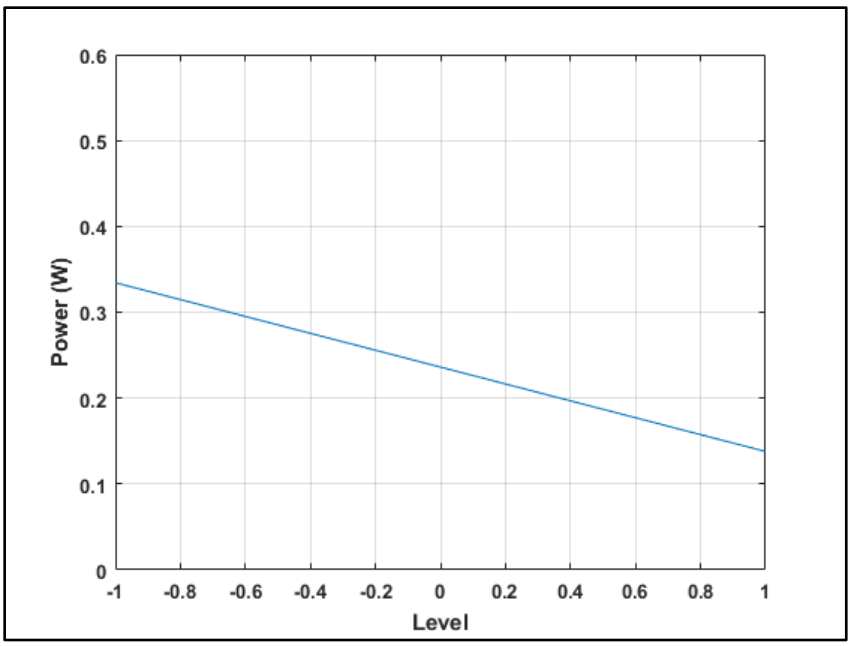

Figure 4-25 Flywheel Setting Effect – Power.

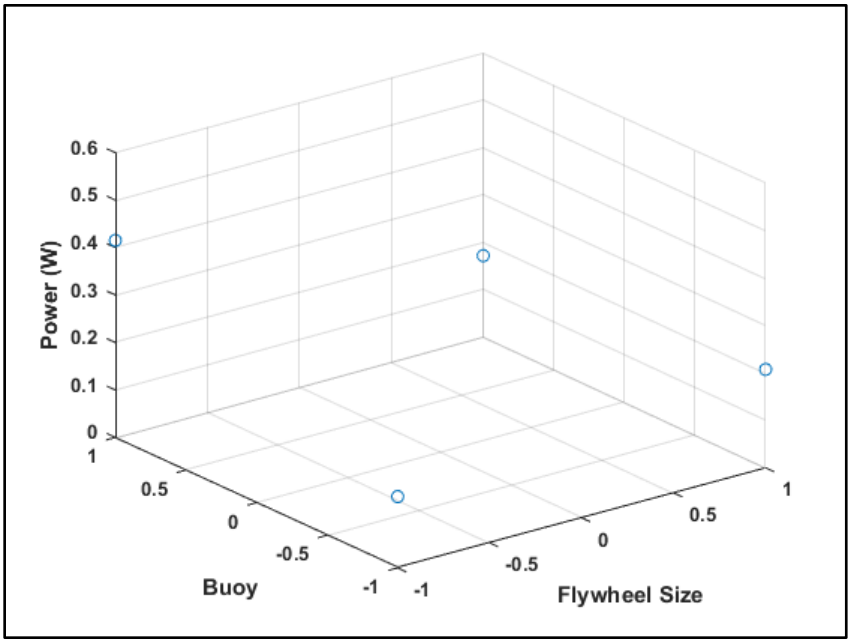

Figure 4-26 Buoy and Flywheel Size Combined Effect – Power.

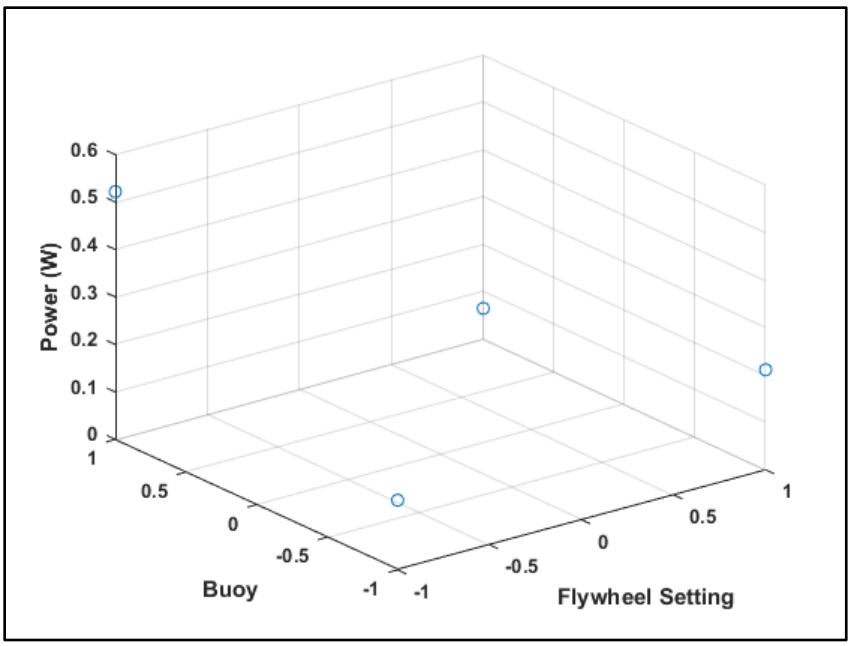

Figure 4-27 Flywheel Size and Setting Combined Effect – Power.

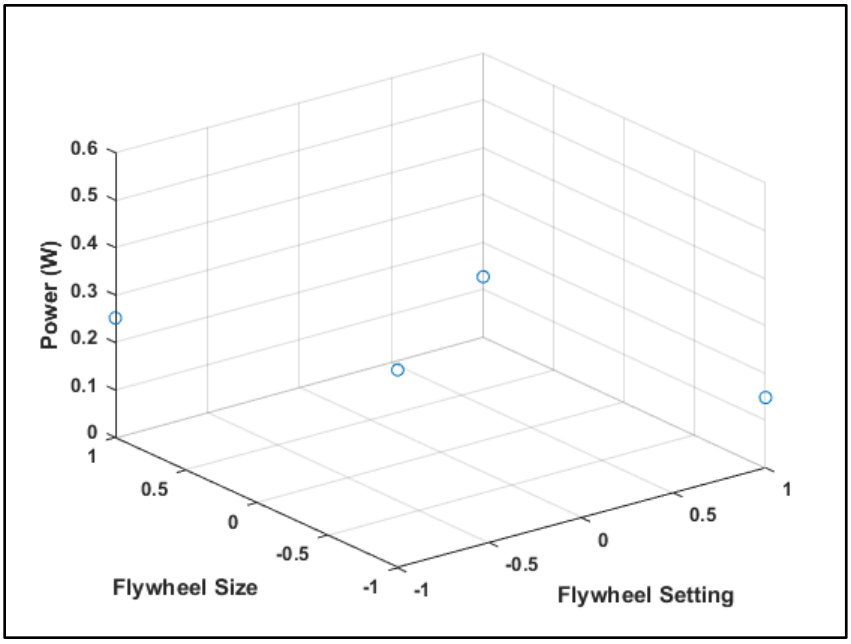

Figure 4-28 Flywheel Size and Setting Combined Effect – Power.

Figures 4-26, 4-27, and 4-28 demonstrate the combined effects for output power of the crank shaft that have been calculated by using the RMS values instead of the maximum values of torque and speed. As can be seen from these plots, the spherical buoy

(+1) and the lower flywheel setting (-1) results in the highest power output (Figure 4-27) of approximately 0.5 W. Table 4-4 shows the calculated power output at the crank shaft for all the iterations of the full factorial analysis.

DOE Power (Watts)																								
	I	Buoy	Flywheel Size	Flywheel Setting	Wave Generator																			Power
		A	B	C	D	AB	AC	AD	BC	BD	CD	ABC	ABD	ACD	BCD	ABCD								
	1	-1	-1	-1	-1	1	1	1	1	1	1	-1	-1	-1	-1	1	0.05074							
	1	1	-1	-1	-1	-1	-1	-1	1	1	1	1	1	1	-1	-1	0.04318							
	1	-1	1	-1	-1	-1	1	1	-1	-1	1	1	1	-1	1	-1	0.37417							
	1	1	1	-1	-1	1	-1	-1	-1	-1	1	-1	-1	1	1	1	0.07422							
	1	-1	-1	1	-1	1	-1	1	-1	1	-1	1	-1	1	1	-1	0.35142							
	1	1	-1	1	-1	-1	1	-1	-1	1	-1	-1	1	-1	1	1	0.04611							
	1	-1	1	1	-1	-1	-1	1	1	-1	-1	-1	1	1	-1	1	0.08146							
	1	1	1	1	-1	1	1	-1	1	-1	-1	1	-1	-1	-1	-1	0.01089							
	1	-1	-1	-1	1	1	1	-1	-1	-1	1	-1	1	1	1	-1	0.05648							
	1	1	-1	-1	1	-1	-1	1	-1	-1	-1	1	-1	-1	1	1	1.51824							
	1	-1	1	-1	1	-1	-1	-1	1	1	-1	1	-1	1	-1	1	0.10573							
	1	1	1	-1	1	1	1	1	-1	1	-1	-1	1	-1	-1	-1	0.45222							
	1	-1	-1	1	1	-1	-1	-1	-1	-1	1	1	1	-1	-1	1	0.14217							
	1	1	-1	1	1	-1	1	1	-1	-1	1	-1	-1	1	-1	-1	0.05239							
	1	-1	1	1	1	-1	-1	-1	1	1	1	-1	-1	-1	1	-1	0.26744							
	1	1	1	1	1	1	1	1	1	1	1	1	1	1	1	1	0.15091							
	3.78	0.92	-0.74	-1.57	1.71	-1.20	-2.08	2.29	0.58	-0.84	-1.47	1.62	-1.08	-1.95	1.90	0.56								
Effects	1.89	0.11482	-0.092961	-0.19652	0.2141739	-0.15	-0.2604	0.28566	0.07261	-0.1053	-0.1834	0.2	-0.1355	-0.24	0.2375	0.0702								
Coeffs	0.94	0.06	-0.05	-0.10	0.11	-0.07	-0.13	0.14	0.04	-0.05	-0.09	0.10	-0.07	-0.12	0.12	0.04								

Table 4-4 Full Factorial 2^4 Analysis – Power.

Overall, the post-processed results from all the configurations tested for this study are presented in this chapter. Experimental results have been post-processed by using two MATLAB programs. These results have then been analyzed by using a full factorial DOE for speed and a full factorial DOE for torque. The results from this analysis provide the most influential variables from the wave generation system as well as the wave energy conversion mechanism. These results will be discussed in the next chapter to make overall conclusions and discuss possible future scope for this study.

CHAPTER 5. CONCLUSIONS

In the industry's attempts towards realizing the potential of all forms of renewable sources of energy, new techniques are being investigated to harness this energy. Since oceans cover approximately 70% of the earth's surface, investigating different means of tapping ocean wave energy has become an active area of research. Wave energy conversion (WEC) is a technique that converts energy associated with ocean waves into useful forms of energy. The focus of this study has been on building and testing a slider crank mechanism to generate rotational motion from regular and irregular waves. The main purpose of this thesis has been to verify the function of a slider crank mechanism that uses wave input as an excitation source, and to find the variables that are most influential for the speed and torque characteristics of the crank shaft. This mechanism has been designed, built, and tested for the experimentation carried out for this thesis. This chapter lists the main conclusions from this study and possible future work that can be carried out to build on the experimentation done in this study.

5.1 Conclusions

The slider crank mechanism developed for this study was used for thirty-two test configurations in order to identify the torque and speed characteristics of the crank shaft. The power output of the crank shaft was also evaluated. A full factorial Design of Experiments (DOE) was used to analyze the test results. The variables that were investigated in the full factorial analysis are as follows: buoy shape, flywheel size, flywheel setting, and wave generator setting.

The slider crank mechanism designed for this study is modular and can be easily modified to accommodate different parts or design changes. The mechanism was designed to allow an adjustable ratio between the crank radius and the length of the connecting rod. The base of the mechanism was designed such that it can be easily mounted on the wave table. All parts of the mechanism were designed with the aim of minimizing the overall weight. This design can be appropriately scaled for any future study with varying sizes of wave tables or for different configurations of the wave generator.

Overall, the torque and speed characteristics exhibit an inverse relationship, implying that speed is seen to decrease as torque tends to increase. This was clearly observed during experimentation for the flywheel size. While the smaller flywheel resulted in a higher speed with low torque, the larger flywheel resulted in a relatively higher torque with lower speed. The results of the full factorial analysis reveal that the buoy and the flywheel are highly influential in determining the speed of the crank shaft. The buoy and the flywheel setting were also observed to be influential in determining the power output of the crank shaft. Particularly, the combined influence of the flywheel and the buoy is seen to be critical for maximizing the speed. For instance, the high flywheel setting (+1) and the low buoy setting (-1) resulted in a speed of 15 RPM, the highest crank speed out of all the configurations tested in this study. This could be attributed to the fact that the larger flywheel setting had a larger path that it traveled on than the smaller settings. However, because of this larger range of travel there was more unwanted movement (horizontal on the table, not vertical). The low buoy setting (spheroid buoy) captured primarily only the vertical movement of the buoy and not the

horizontal movement. With the larger flywheel setting and the spheroid buoy, the vertical movement and speed was maximized while removing the horizontal movement. This allowed for the maximum speed to be accomplished. The most influential variables for torque were the flywheel and the wave generator setting, particularly the combined effect of these two variables. The buoy is not seen to an influential variable for torque. The test configuration with the highest torque involves the larger flywheel size (+1) and the higher wave generator setting (+1). This setting resulted in a torque of 1700 N-mm. This could be attributed to the combination of the larger waves from the wave generator setting and the extra weight and acceleration that the larger flywheel produced. The added weight for the flywheel helped with the torque, because the torque measurement took the maximum acceleration in both vertical directions of the buoy. This means that because the system was heavier for these tests, the acceleration would be higher and thus yielded a larger torque value. This combination should also be helpful in future testing, because the system has more energy in the portion of rotation in which the buoy is moving down. This extra energy then helps to initially propel the mechanism around the portion of rotation where the wave is pushing the buoy up. The full factorial analysis has been very useful since this analysis easily allows an investigation into the combined effects of variables, these combined effects have been found to be crucial even when the single variable was not highly influential in some cases. The only constraint posed by this analysis is the choice of the high and low settings in a two-level configuration. This can be mitigated in the future by using a three-level configuration with critical variables identified in this study, as discussed in the next section.

5.2 Future Scope

Possible future scope of this study could involve a further investigation into some of the critical variables identified from the full factorial analysis. The slider crank mechanism developed for this study worked well and can be used or adapted for future studies of interaction effects or possibly a three-level full factorial analysis in order to further comprehend the influence of some of the critical variables. Since a large number of variables was being investigated in this study, the full factorial analysis was limited to two levels in order to restrict the overall number of tests to a manageable number. Although the full factorial analysis has been able to determine the most influential variables, additional experimentation will be required to validate the results and to fully determine the underlying reasons. Nonlinearities, if any, can be detected by using a three-level full factorial analysis.

For many configurations tested in this study, the crank shaft exhibited intermittent motion instead of continuous rotational motion. Several adjustments can be made to the mechanism to maximize the rotational motion of the crank shaft. Additionally, a control strategy can be investigated to enhance the rotational motion of the crank shaft in order to maximize energy generation.

Some design changes can also be incorporated as part of future scope. To create variability in the flywheel settings, various threaded holes were incorporated into the flywheel design. During testing, it was observed that the flywheel would get out of alignment for some of the settings. This issue can be fixed by either using a jig for tapping the threaded holes or by using bearings. This may mean some design changes to

the mechanism, but this should solve the alignment issue and offer better results accordingly.

Also, a regression analysis could be done in the future to further investigate the results from the full factorial analysis. This regression analysis can be used to form an equation that can be used to predict the response.

REFERENCES

1. Sang, Y., Karayaka, H. B., Yan, Y., & Zhang, J. Z. (2014). Resonance control strategy for a slider crank WEC power take-off system. 2014 Oceans - St. Johns. doi:10.1109/oceans.2014.7003180
2. Green energy Definition in the Cambridge English Dictionary. (n.d.). Retrieved March 05, 2017, from http://dictionary.cambridge.org/us/dictionary/english/green-energy
3. Senten, J. R. (1994). OCEAN ENERGIES (Book). International Journal Of Environmental Studies, 46(2/3), 225.
4. Falcão, A. O. (2010). Wave energy utilization: A review of the technologies. Renewable & Sustainable Energy Reviews, 14(3), 899-918. doi:10.1016/j.rser.2009.11.003
5. Ozkop, E., & Altas, I. H. (2017). Control, power and electrical components in wave energy conversion systems: A review of the technologies. Renewable & Sustainable Energy Reviews, 67106-115. doi:10.1016/j.rser.2016.09.012
6. Nunes, G., Valério, D., Beirão, P., & Sá da Costa, J. (2011). Modelling and control of a wave energy converter. Renewable Energy: An International Journal, 36(7), 1913-1921. doi:10.1016/j.renene.2010.12.018
7. Sheng, W., & Lewis, A. (2016). Power Takeoff Optimization for Maximizing Energy Conversion of Wave-Activated Bodies. *IEEE Journal of Oceanic Engineering, 41*(3), 529-540. doi:10.1109/joe.2015.2489798

8. Sang, Y. (2015). *A suboptimal control strategy for a slider crank wave energy converter power take-off system* (Master's thesis). Sylva: Western Carolina Universtiy.
9. Sang, Y., Karayaka, H. B., Yan, Y., Zhang, J. Z., Muljadi, E., & Yu, Y. (2015). Energy extraction from a slider-crank wave energy converter under irregular wave conditions. *OCEANS 2015 - MTS/IEEE Washington*. doi:10.23919/oceans.2015.7401873
10. Falnes, J. (2007). A review of wave-energy extraction. Marine Structures, 20(4), 185-201. doi:10.1016/j.marstruc.2007.09.001
11. Design of Machinery, Fifth Edition, Robert L. Norton, McGraw Hill, NY, 2012

Appendix A

RPM MATLAB Code

```
close all
clear

% Pull data from excel
Data = xlsread('Test2.xls');
t=Data(:,1);
x=Data(:,2);
y=Data(:,3);
r=Data(:,4);

% Center point of circle
x0=200;
y0=600;

% Arc Angle Calculation

for i=1:length(x)-1
    pheta(i)=atan2d(y(i+1)-y0,x(i+1)-x0)-atan2d(y(i)-y0,x(i)-x0);
end


for i=1:length(x)-1
    arclength(i)=(pheta(i)./360);
end

% Time between points
for i=1:(length(t)-1)
    T(i)=t(i+1)-t(i);
end

% Calculate Revolutions per Second

for i=1:length(x)-1
    RPs(i)=arclength(i)/T(i);
end


RPM=RPs.*60;

% Filter Data
indices = find(abs(RPM)>80);
    RPM(indices) = [ ];
figure
plot(RPM)
xlabel('Time in Seconds')
ylabel('Revolutions per Minute (RPM)')
title('Speed')
```

```
figure
scatter(x,y)
xlabel('Position X')
ylabel('Position Y')
title('Position')

maximum=max(abs(RPM))
```

Torque MATLAB Code

```
close all
clear
% Slider crank mechanism for buoy

% Data from Test 1 spreadsheet
%%%%%%%%%%%%%%%%%%%%%%%%%%%%%%%%%%%%%%%%%%%%%%%%%%%
m2=336.6/1000;% Units: kg
m3=20.2/1000;% Units: kg
m4=356.3/1000;% Units: kg
I2=15.8563280*25.4*25.4/(2.2*1000*1000);% Units: kg-m^2
I3=0.0104837*25.4*25.4/(2.2*1000*1000);% Units: kg-m^2
r=3.6*25.4/1000; % Units: meters
l=6*25.4/1000; % Units: meters

w2=1.8589*2*pi/60; %Units: rad/s
alp2=0; % steady state
%%%%%%%%%%%%%%%%%%%%%%%%%%%%%%%%%%%%%%%%%%%%%%%%%%%
% Data from Test 1 spreadsheet and the acceleration data
FP= (m4)*1.9619*9.81; % Note: m4=356.3 from Test 1 & use acceleration
test data (Units of FP: N)
% This can also be made into a force history of 361 data points for one
full revolution
%%%%%%%%%%%%%%%%%%%%%%%%%%%%%%%%%%%%%%%%%%%%%%%%%%%

T =[];
for tht2=0:1:360 % Units: degrees

tht3=acosd(-r*cosd(tht2))/l;
y=-r*sind(tht2)-l*sind(tht3);

w3=-(r*w2*sind(tht2))/(l*sind(tht3));

yd=-(r*w2*cosd(tht2))-(l*w3*cosd(tht3));

alp3= (-(r*alp2*sind(tht2))-(r*w2^2*cosd(tht2))-
(l*w3^2*cosd(tht3)))/(l*sind(tht3));

ydd= -(r*alp2*cosd(tht2))+(r*w2^2*sind(tht2))-
(l*alp3*cosd(tht3))+(l*w3^2*sind(tht3));

% Position vectors
R12x=(r/2)*cosd(tht2-180); R12y=(r/2)*sind(tht2-180);
R32x=(r/2)*cosd(tht2); R32y=(r/2)*sind(tht2);
```

```
R23x=(l/2)*cosd(tht3-180); R23y=(l/2)*sind(tht3-180);
R43x=(l/2)*cosd(tht3); R43y=(l/2)*sind(tht3);

% Acceleration vectors
aG2x=-(r/2)*alp2*sind(tht2)-(r/2)*w2^2*cosd(tht2);
aG2y=(r/2)*alp2*cosd(tht2)-(r/2)*w2^2*sind(tht2);
aG3x=-(r*alp2)*sind(tht2)-(r*w2^2)*cosd(tht2)-(l*alp3/2)*sind(tht3)-
(l*w3^2/2)*cosd(tht3);
aG3y=(r*alp2)*cosd(tht2)-(r*w2^2)*sind(tht2)+(l*alp3/2)*cosd(tht3)-
(l*w3^2/2)*sind(tht3);
aG4y=ydd;

% matrix Solution
A=[1 0 1 0 0 0 0 0; ...
    0 1 0 1 0 0 0 0; ...
    -R12y R12x -R32y R32x 0 0 0 1; ...
    0 0 -1 0 1 0 0 0; ...
    0 0 0 -1 0 1 0 0; ...
    0 0 R23y -R23x -R43y R43x 0 0; ...
    0 0 0 0 -1 0 1 0; ...
    0 0 0 0 0 -1 0 0];

B=[m2*aG2x;m2*aG2y;I2*alp2;m3*aG3x;m3*aG3y;I3*alp3;0;m4*aG4y-FP];

F=inv(A)*B;

T=[T F(8,1)];
end

Tmax=max(abs(T)) % absolute maximum torque in N-m
plot(0:1:360,T*1000,'LineWidth',2),grid
xlim([0 360])
xlabel('Crank angle (deg.)'), ylabel('Torque (N-mm)')
```

Effects MATLAB Code

```
clear all
close all

% Normal Probability Plot RPM

effectRPM=[-5.2044375 -5.2510625 -2.0546625 3.7070125 -0.4886625 -6.7275125 5.7487625 -6.0939875
-2.3246125 -1.1860625 9.2920125 -3.1180125 -4.4177125 5.8448625 -1.3416375];
figure
normplot(effectRPM)

% Normal Probability Plot Torque

effecttorque=[141.78 722.92 96.03 261.92 -213.07 -17.18 172.03 -14.17 332.42 -346.27 11.77 230.88 -
10.23 -68.57 300.22];
figure
normplot(effecttorque)
```

```
% RPM Effects

X=[-1 1];
x=[-1 -1 1 1];
y=[-1 1 -1 1];

A=[12.32268 7.118238];
B=[12.34599 7.094925];
C=[10.7477875 8.693125];
D=[7.86695 11.5739625];
AB=[14.7039 9.94 9.99 4.248];
AC=[9.99 14.66 11.509 2.73];
AD=[13.34 11.30 2.39 11.85];
BC=[10.33 14.366 11.17 3.02];
BD=[9.33 15.3618 6.404 7.79];
CD=[8.30 13.19 7.43 9.95];

% RPM Effects plots

figure
plot(X,A), grid
xlabel('Level')
ylabel('RPM')
ylim([4 15])

figure
plot(X,B), grid
xlabel('Level')
ylabel('RPM')
ylim([4 15])

figure
plot(X,C), grid
xlabel('Level')
ylabel('RPM')
ylim([4 15])

figure
plot(X,D), grid
xlabel('Level')
ylabel('RPM')
ylim([4 15])

figure
scatter3(y,x,AB), grid on
ylabel('Buoy')
xlabel('Flywheel Size')
zlabel('RPM')
zlim([4 15])

figure
scatter3(y,x,AC), grid on
ylabel('Buoy')
```

```
xlabel('Flywheel Setting')
zlabel('RPM')
zlim([4 15])

figure
scatter3(y,x,AD), grid on
ylabel('Buoy')
xlabel('Wave Generator')
zlabel('RPM')
zlim([4 15])

figure
scatter3(y,x,BC), grid on
ylabel('Flywheel Size')
xlabel('Flywheel Setting')
zlabel('RPM')
zlim([4 15])

figure
scatter3(y,x,BD), grid on
ylabel('Flywheel Size')
xlabel('Wave Generator')
zlabel('RPM')
zlim([4 15])

figure
scatter3(y,x,CD), grid on
ylabel('Flywheel Setting')
xlabel('Wave Generator')
zlabel('RPM')
zlim([4 15])



% Torque Effects

a=[972.77 1114.6];
b=[682.2 1405.12];
c=[995.6475 1091.675];
d=[912.7 1174.6225];

ab=[504.775 1440.77 859.625 1369.48];
ac=[916.17 1029.38 1075.13 1153.98];
ad=[927.825 1017.72 897.575 1331.53];
bc=[627.1 737.3 1364.2 1446.05];
bd=[717.45 646.95 1107.95 1702.3];
cd=[691.55 1299.75 1133.85 1049.5];

% Torque Effects Plots

figure
plot(X,a), grid
xlabel('Level')
ylabel('Torque (N-mm)')
```

```
ylim([600 1500])

figure
plot(X,b), grid
xlabel('Level')
ylabel('Torque (N-mm)')
ylim([600 1500])

figure
plot(X,c), grid
xlabel('Level')
ylabel('Torque (N-mm)')
ylim([600 1500])

figure
plot(X,d), grid
xlabel('Level')
ylabel('Torque (N-mm)')
ylim([600 1500])

figure
scatter3(y,x,ab), grid on
ylabel('Buoy')
xlabel('Flywheel Size')
zlabel('Torque (N-mm)')
zlim([600 1500])

figure
scatter3(y,x,ac), grid on
ylabel('Buoy')
xlabel('Flywheel Setting')
zlabel('Torque (N-mm)')
zlim([600 1500])

figure
scatter3(y,x,ad), grid on
ylabel('Buoy')
xlabel('Wave Generator')
zlabel('Torque (N-mm)')
zlim([600 1500])

figure
scatter3(y,x,bc), grid on
ylabel('Flywheel Size')
xlabel('Flywheel Setting')
zlabel('Torque (N-mm)')
zlim([600 1500])

figure
scatter3(y,x,bd), grid on
ylabel('Flywheel Size')
xlabel('Wave Generator')
zlabel('Torque (N-mm)')
zlim([600 1500])
```

```
figure
scatter3(y,x,cd), grid on
ylabel('Flywheel Setting')
xlabel('Wave Generator')
zlabel('Torque (N-mm)')
zlim([600 1500])
```

Appendix B

Position Plots

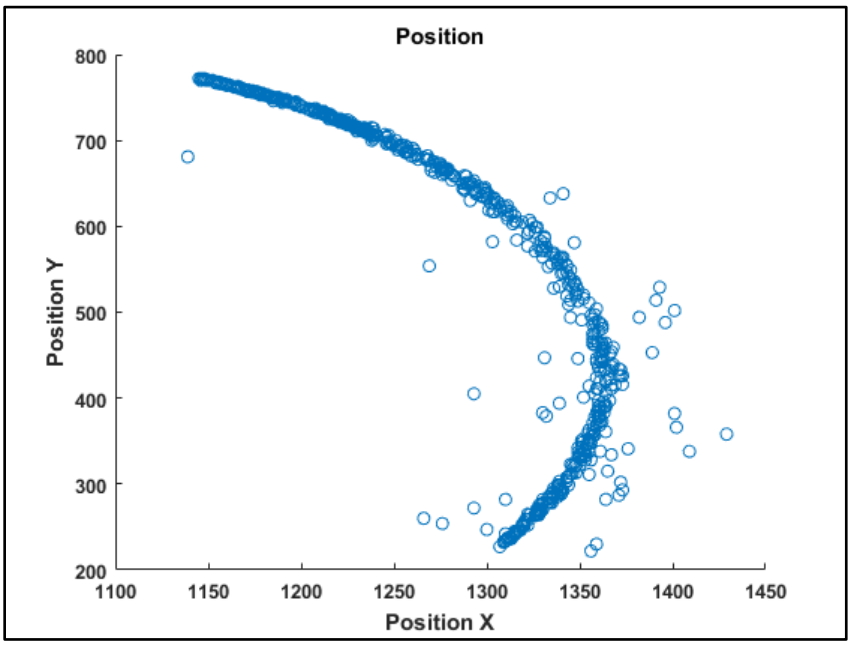

Figure B- 1 Position Plot - Test 1.

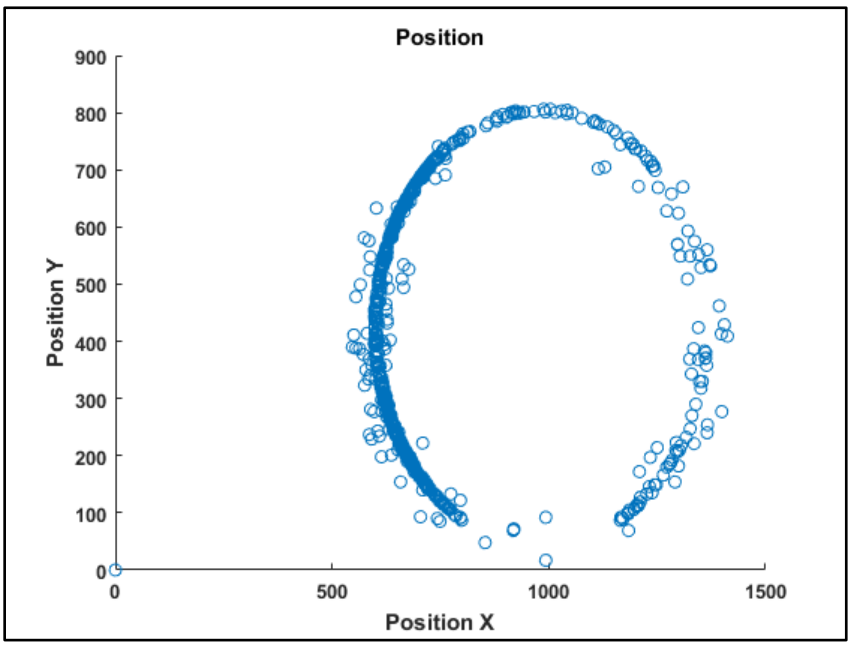

Figure B- 2 Position Plot - Test 2.

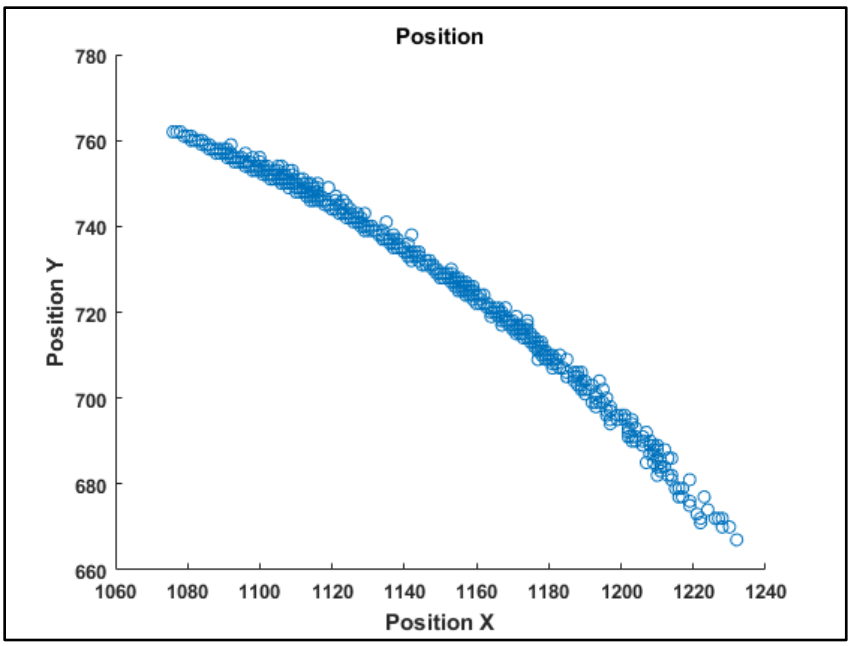

Figure B- 3 Position Plot - Test 3.

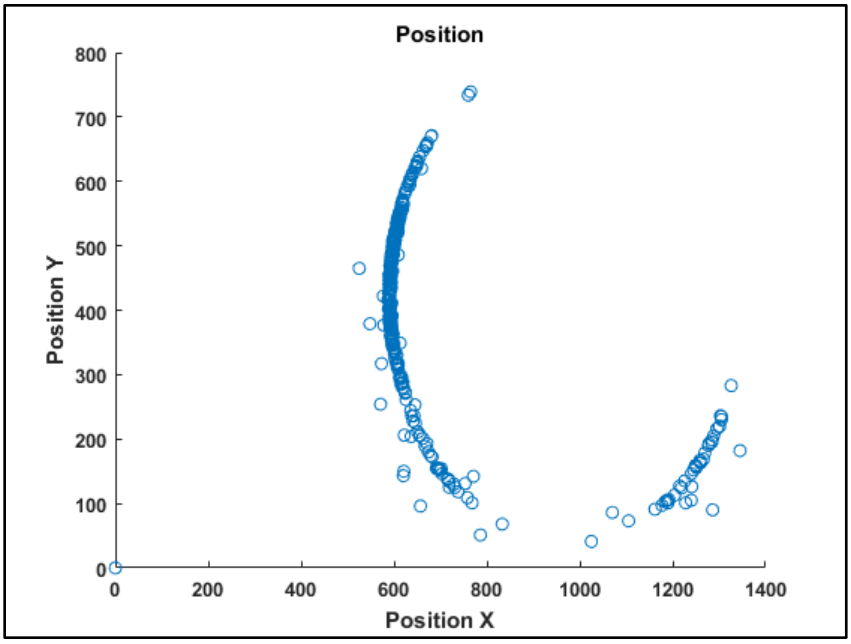

Figure B- 4 Position Plot - Test 4.

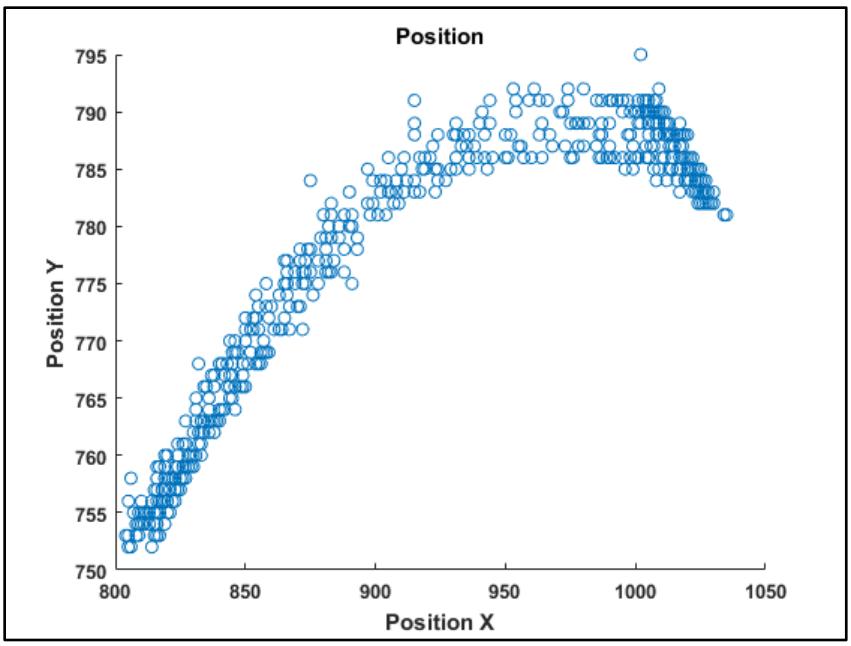

Figure B- 5 Position Plot - Test 5.

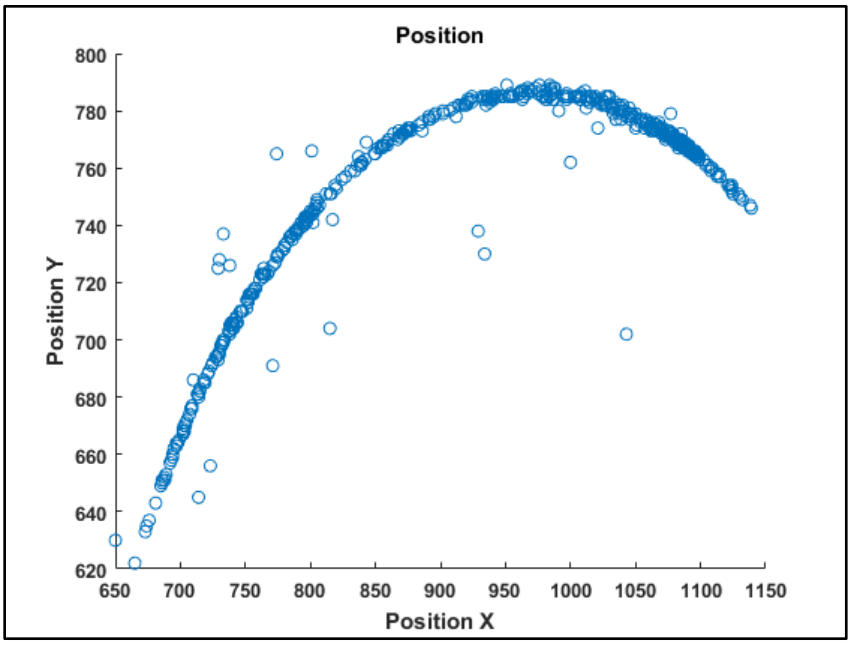

Figure B- 6 Position Plot - Test 6.

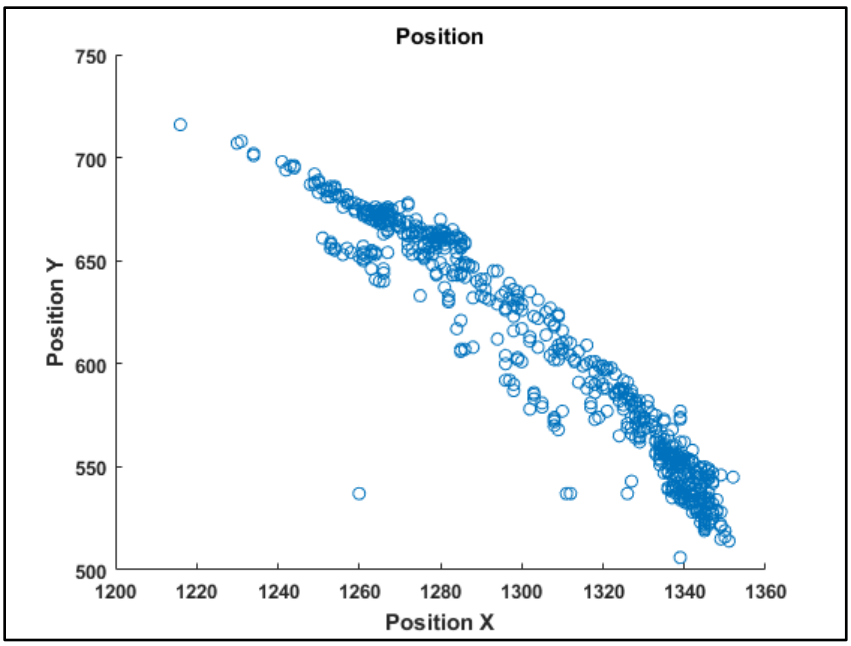

Figure B- 7 Position Plot - Test 7.

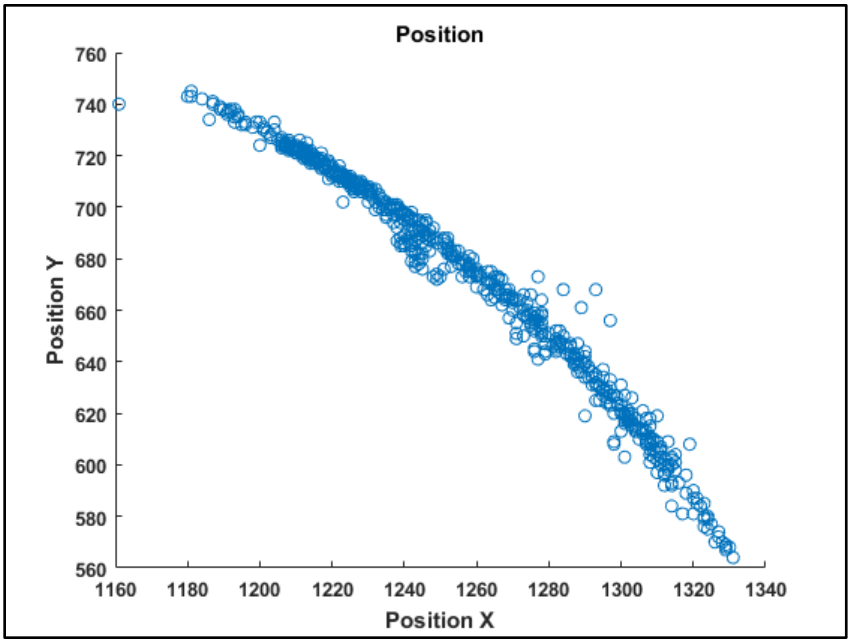

Figure B- 8 Position Plot - Test 8.

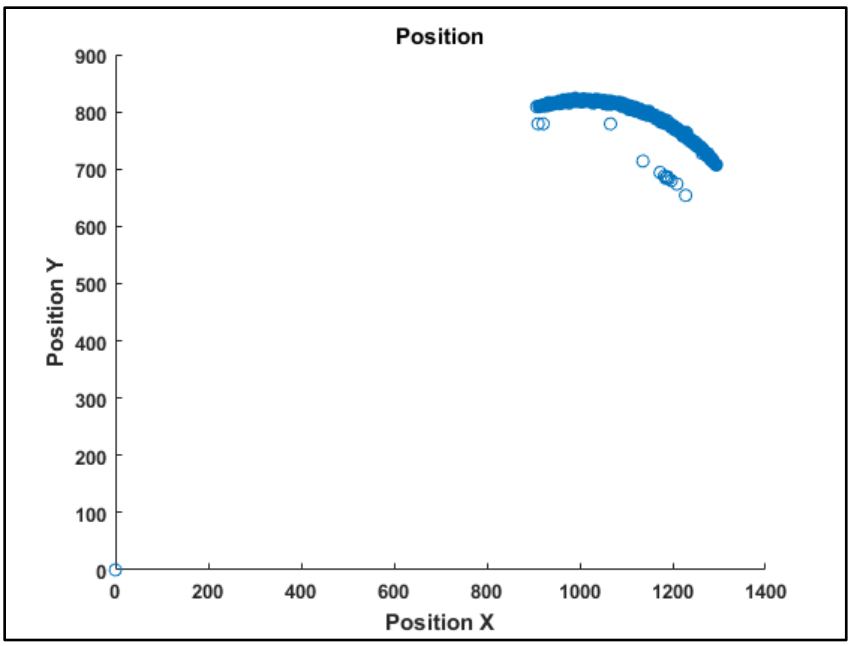

Figure B- 9 Position Plot - Test 9.

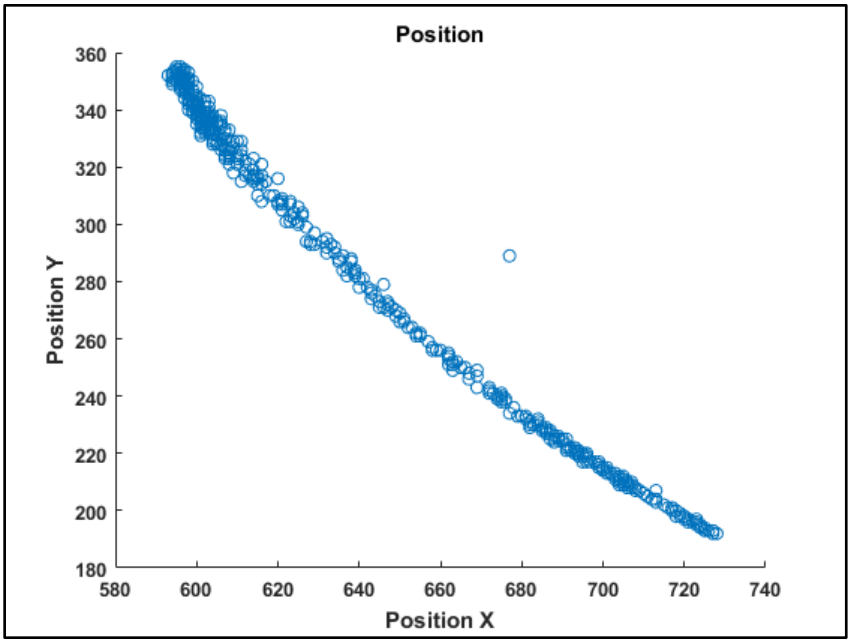

Figure B- 10 Position Plot - Test 11.

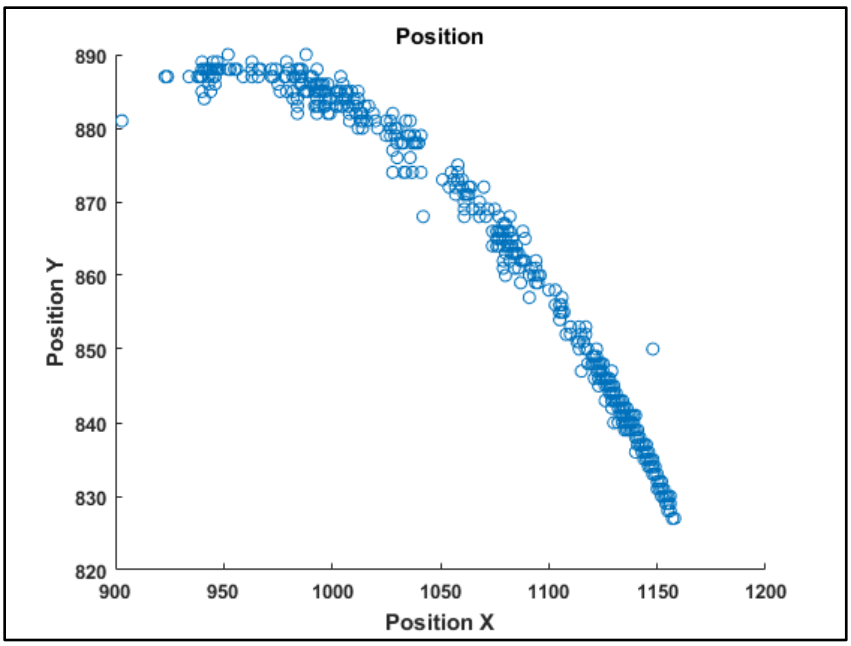

Figure B- 11 Position Plot - Test 12.

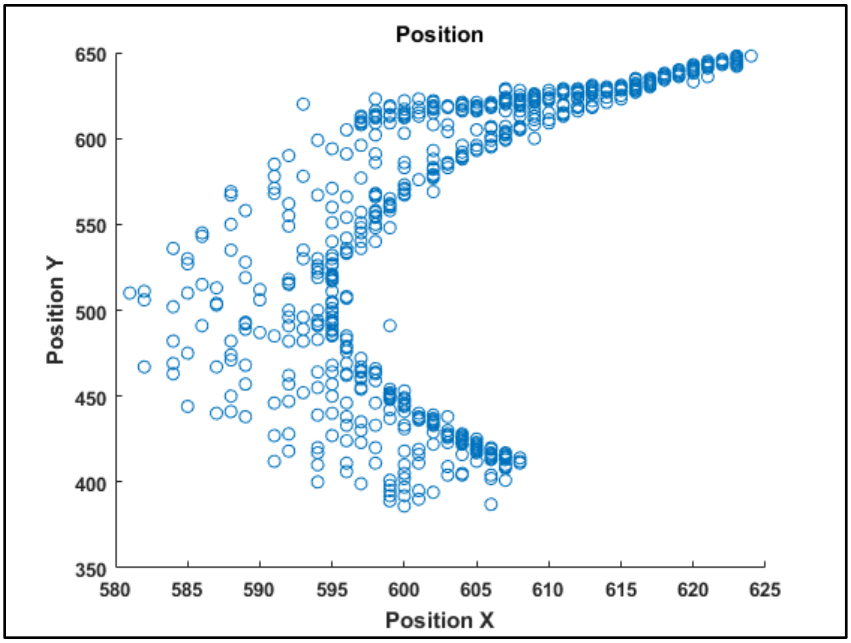

Figure B- 12 Position Plot - Test 13.

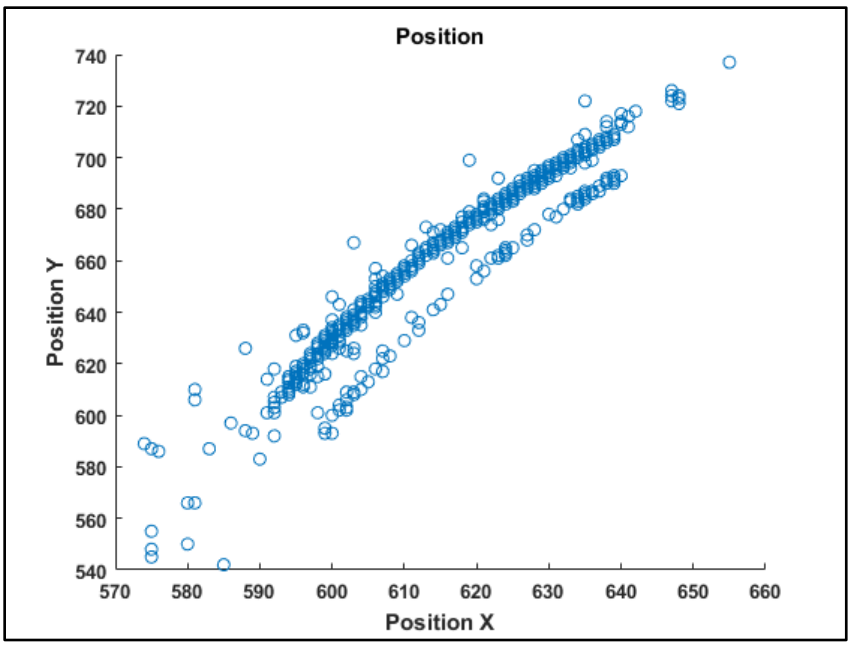

Figure B- 13 Position Plot - Test 14.

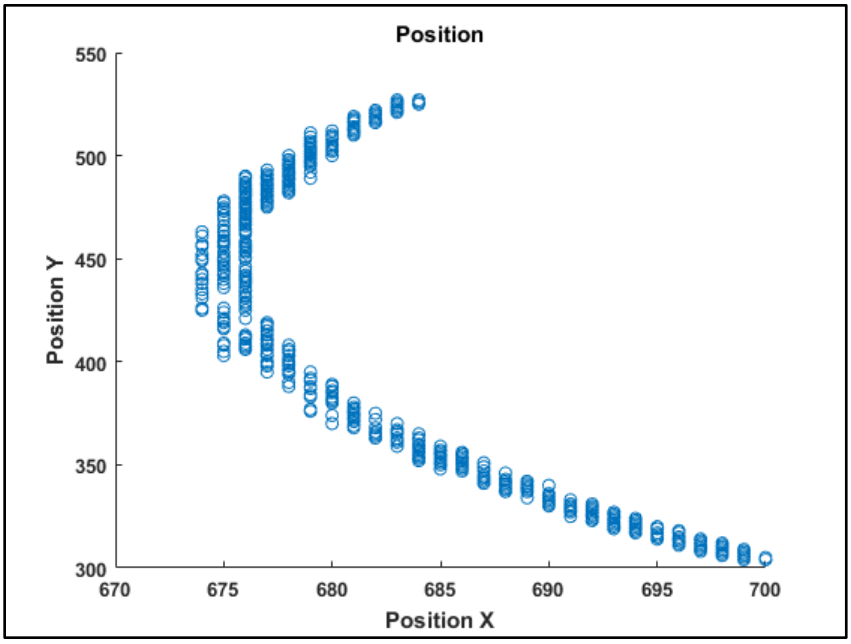

Figure B- 14 Position Plot - Test 15.

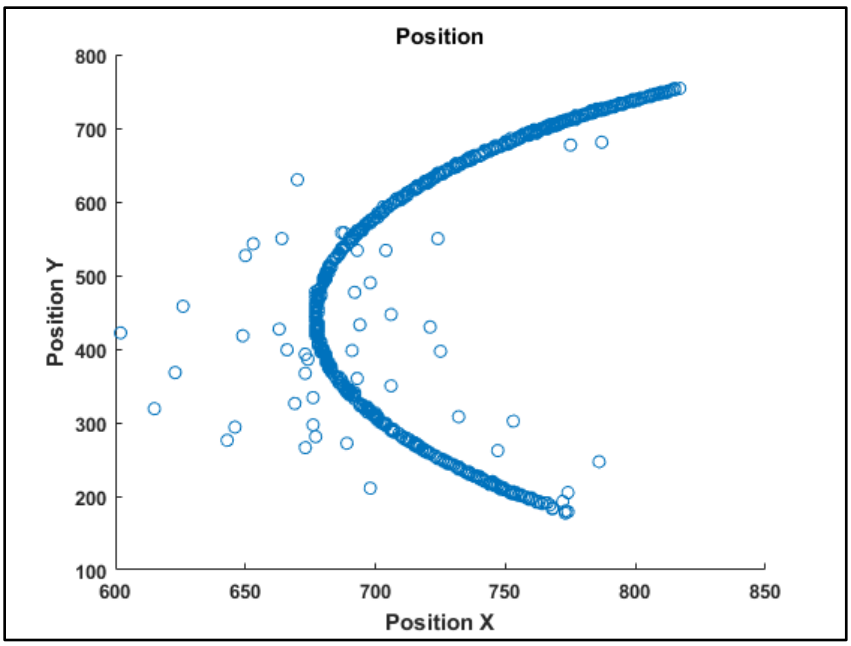

Figure B- 15 Position Plot - Test 16.

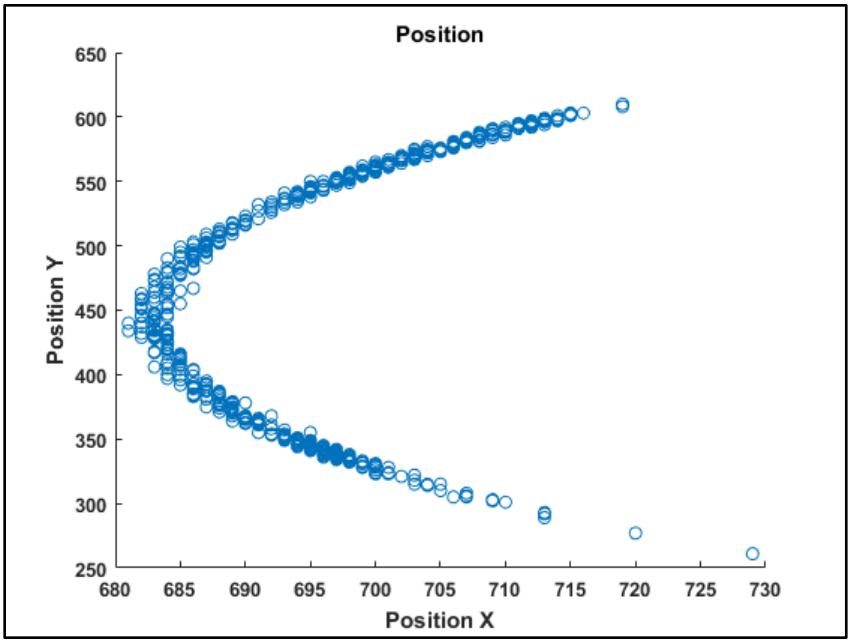

Figure B- 16 Position Plot - Test 17.

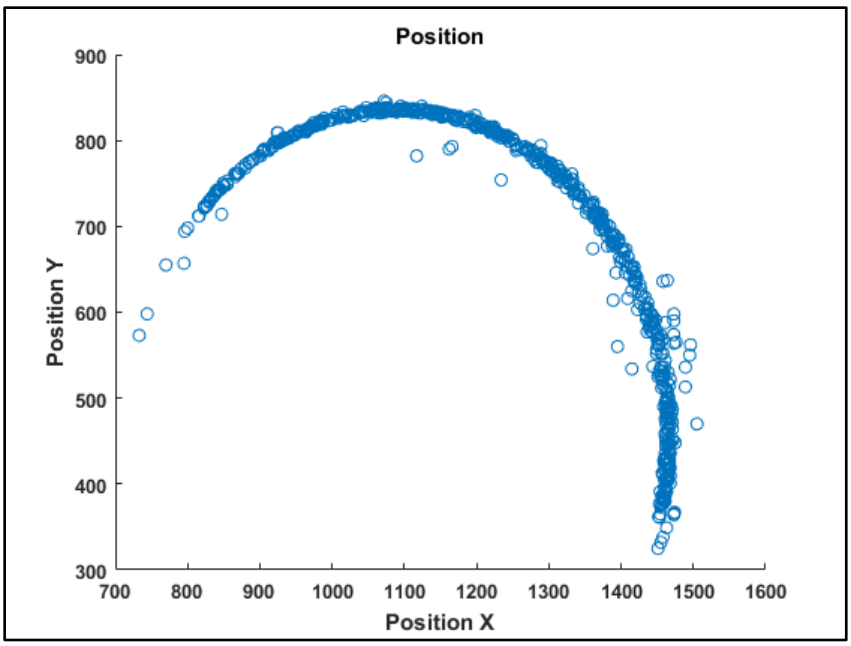

Figure B- 17 Position Plot - Test 18.

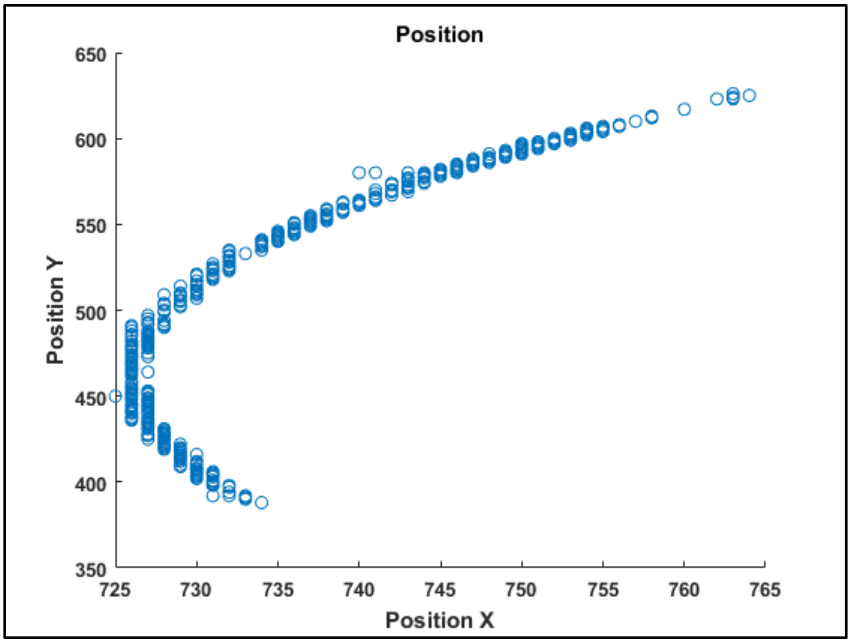

Figure B- 18 Position Plot - Test 19.

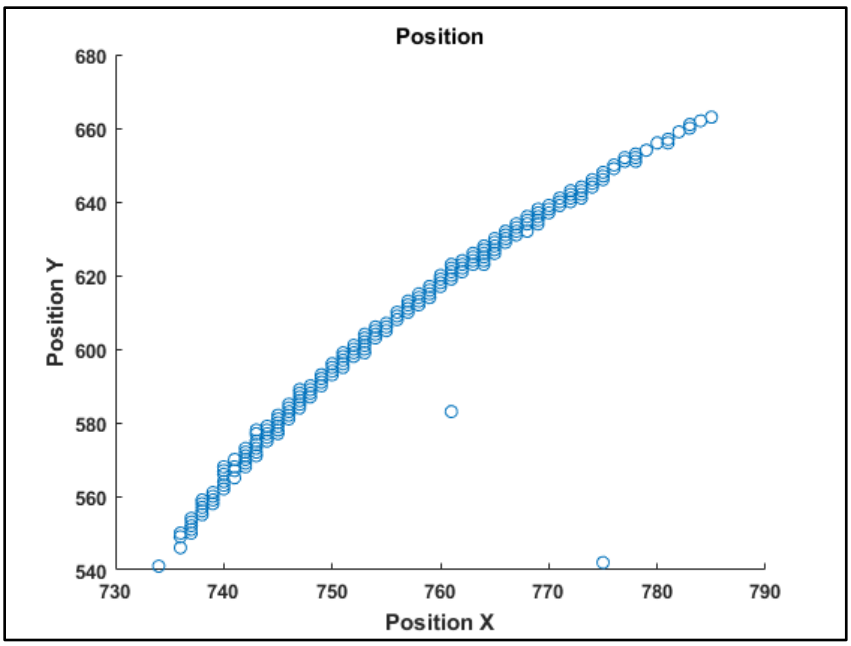

Figure B- 19 Position Plot - Test 20.

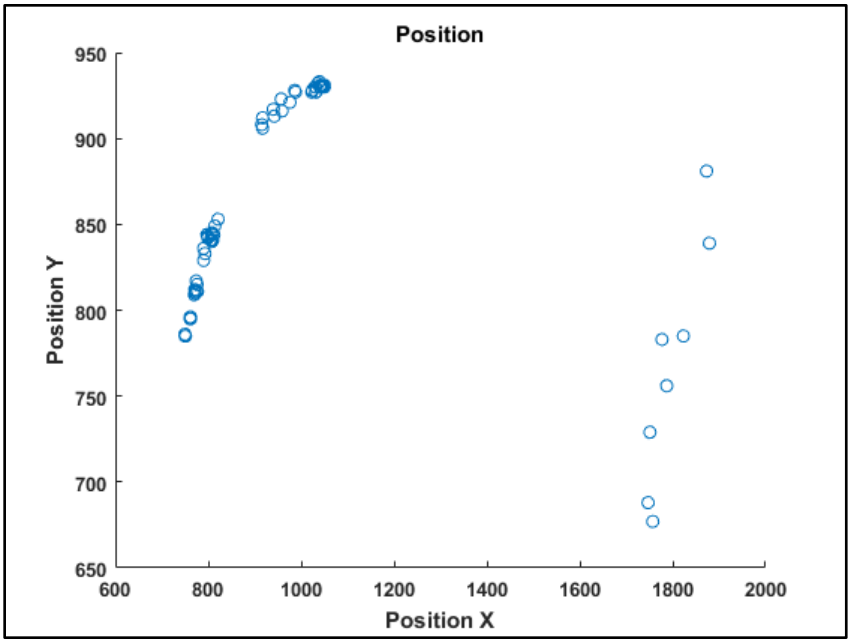

Figure B- 20 Position Plot - Test 21.

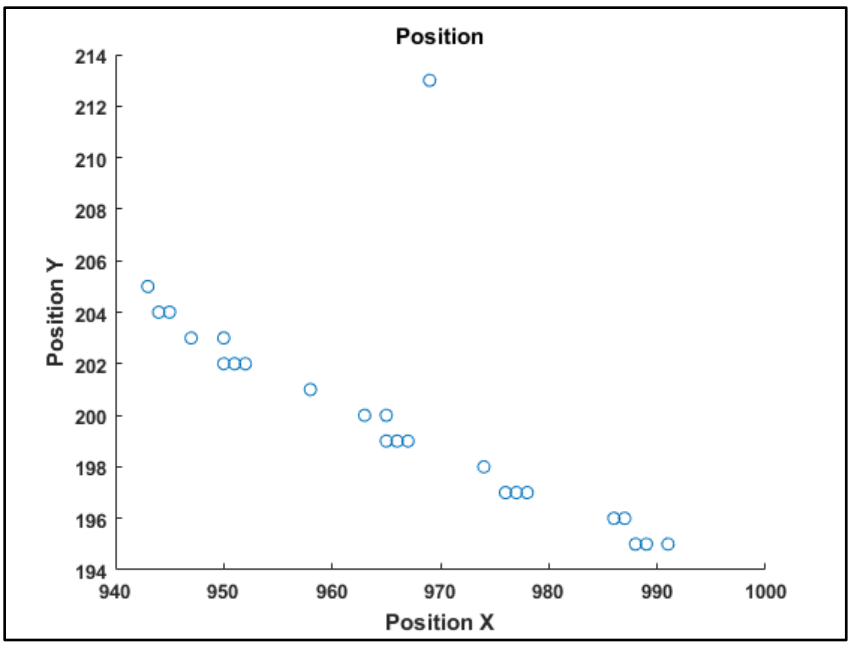

Figure B- 21 Position Plot - Test 23.

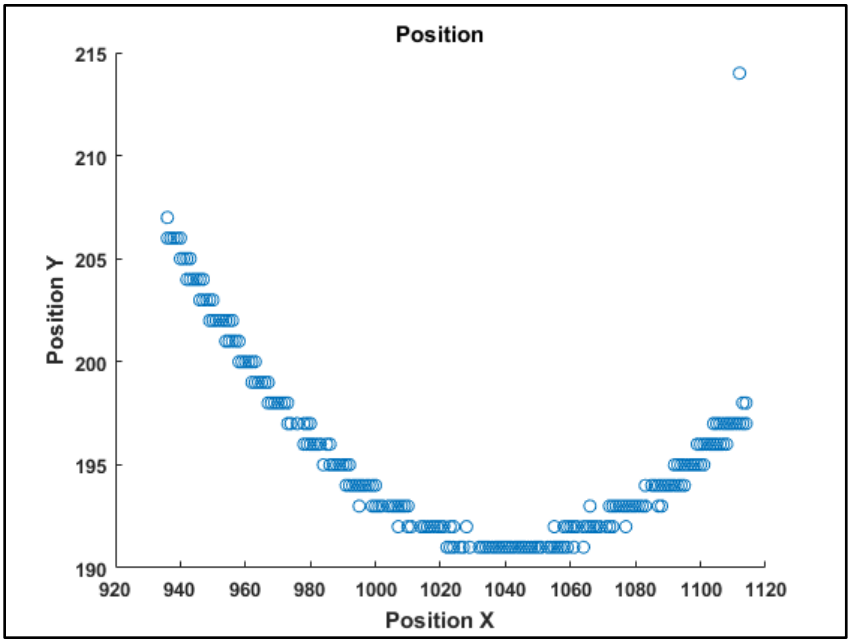

Figure B- 22 Position Plot - Test 24.

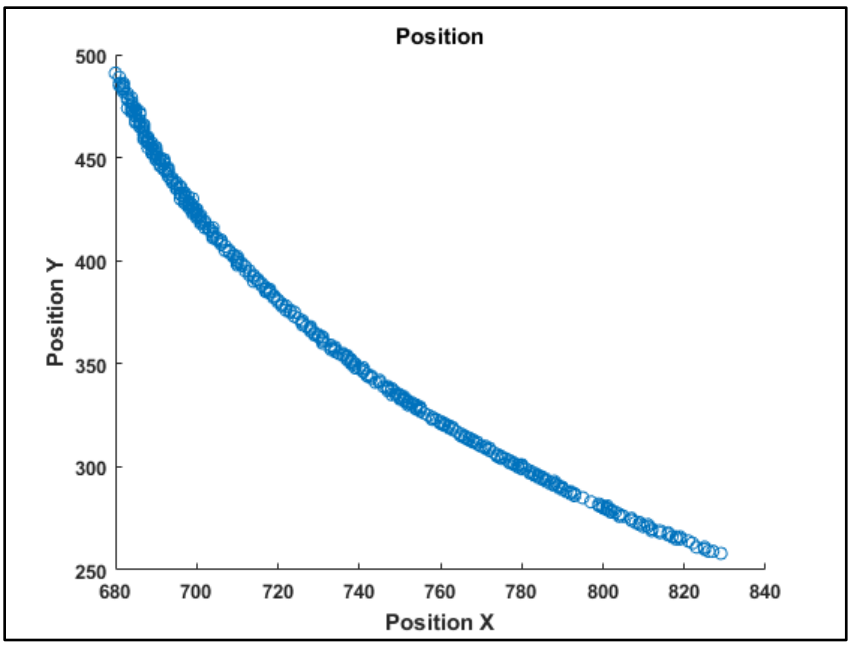

Figure B- 23 Position Plot - Test 25.

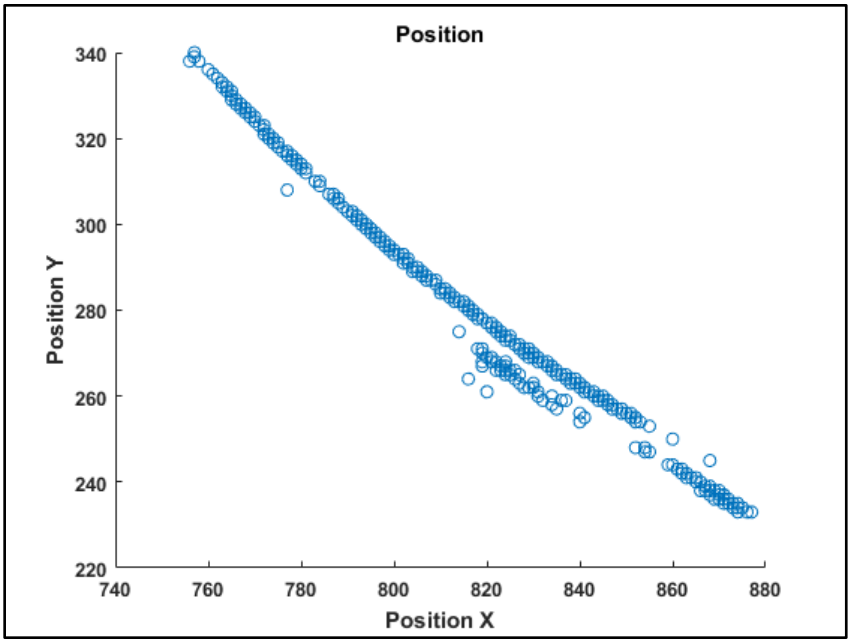

Figure B- 24 Position Plot - Test 26.

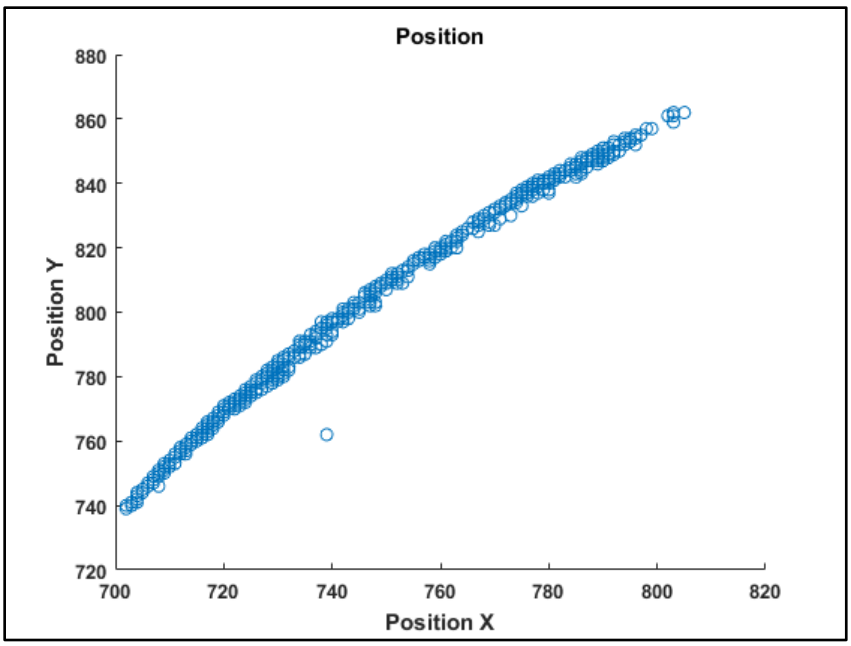

Figure B- 25 Position Plot - Test 27.

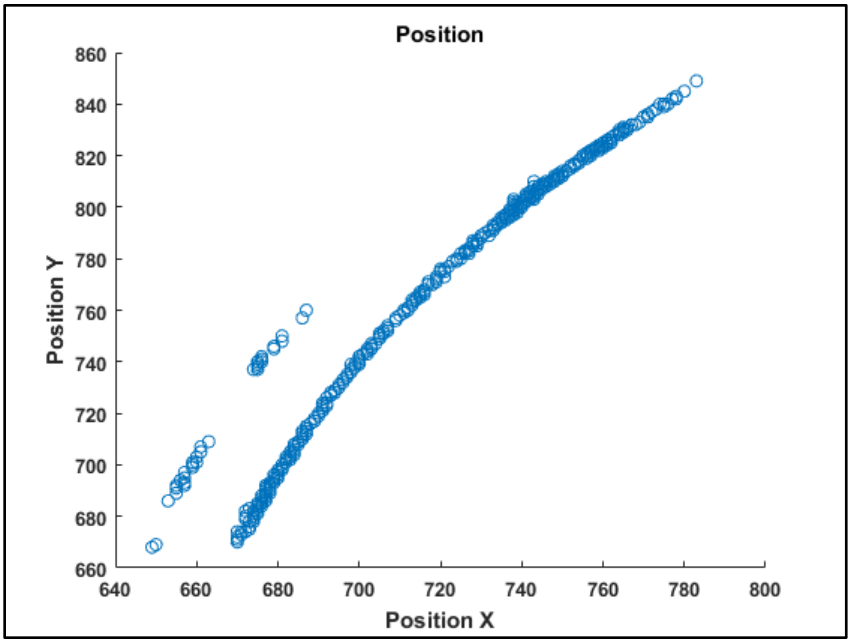

Figure B- 26 Position Plot - Test 28.

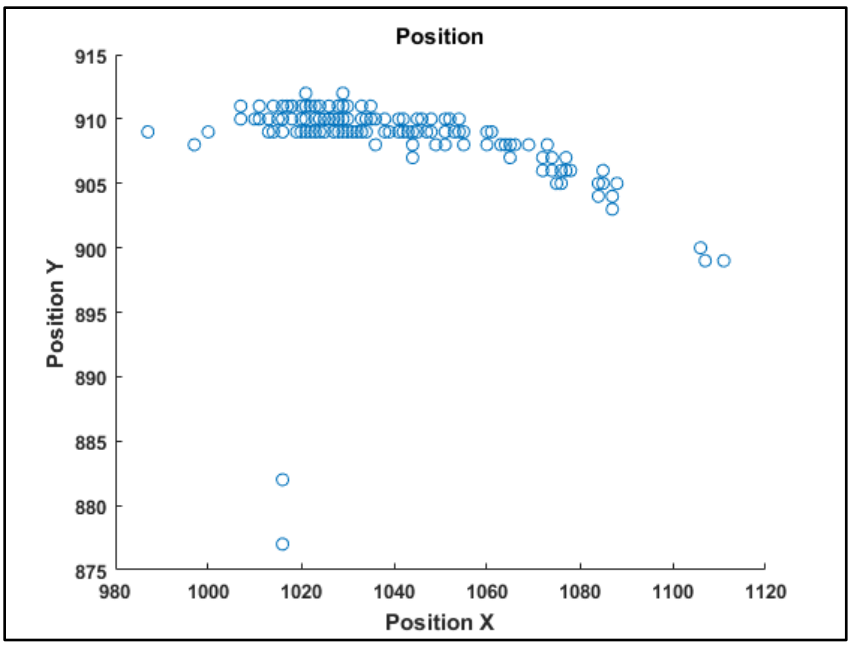

Figure B- 27 Position Plot - Test 29.

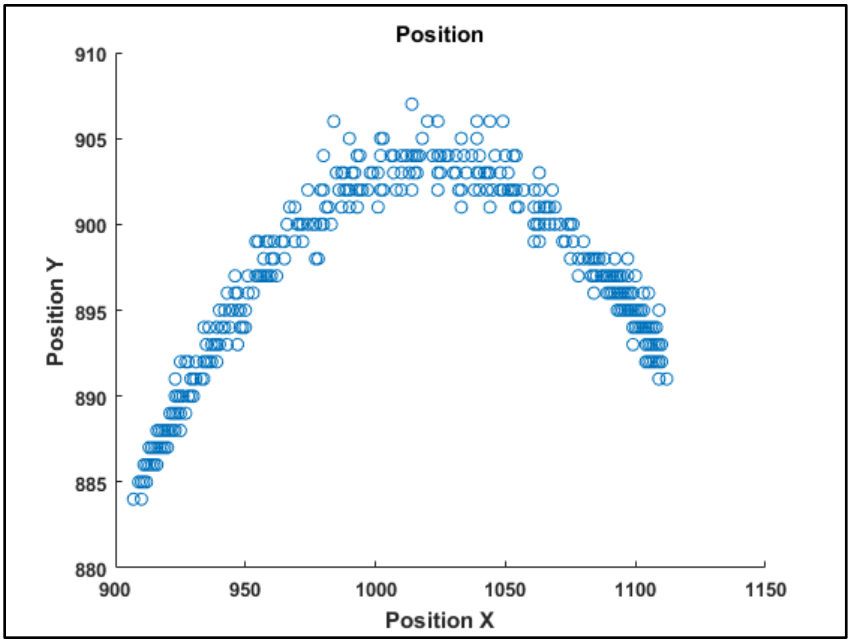

Figure B- 28 Position Plot - Test 30.

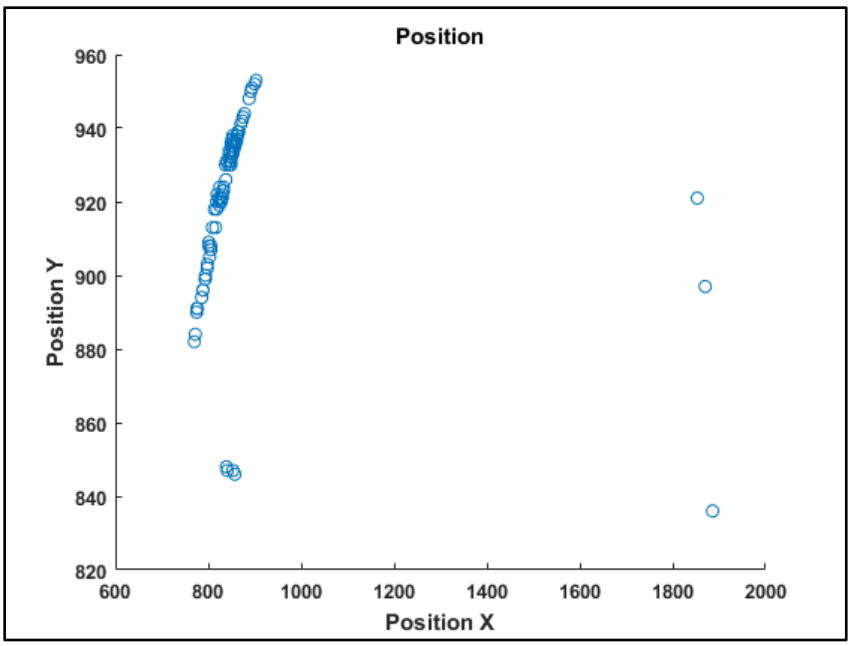

Figure B- 29 Position Plot - Test 31.

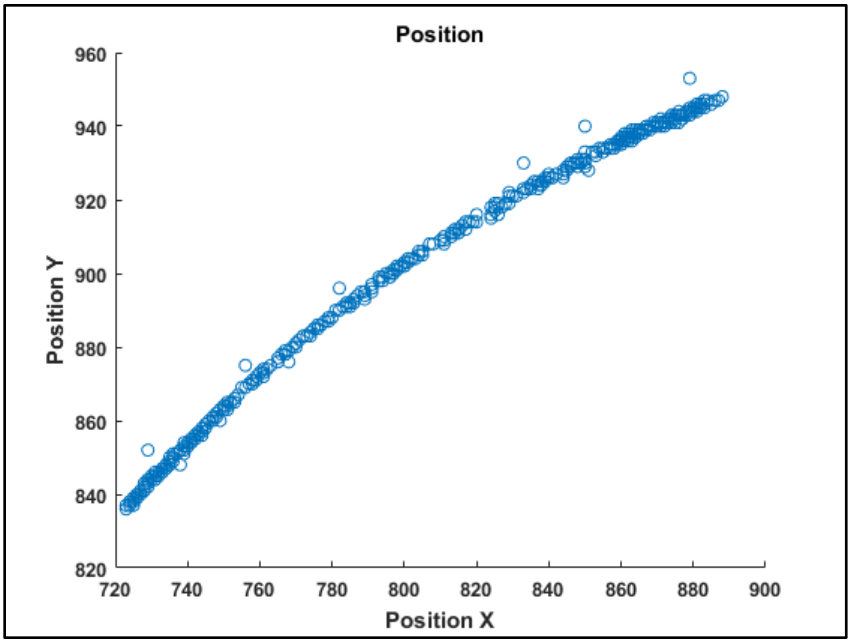

Figure B- 30 Position Plot - Test 32.

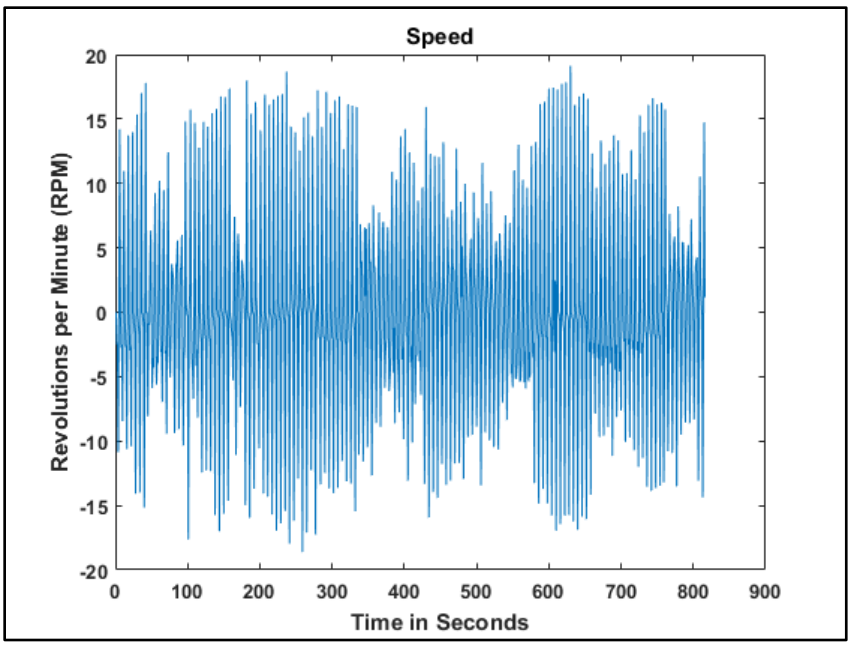

Figure B- 31 Speed (RPM) Plot - Test 1.

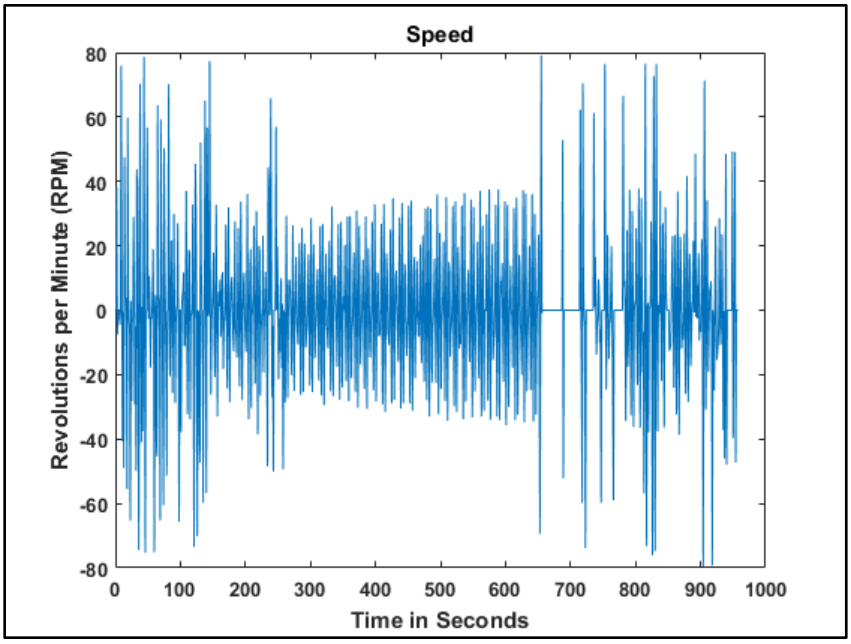

Figure B- 32 Speed (RPM) Plot - Test 2.

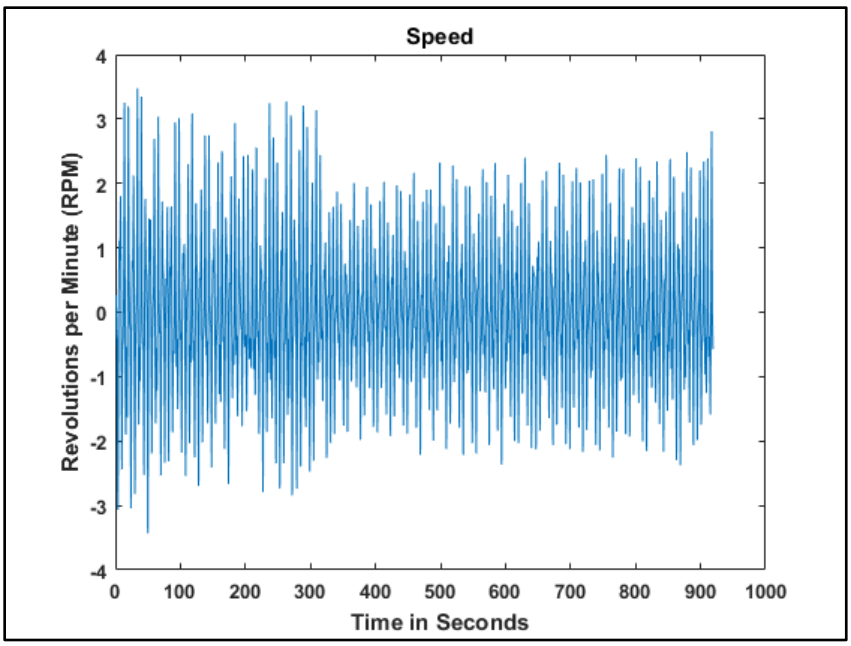

Figure B- 33 Speed (RPM) Plot - Test 3.

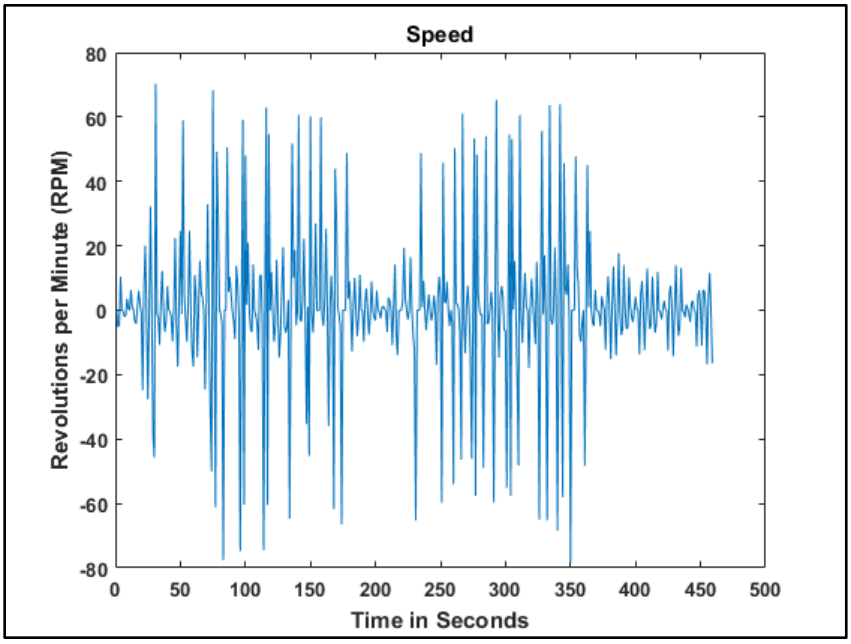

Figure B- 34 Speed (RPM) Plot - Test 4.

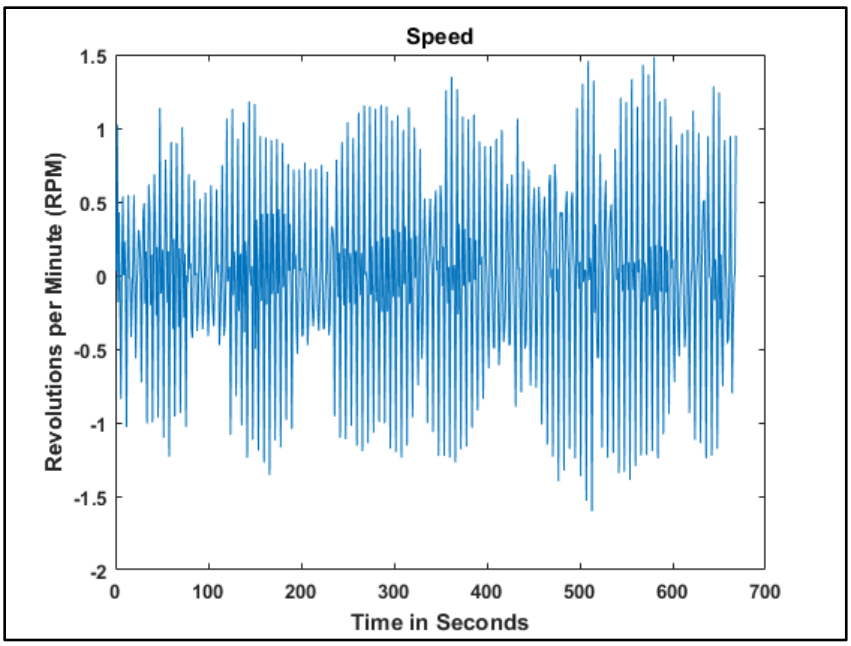

Figure B- 35 Speed (RPM) Plot - Test 5.

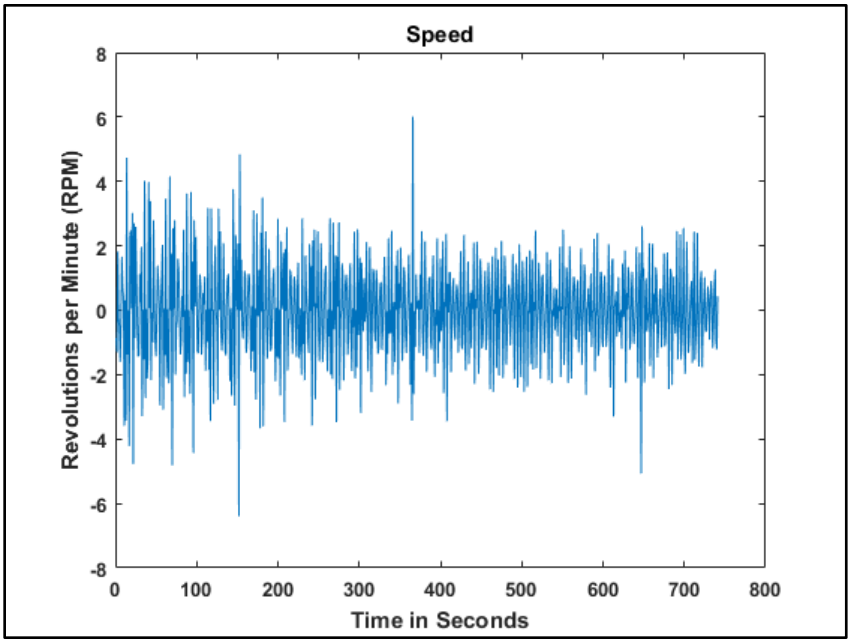

Figure B- 36 Speed (RPM) Plot - Test 6.

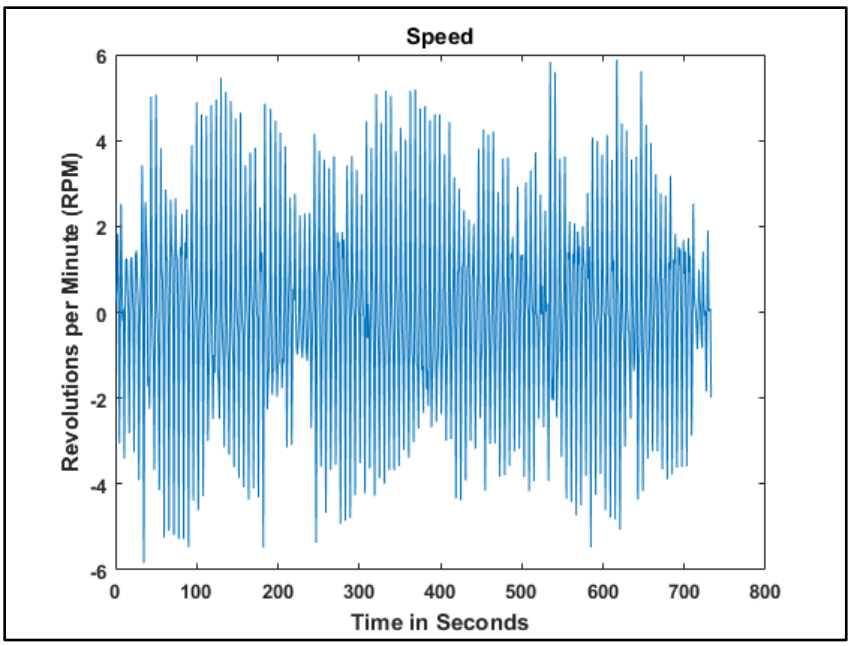

Figure B- 37 Speed (RPM) Plot - Test 7.

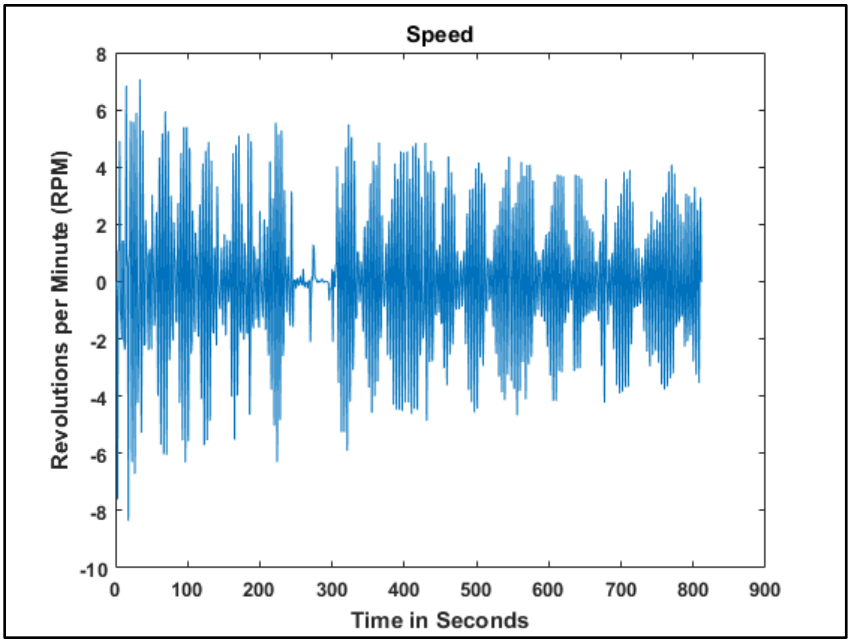

Figure B- 38 Speed (RPM) Plot - Test 8.

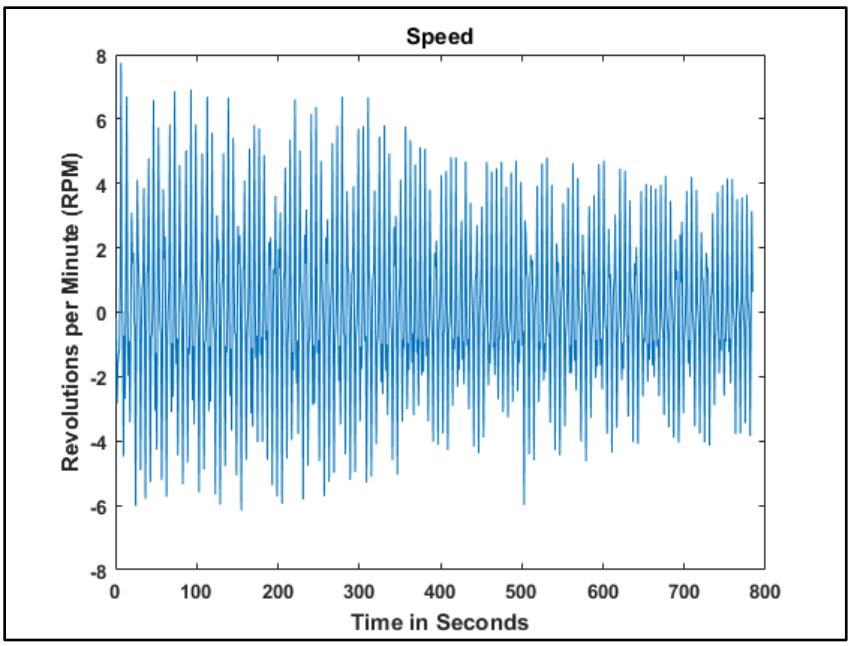

Figure B- 39 Speed (RPM) Plot - Test 9.

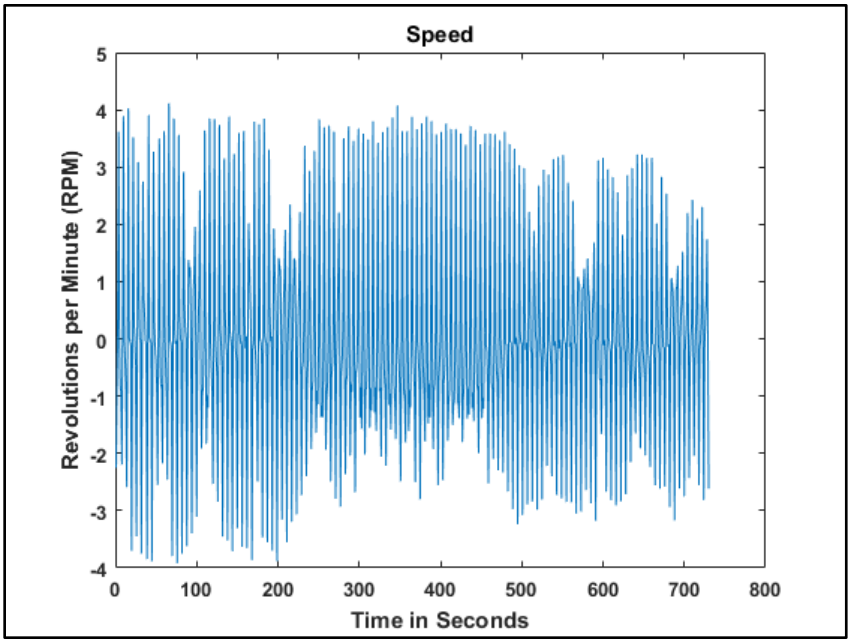

Figure B- 40 Speed (RPM) Plot - Test 11.

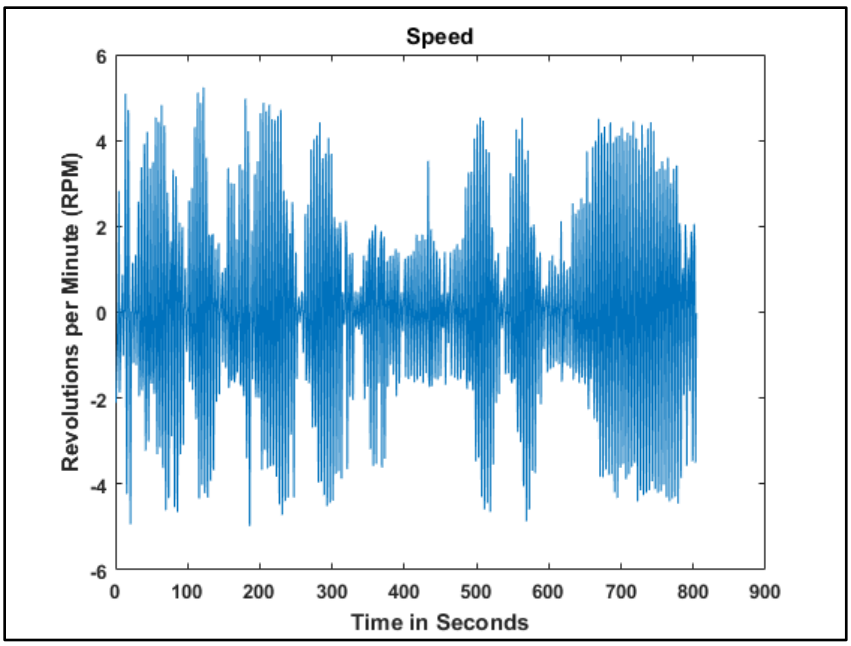

Figure B- 41 Speed (RPM) Plot - Test 12.

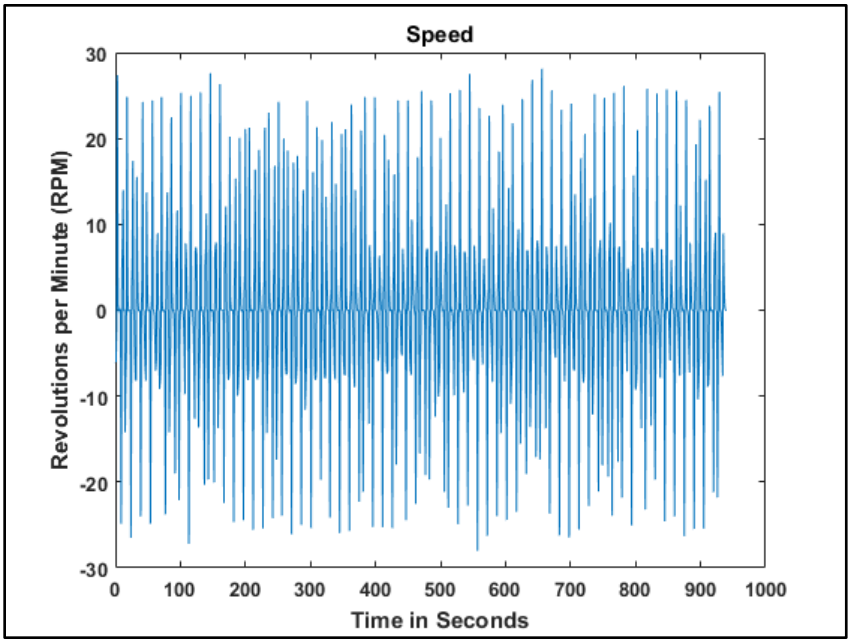

Figure B- 42 Speed (RPM) Plot - Test 13.

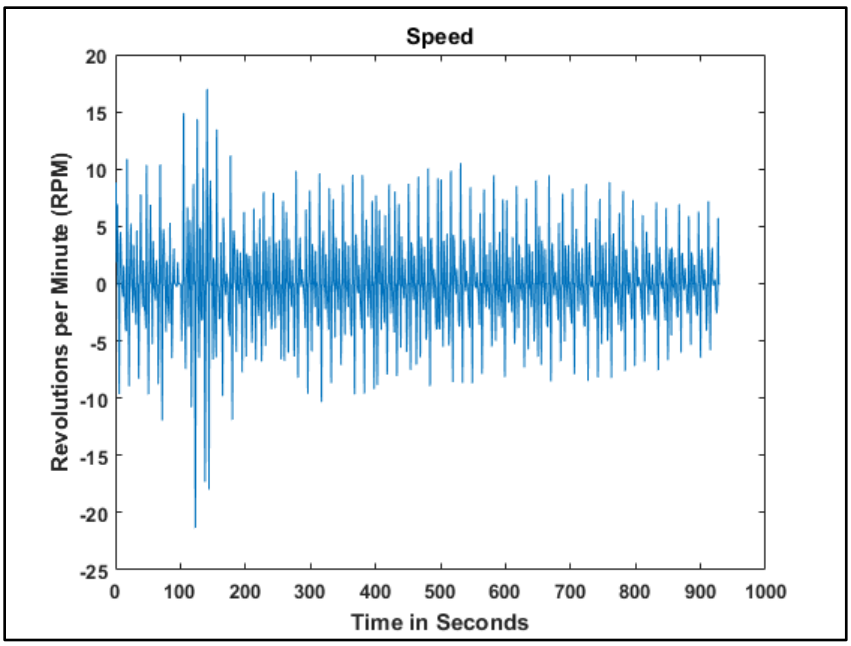

Figure B- 43 Speed (RPM) Plot - Test 14.

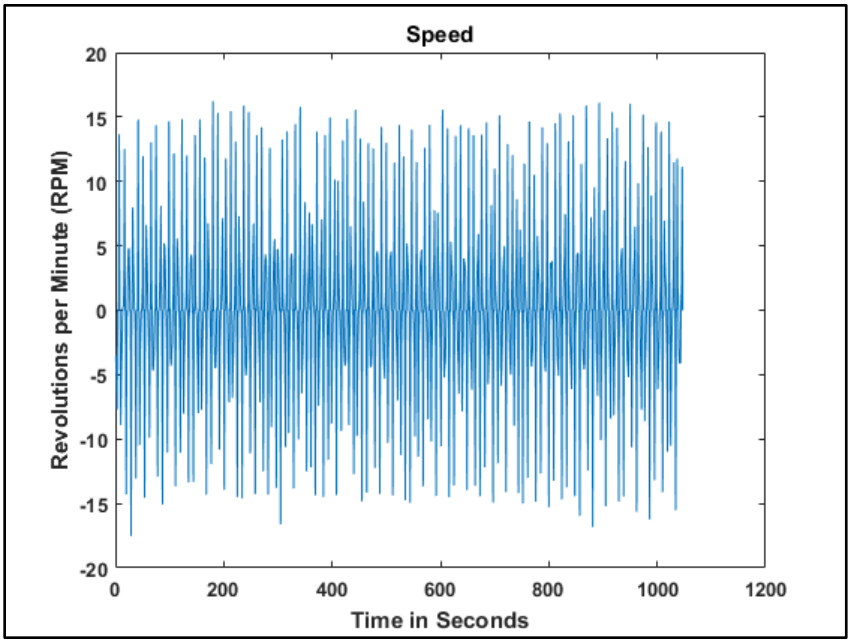

Figure B- 44 Speed (RPM) Plot - Test 15.

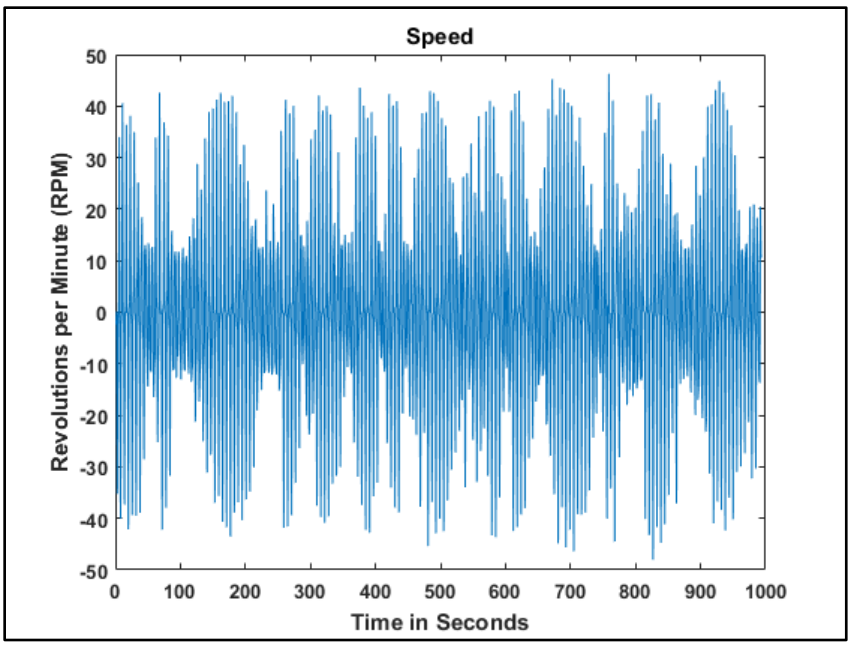

Figure B- 45 Speed (RPM) Plot - Test 16.

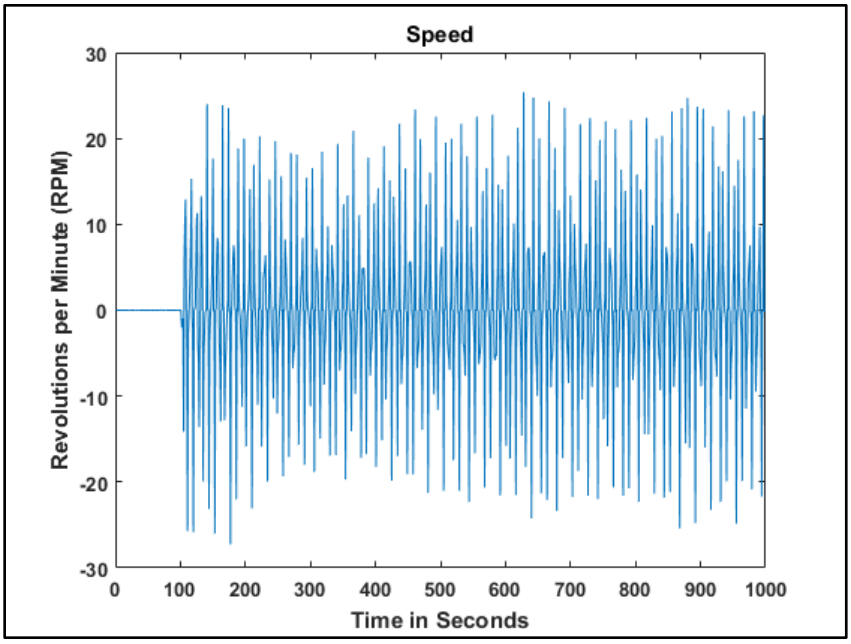

Figure B- 46 Speed (RPM) Plot - Test 17.

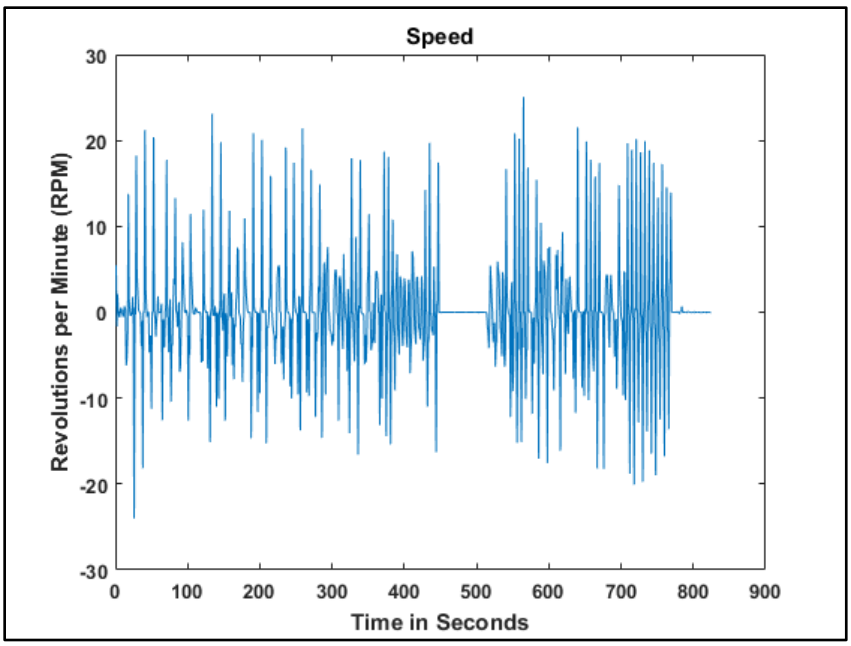

Figure B- 47 Speed (RPM) Plot - Test 18.

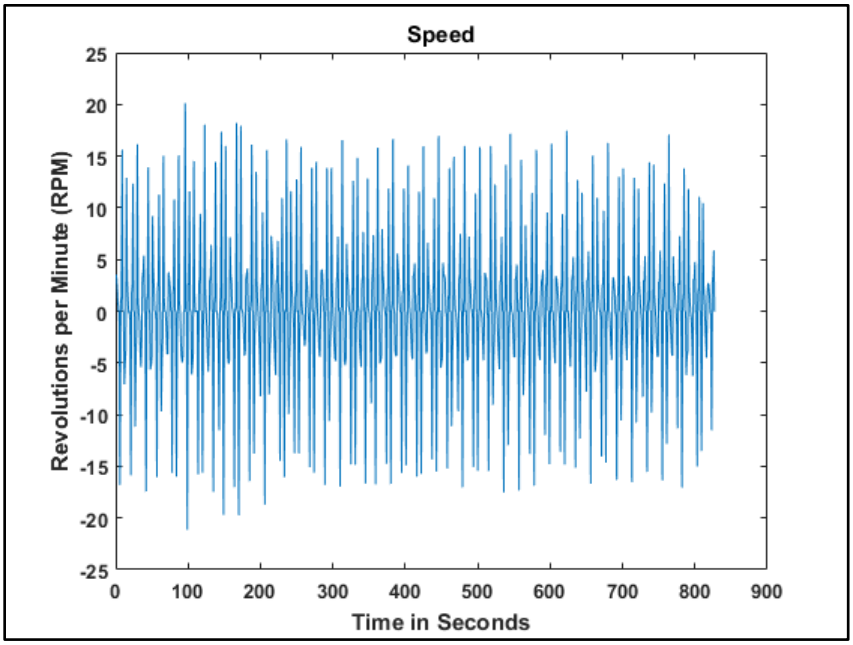

Figure B- 48 Speed (RPM) Plot - Test 19.

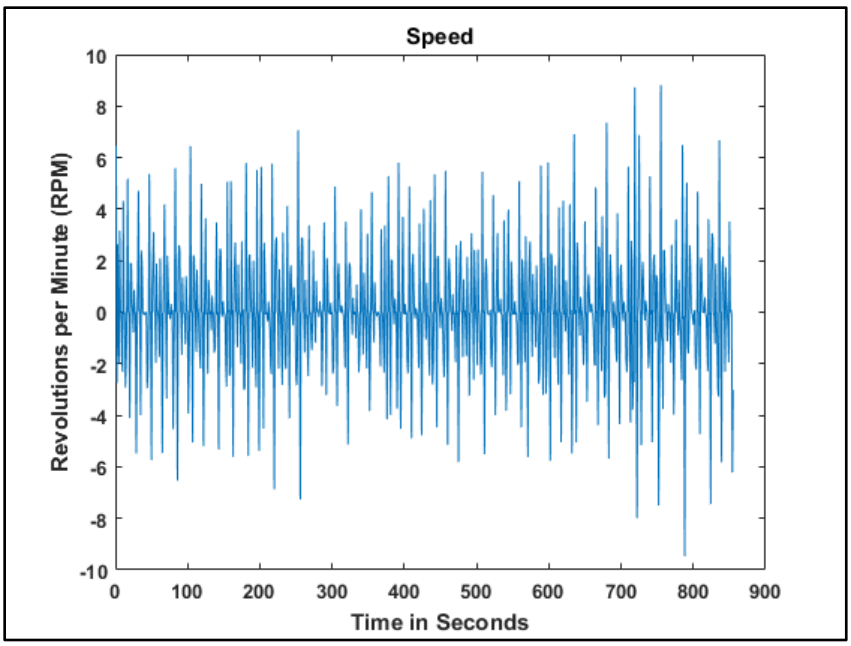

Figure B- 49 Speed (RPM) Plot - Test 20.

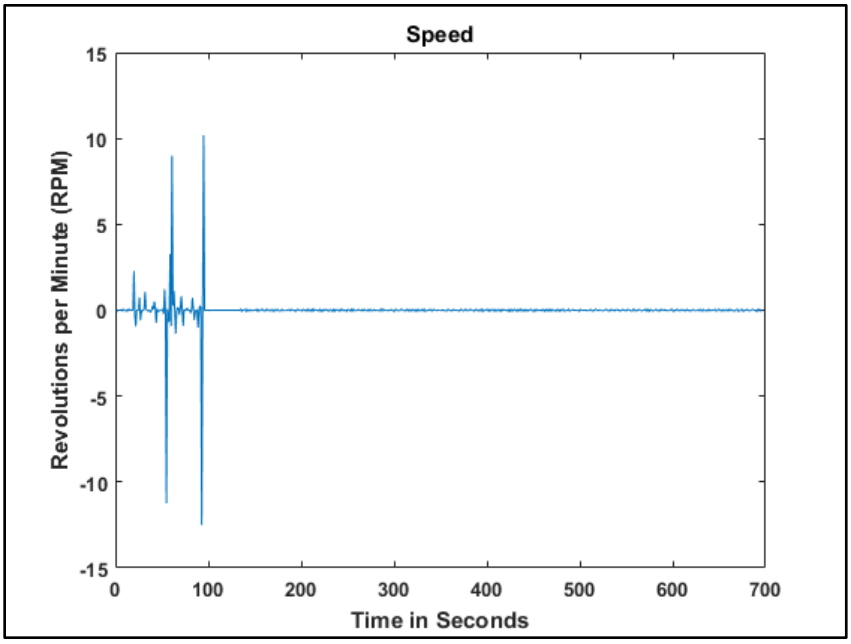

Figure B- 50 Speed (RPM) Plot - Test 21.

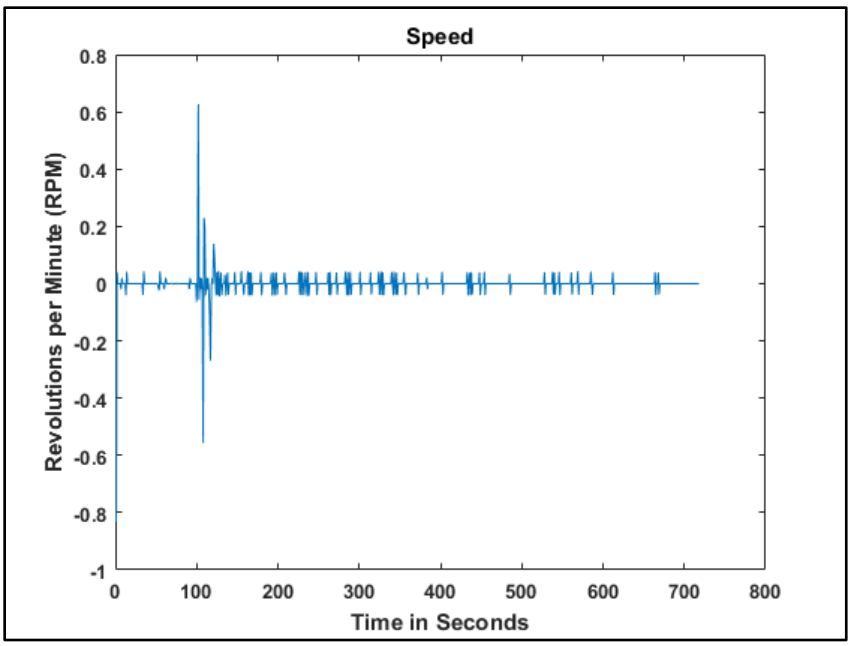

Figure B- 51 Speed (RPM) Plot - Test 23.

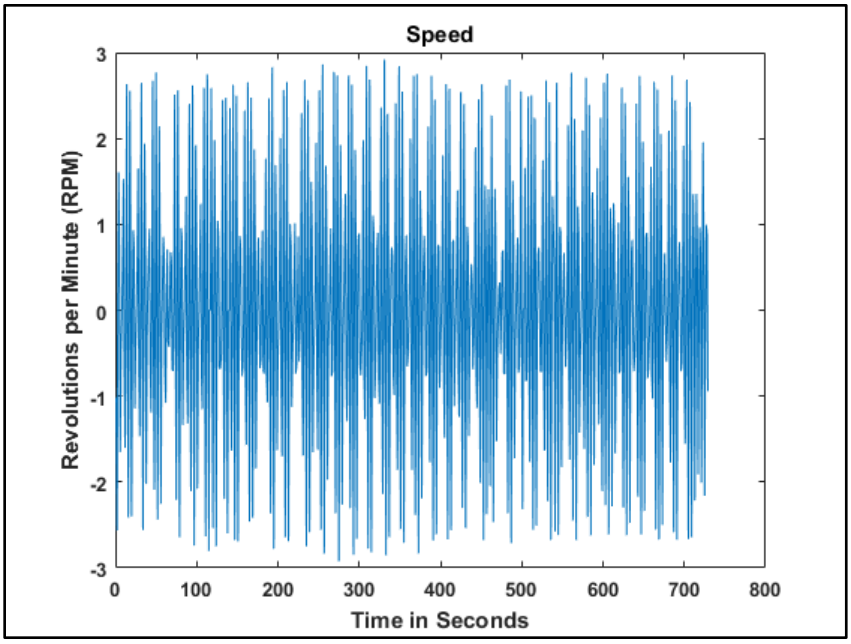

Figure B- 52 Speed (RPM) Plot - Test 24.

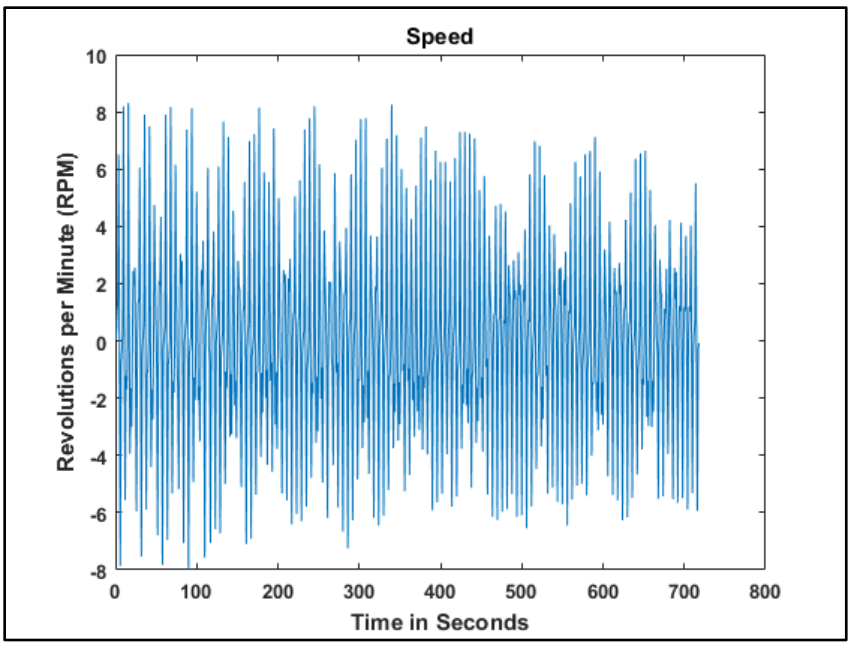

Figure B- 53 Speed (RPM) Plot - Test 25.

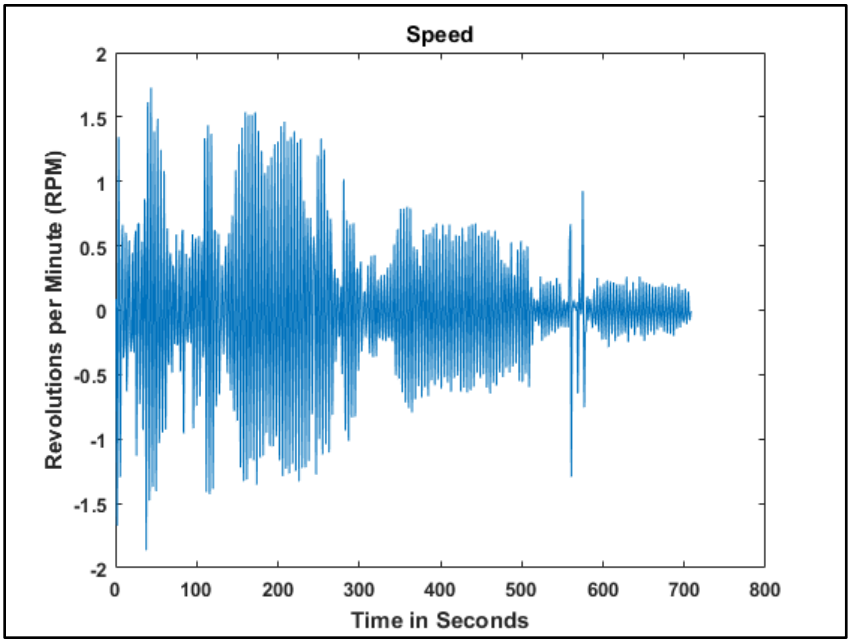

Figure B- 54 Speed (RPM) Plot - Test 26.

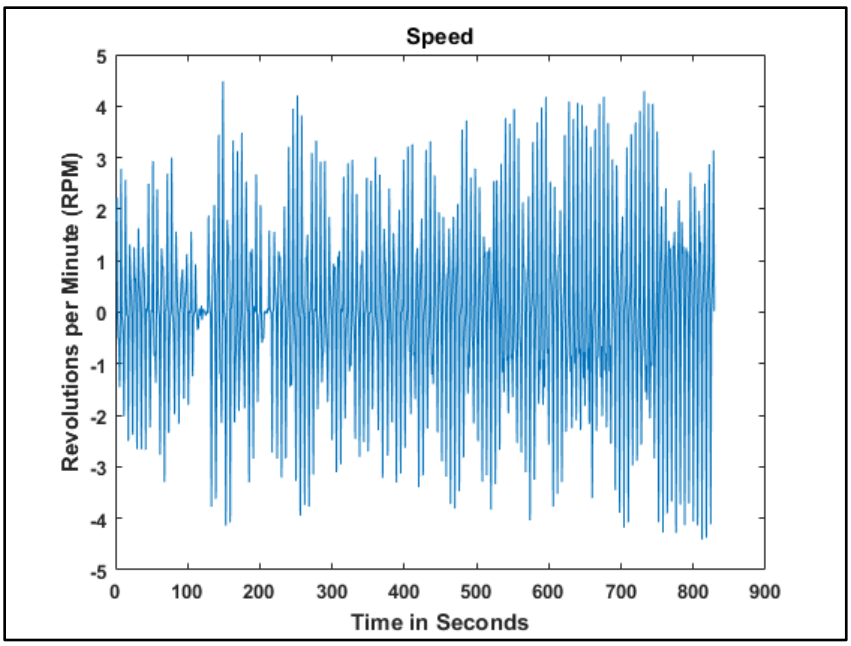

Figure B- 55 Speed (RPM) Plot - Test 27.

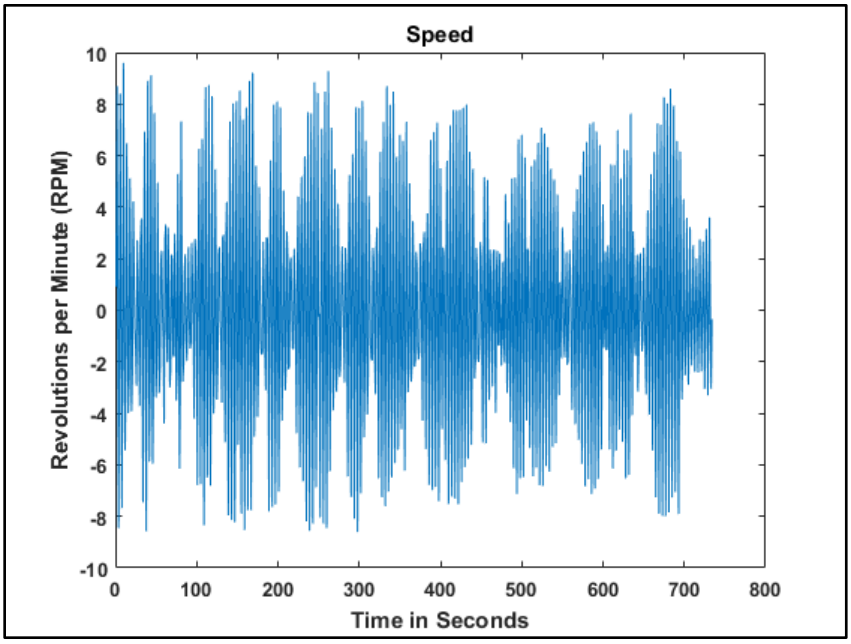

Figure B- 56 Speed (RPM) Plot - Test 28.

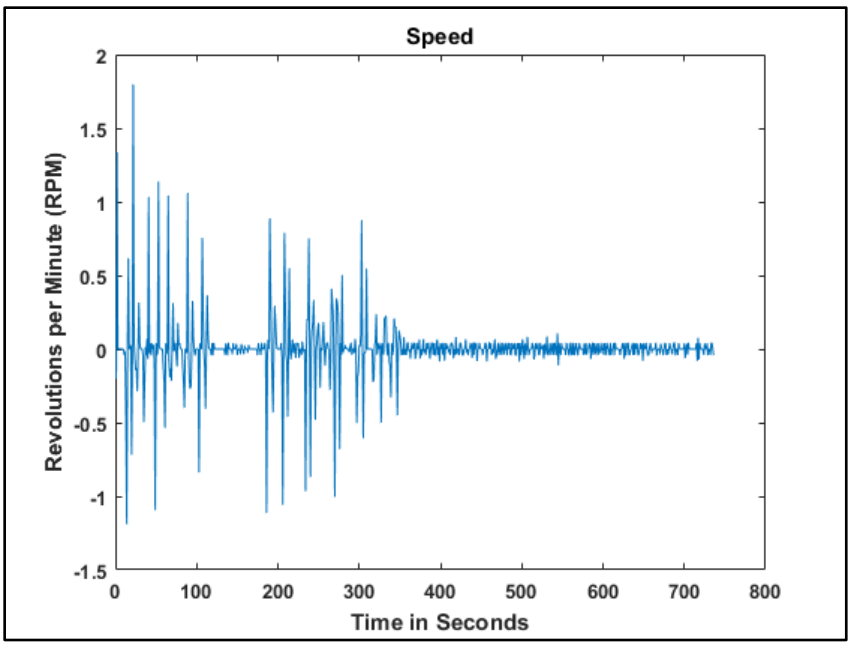

Figure B- 57 Speed (RPM) Plot - Test 29.

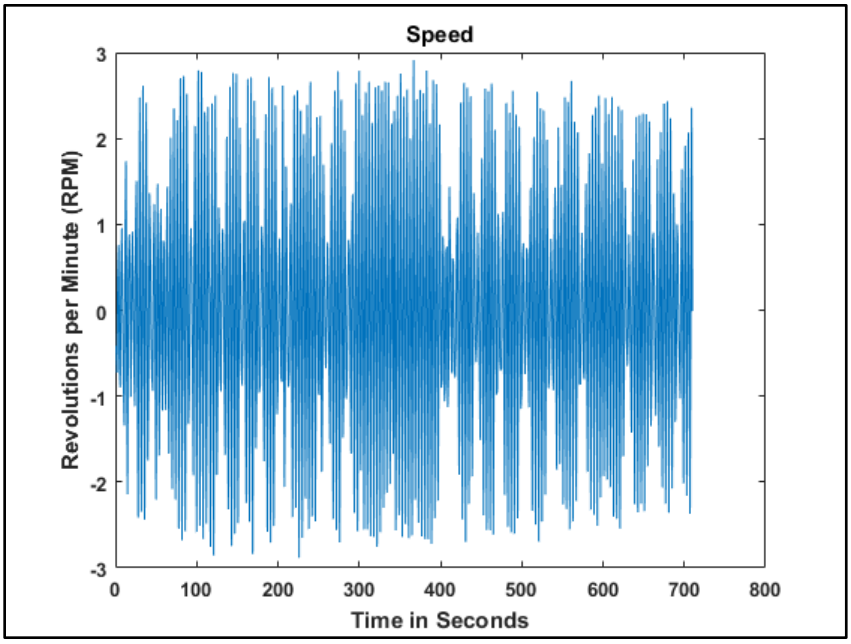

Figure B- 58 Speed (RPM) Plot - Test 30.

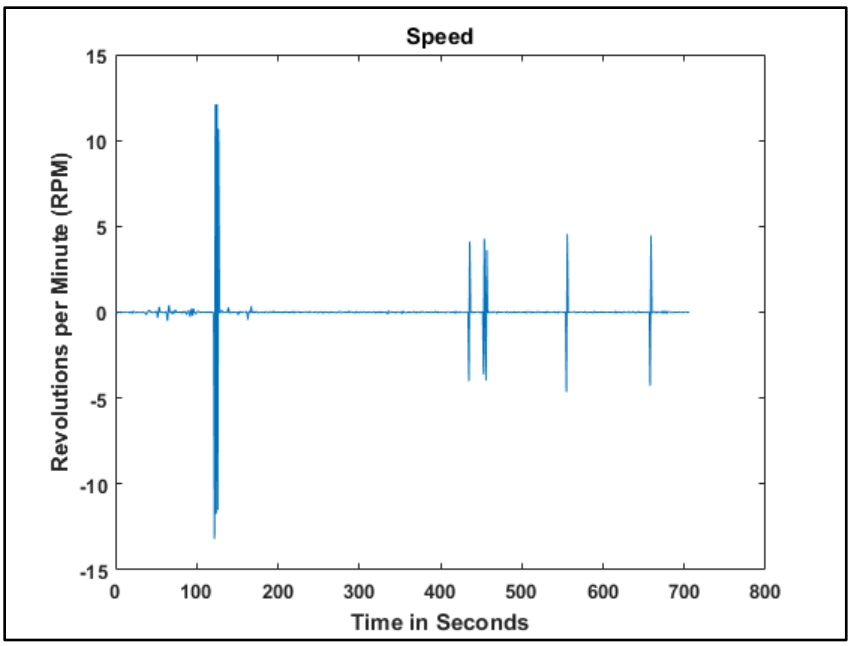

Figure B- 59 Speed (RPM) Plot - Test 31.

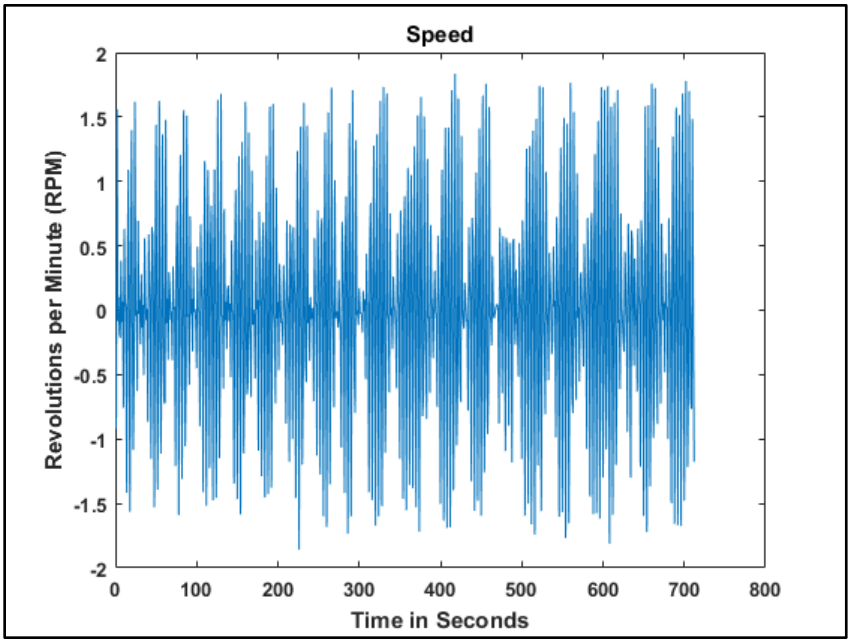

Figure B- 60 Speed (RPM) Plot - Test 32.

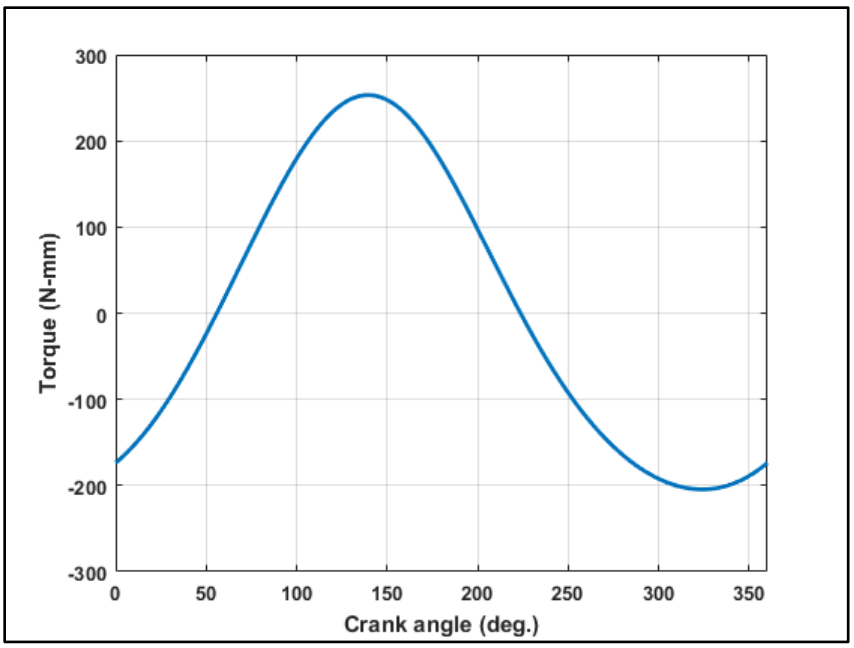

Figure B- 61 Torque Plot - Test 1.

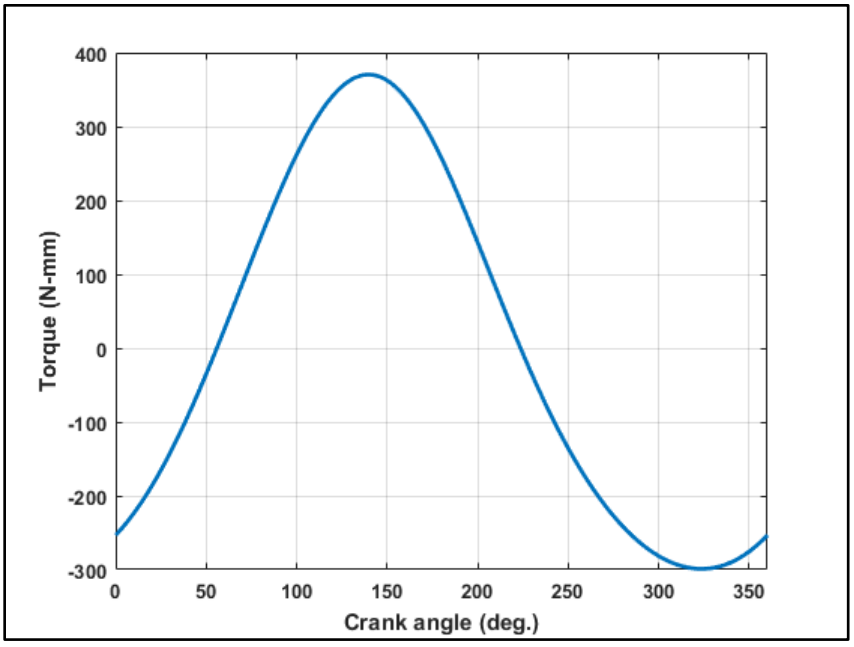

Figure B- 62 Torque Plot - Test 2.

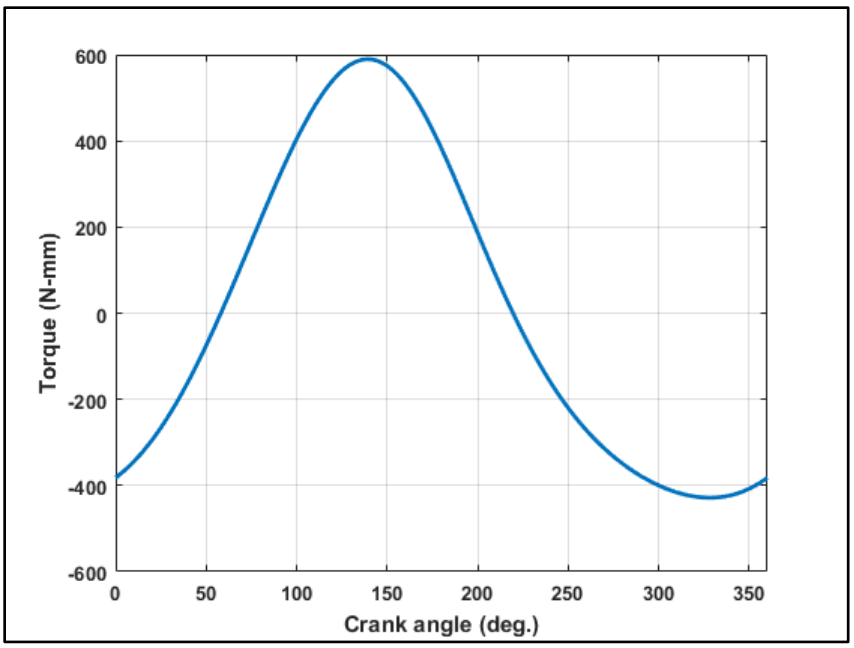

Figure B- 63 Torque Plot - Test 3.

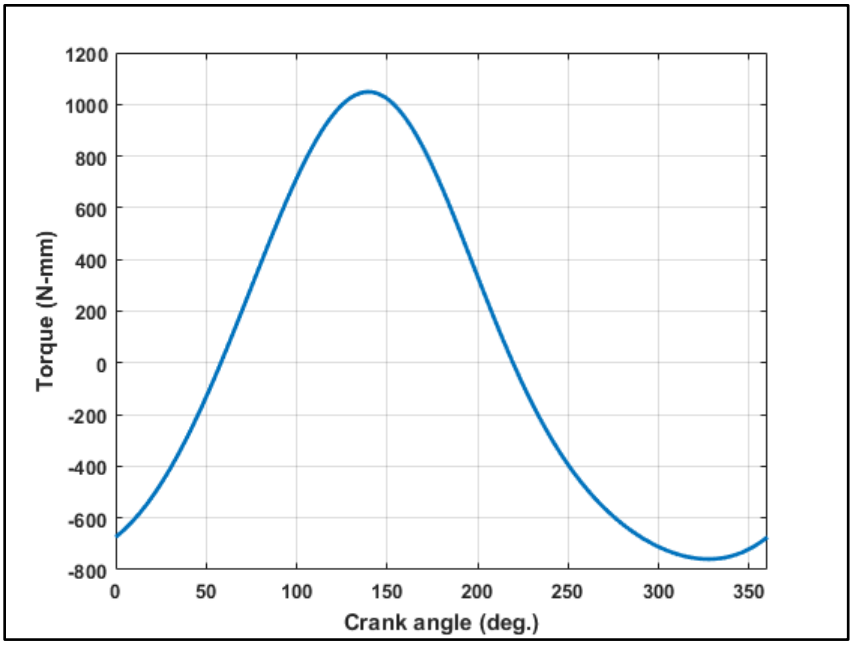

Figure B- 64 Torque Plot - Test 4.

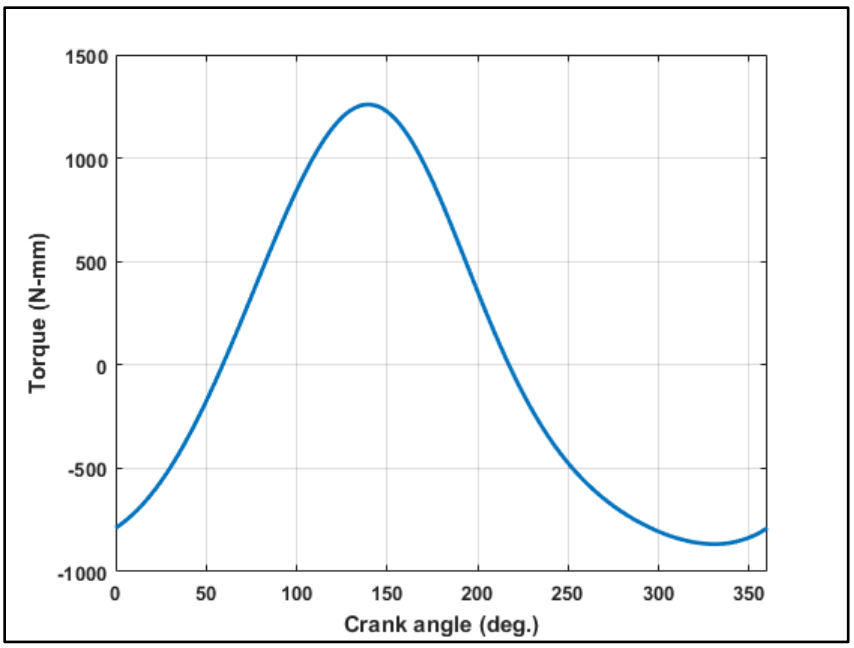

Figure B- 65 Torque Plot - Test 5.

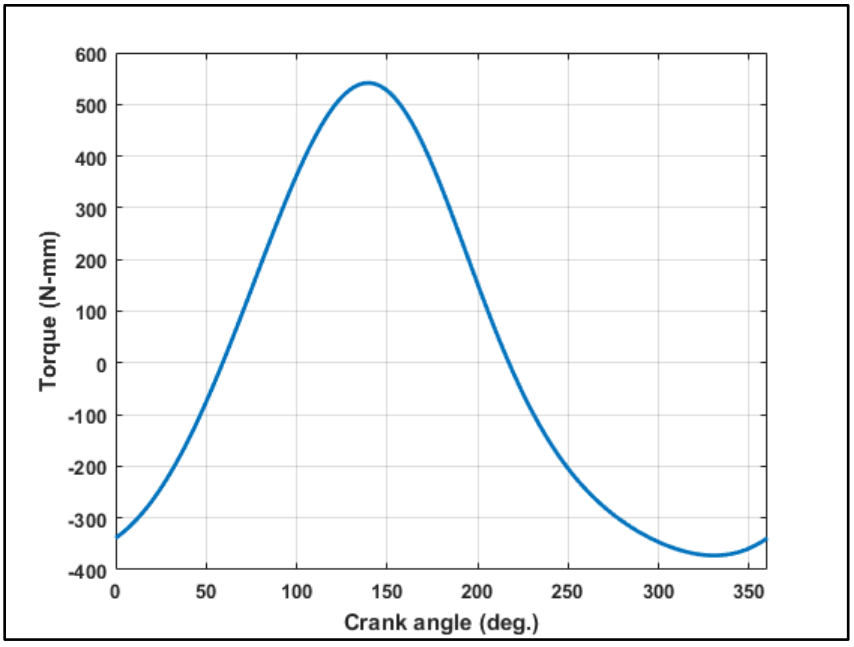

Figure B- 66 Torque Plot - Test 6.

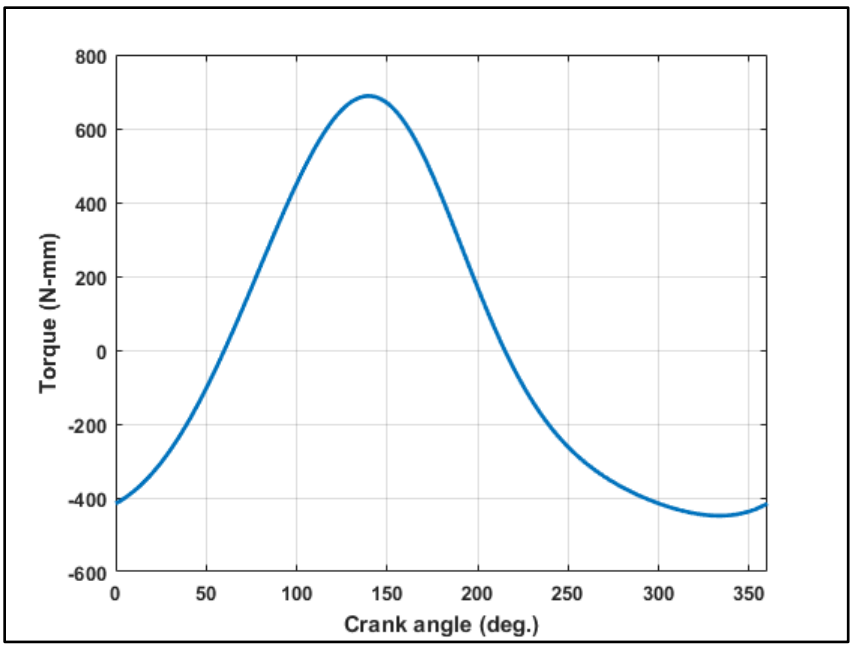

Figure B- 67 Torque Plot - Test 7.

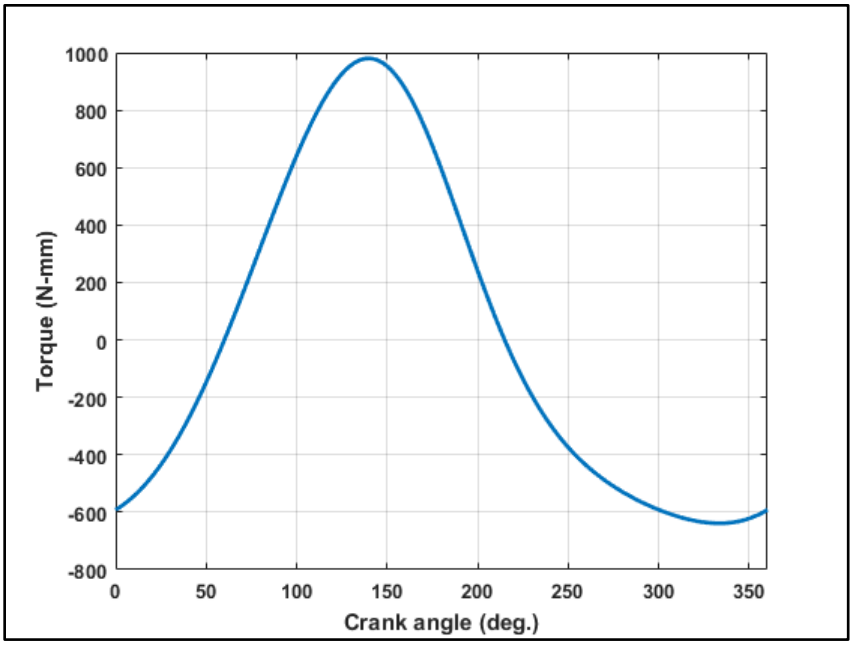

Figure B- 68 Torque Plot - Test 8.

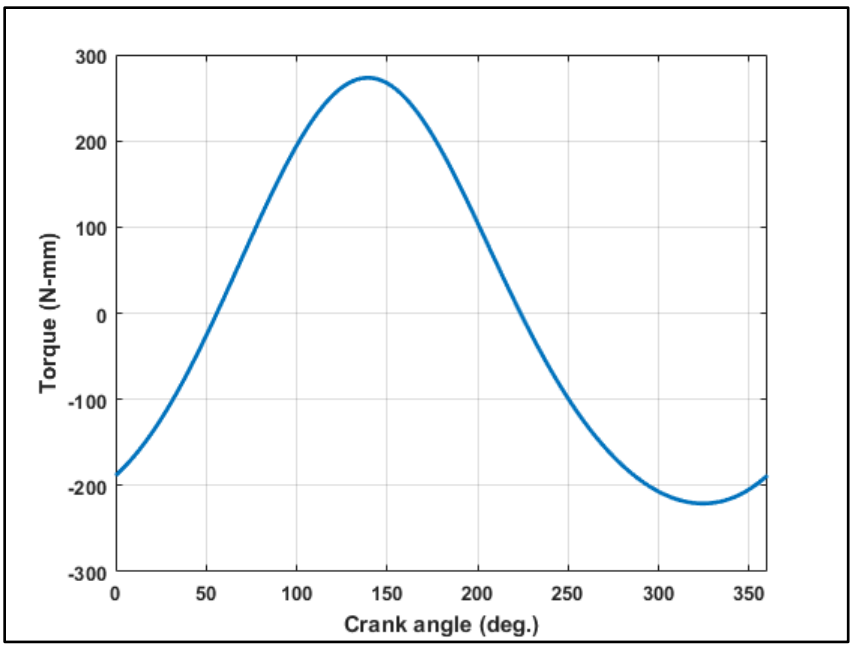

Figure B- 69 Torque Plot - Test 9.

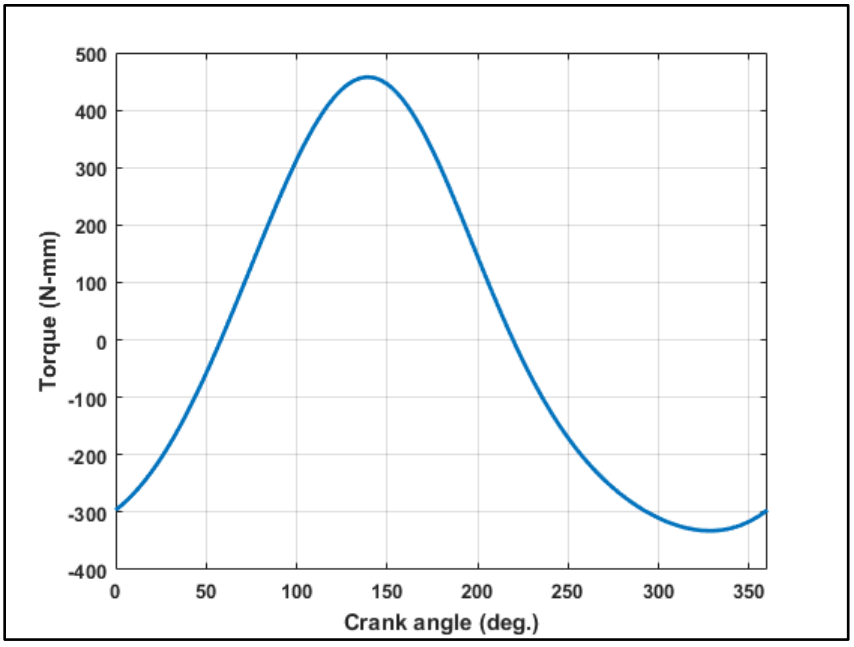

Figure B- 70 Torque Plot - Test 11.

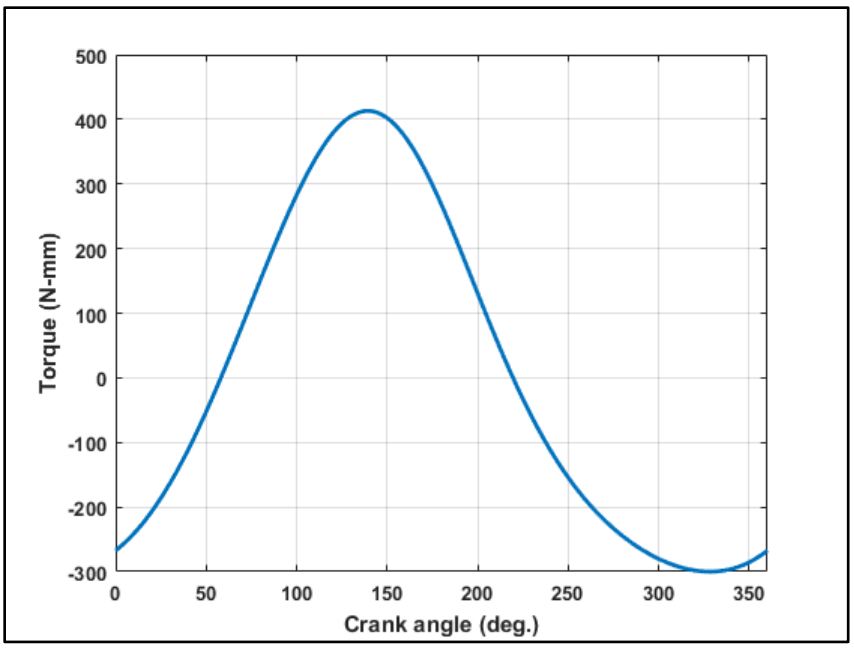

Figure B- 71 Torque Plot - Test 12.

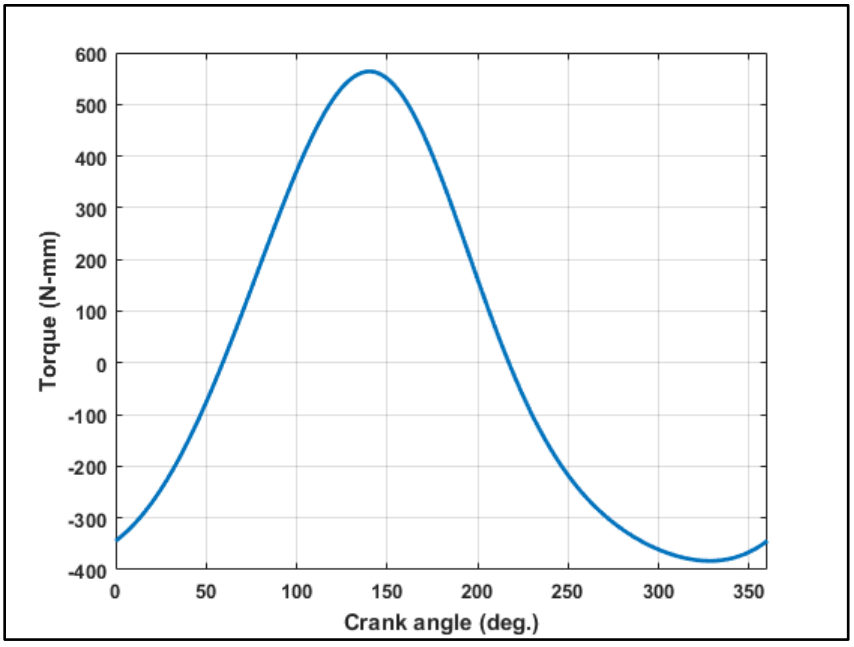

Figure B- 72 Torque Plot - Test 13.

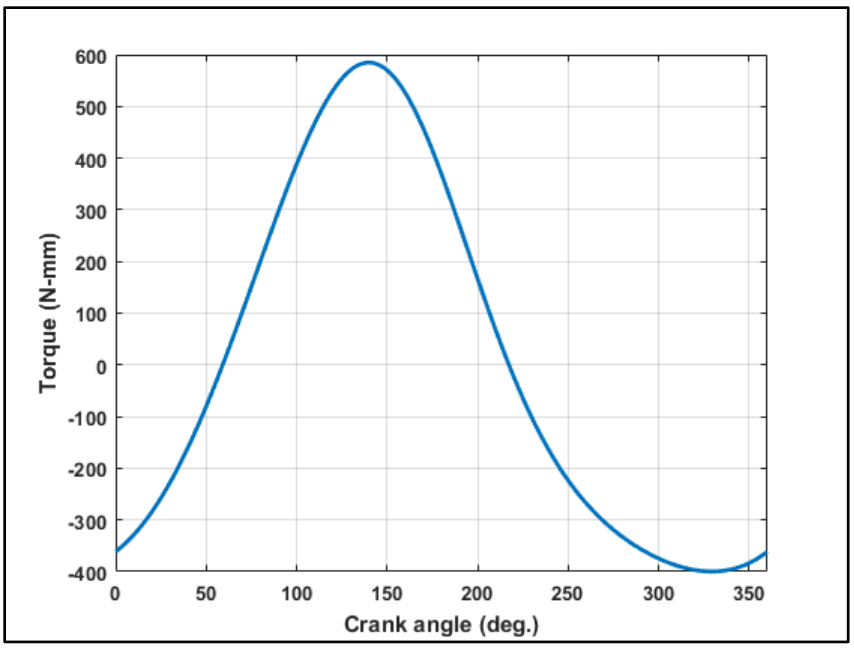

Figure B- 73 Torque Plot - Test 14.

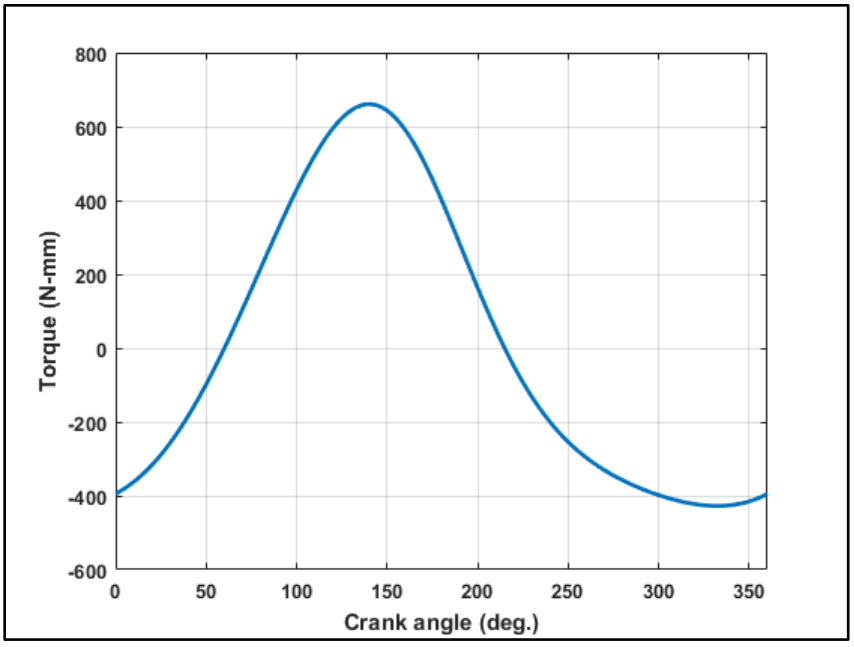

Figure B- 74 Torque Plot - Test 15.

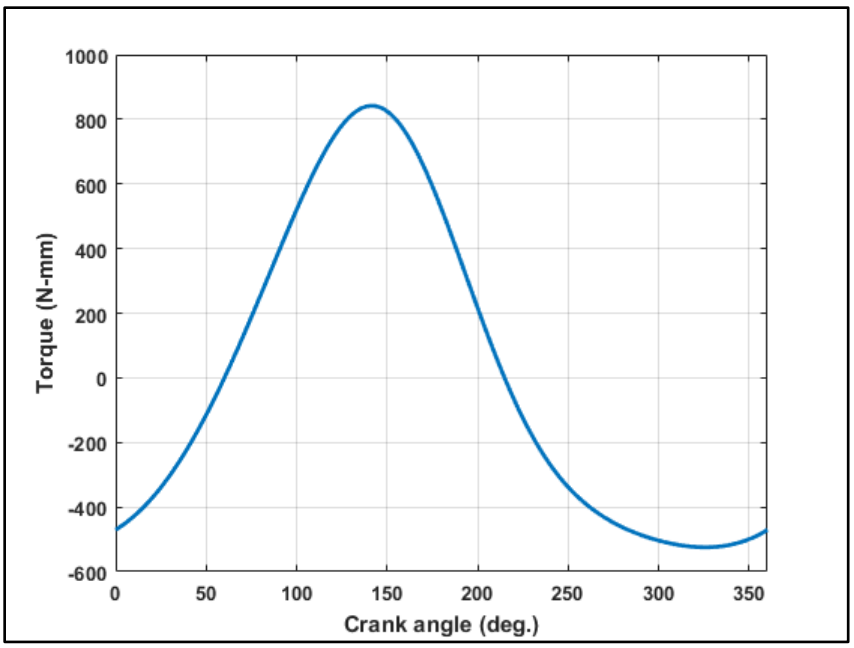

Figure B- 75 Torque Plot - Test 16.

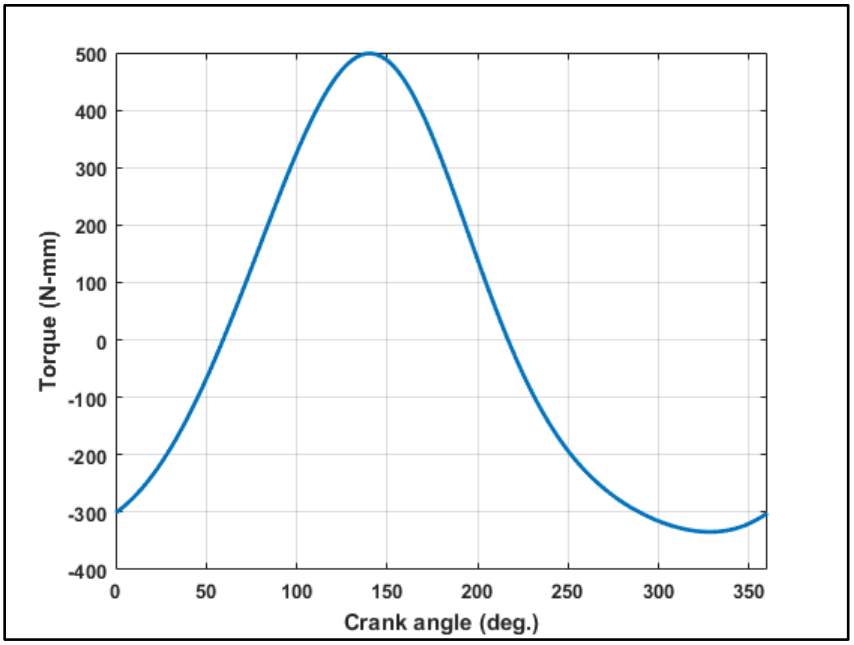

Figure B- 76 Torque Plot - Test 17.

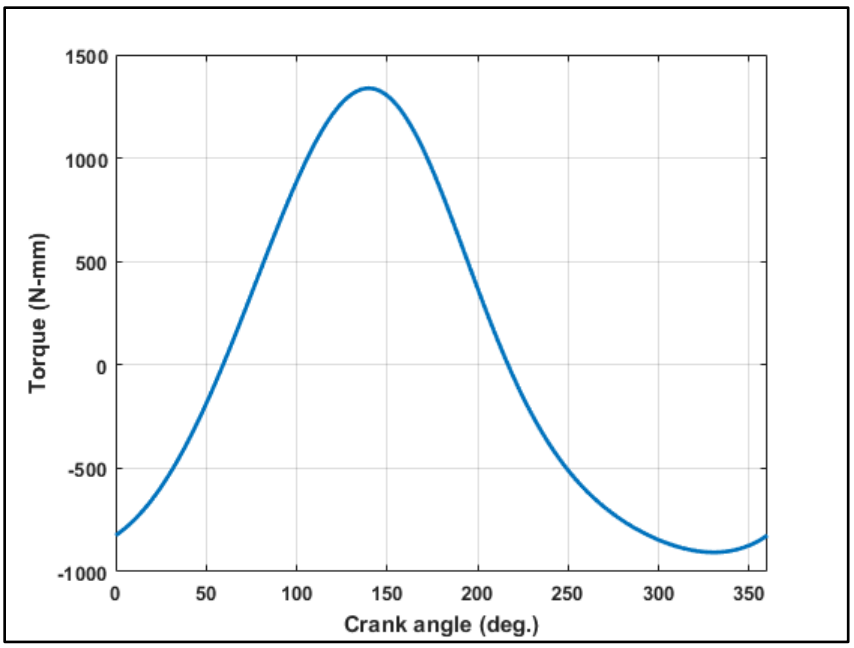

Figure B- 77 Torque Plot - Test 18.

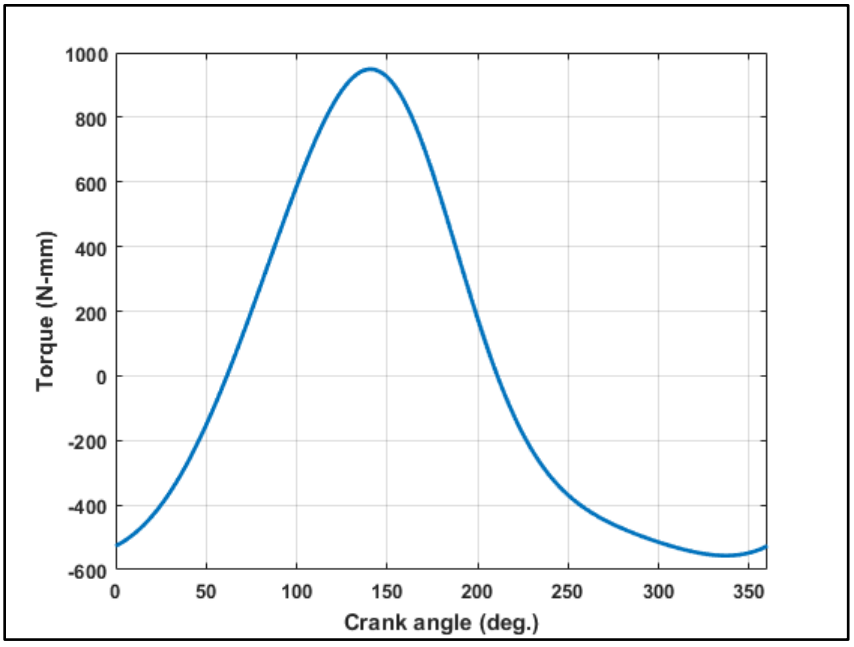

Figure B- 78 Torque Plot - Test 19.

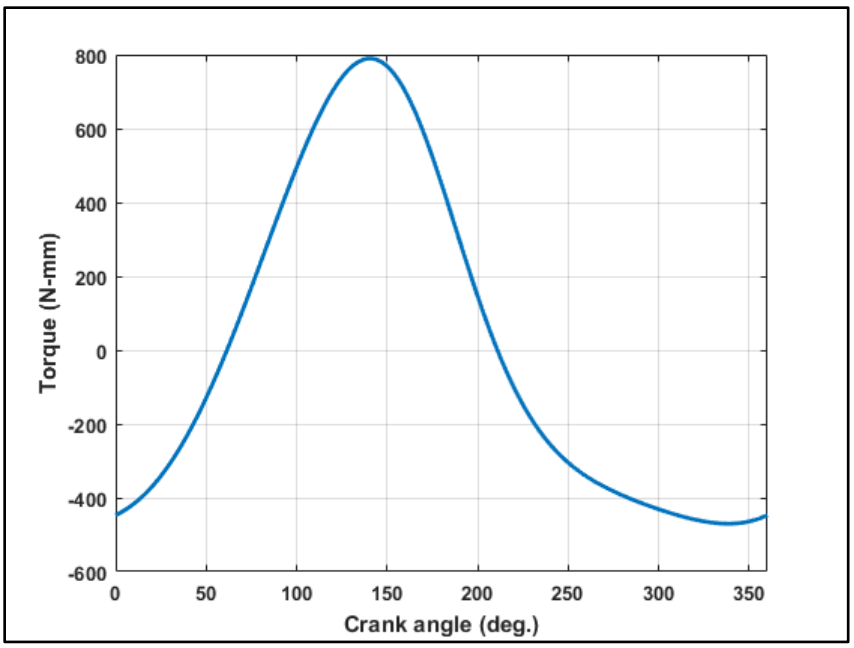

Figure B- 79 Torque Plot - Test 20.

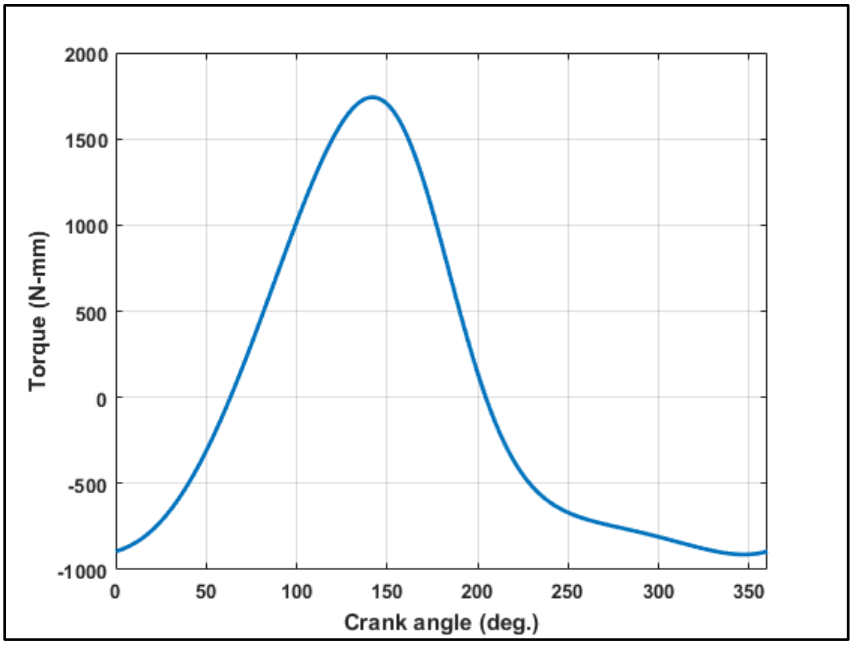

Figure B- 80 Torque Plot - Test 21.

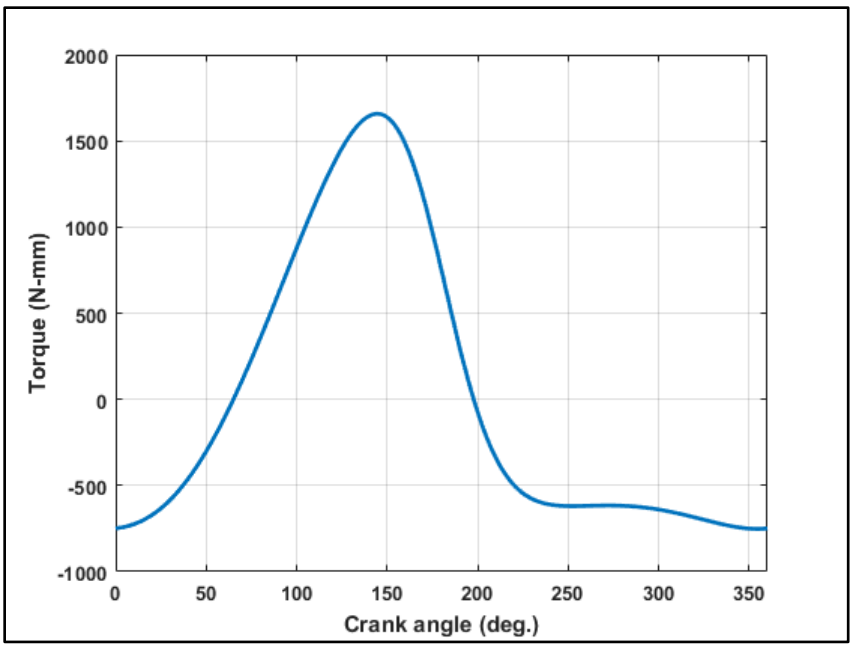

Figure B- 81 Torque Plot - Test 23.

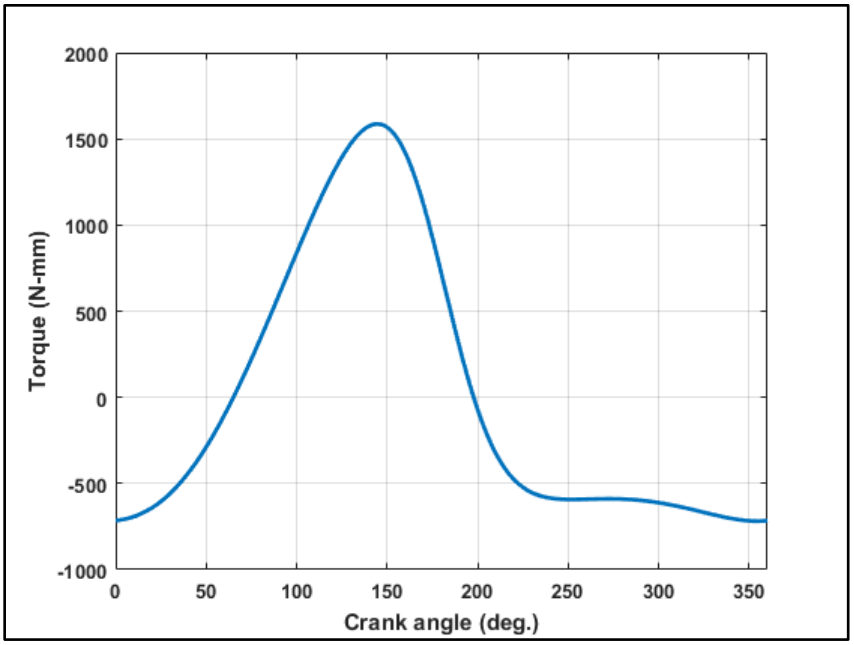

Figure B- 82 Torque Plot - Test 24.

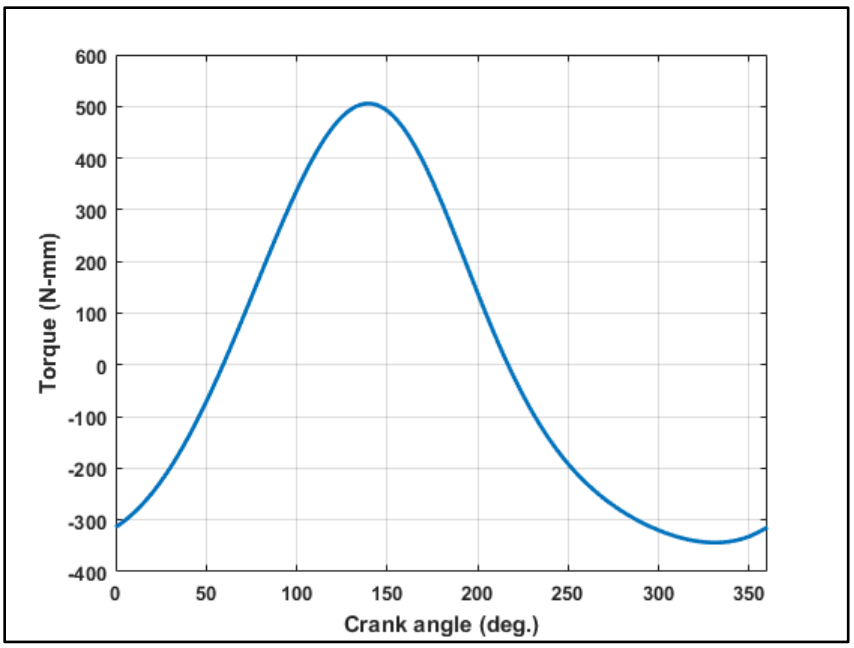

Figure B- 83 Torque Plot - Test 25.

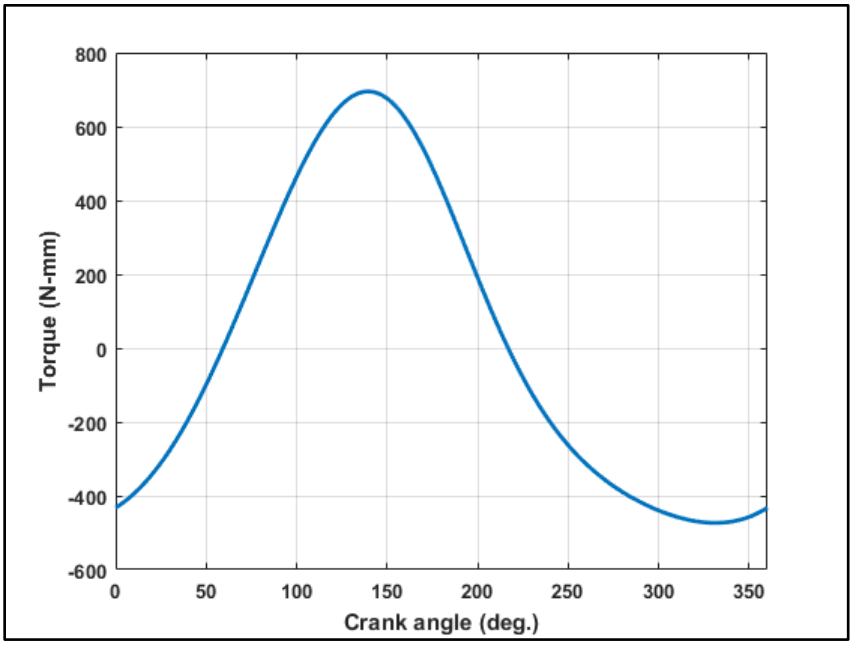

Figure B- 84 Torque Plot - Test 26.

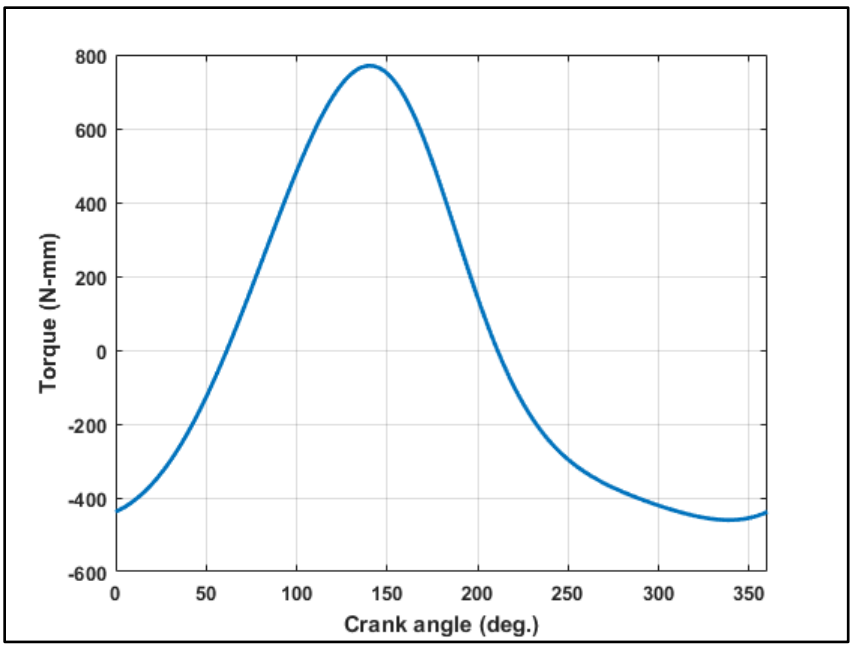

Figure B- 85 Torque Plot - Test 27.

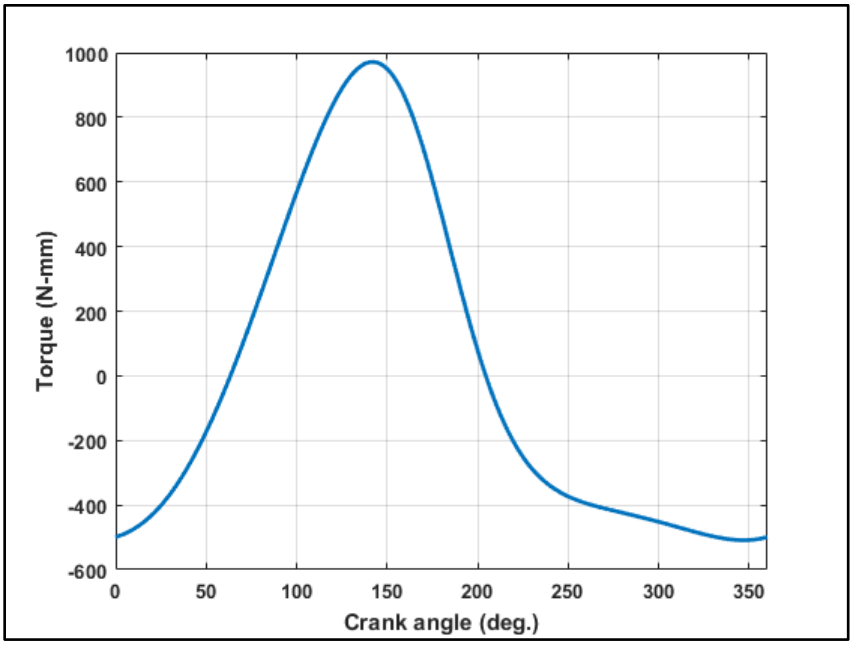

Figure B- 86 Torque Plot - Test 28.

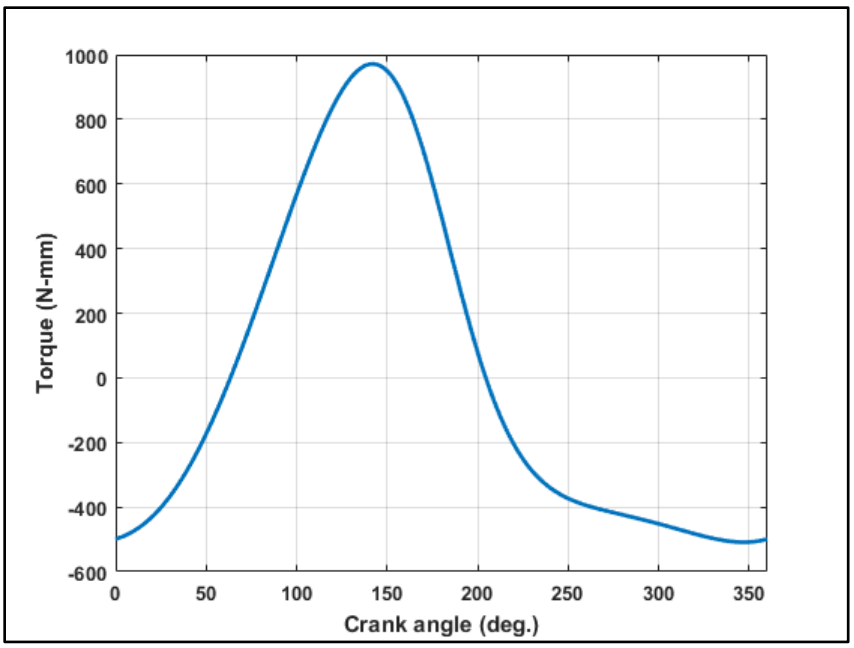

Figure B- 87 Torque Plot - Test 29.

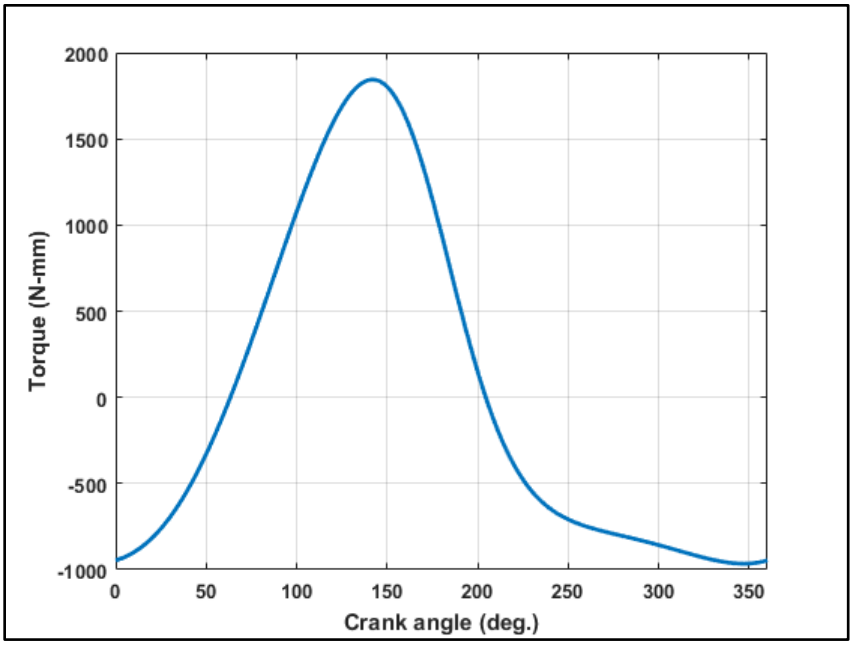

Figure B- 88 Torque Plot - Test 30.

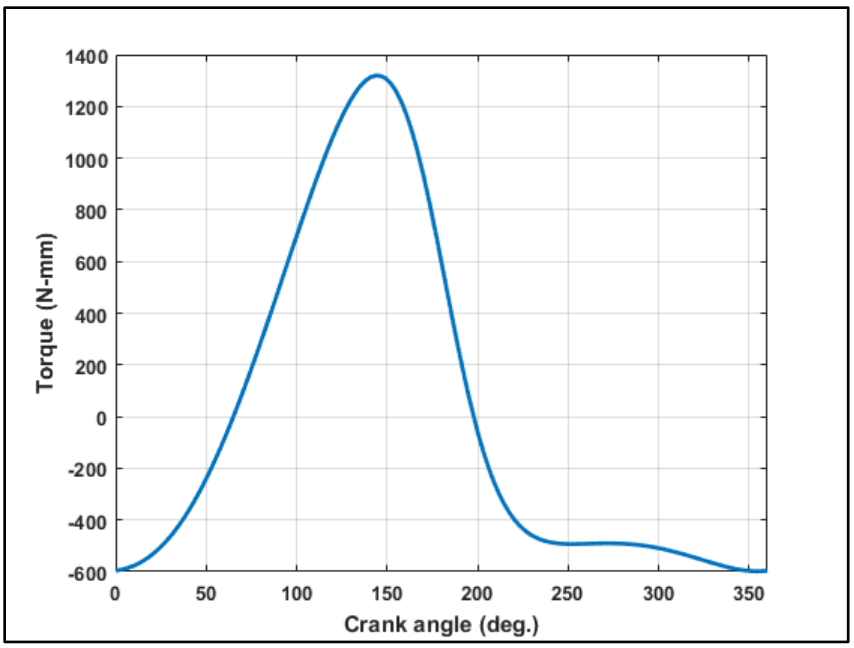

Figure B- 89 Torque Plot - Test 31.

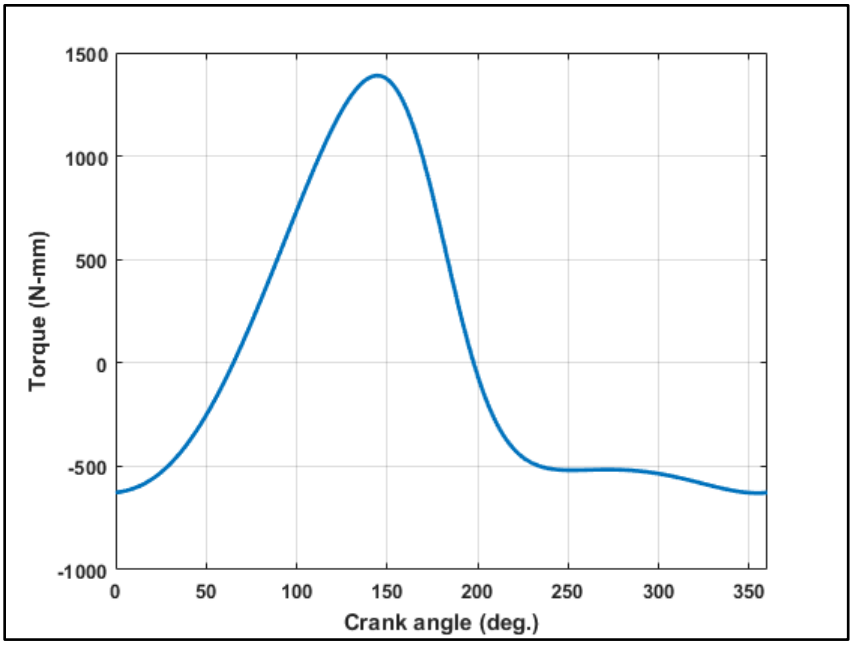

Figure B- 90 Torque Plot - Test 32.

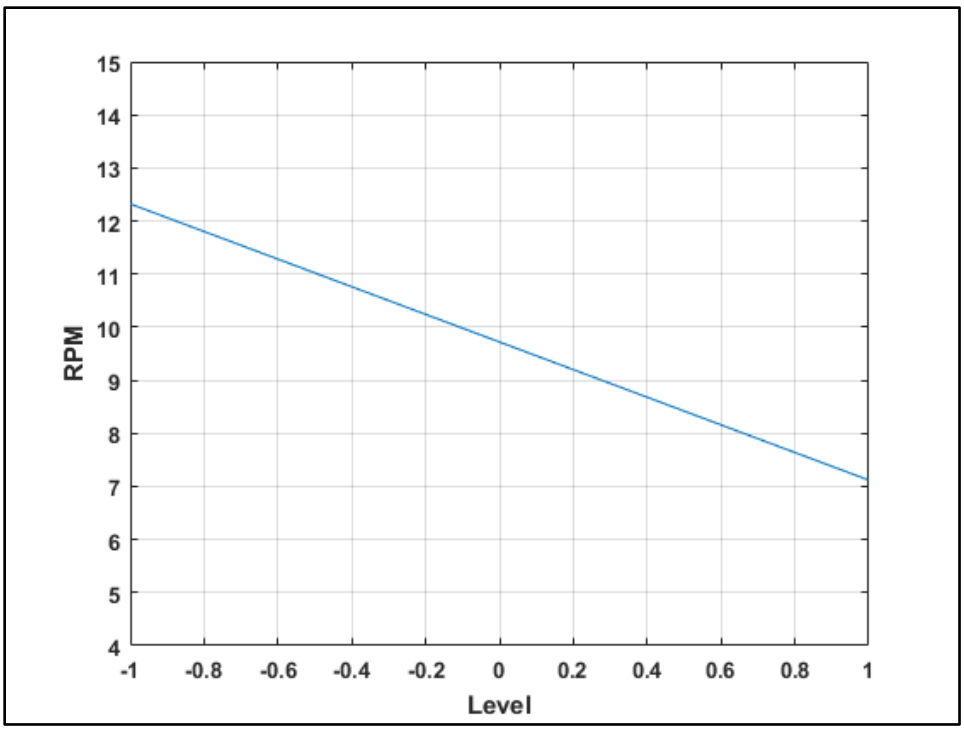

Figure B- 91 Buoy Effect - Speed.

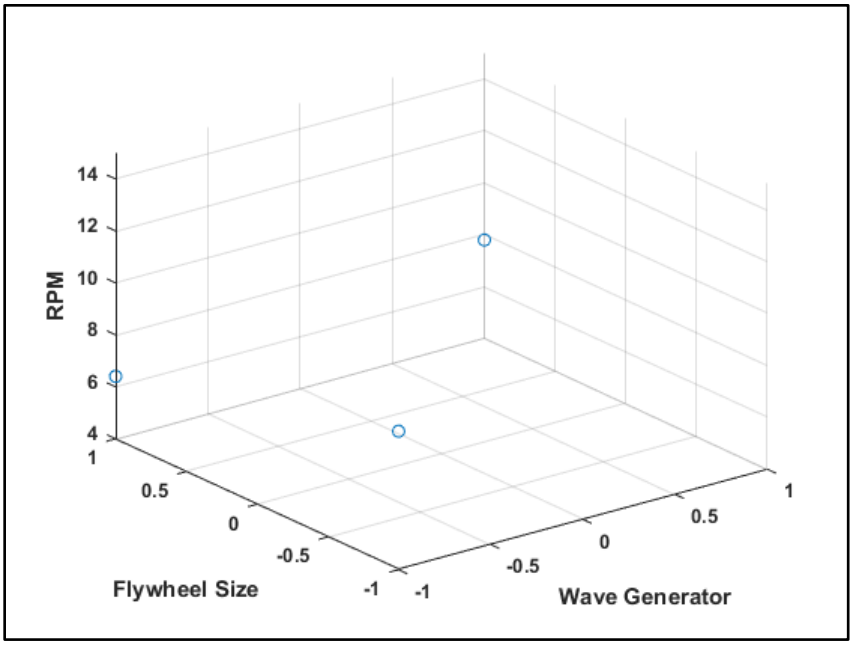

Figure B- 92 Flywheel Size and Wave Generator Setting Combined Effect - Speed.

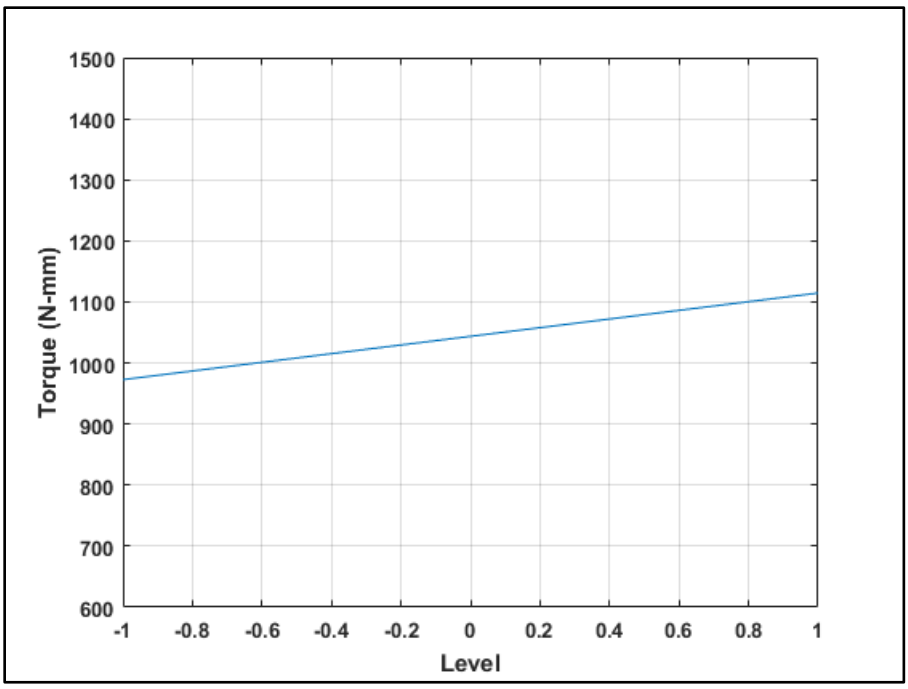

Figure B- 93 Buoy Effect - Torque.

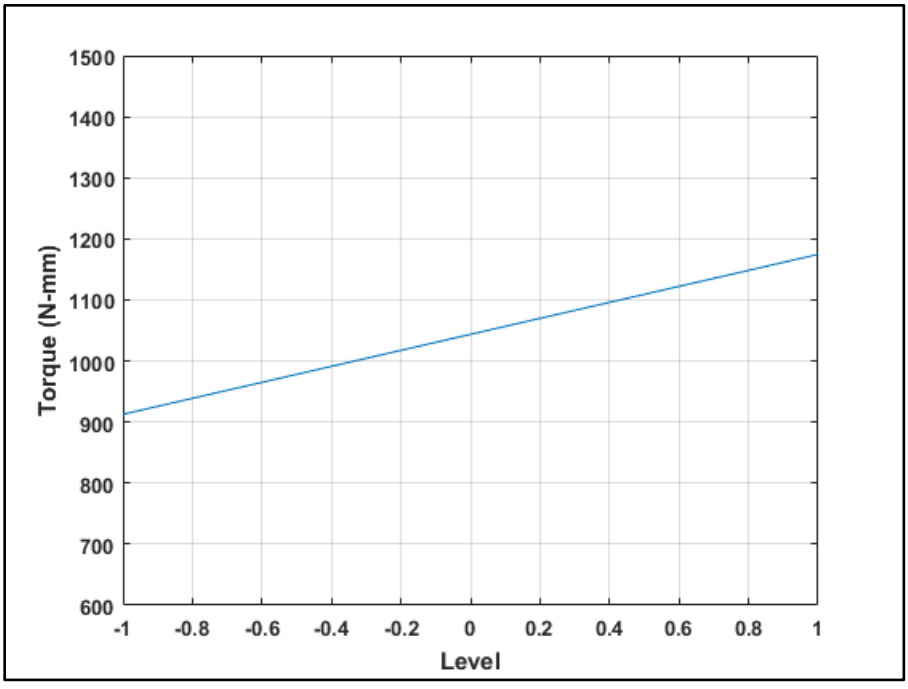

Figure B- 94 Wave Generator Setting Effect - Torque.

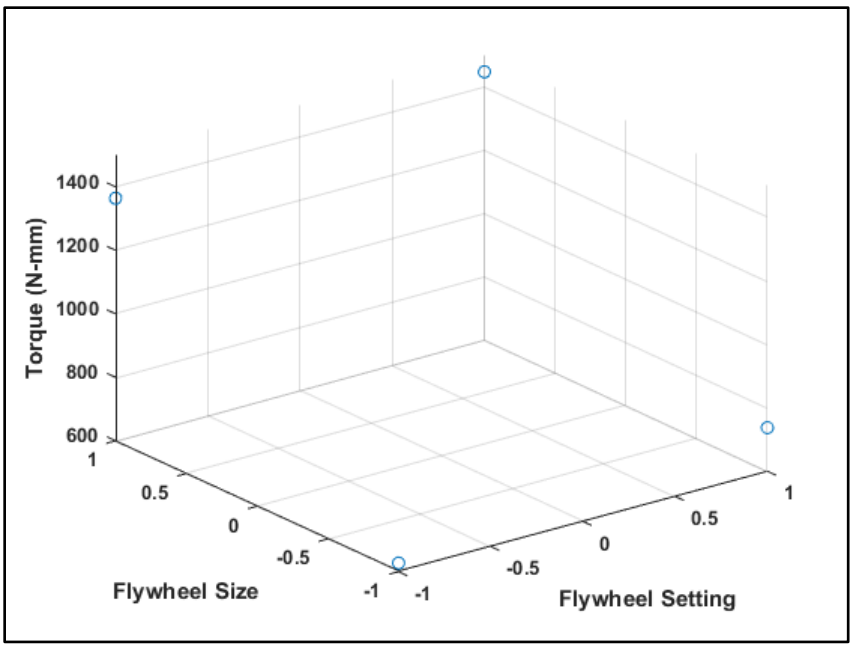

Figure B- 95 Flywheel Size and Flywheel Setting Combined Effect – Torque.

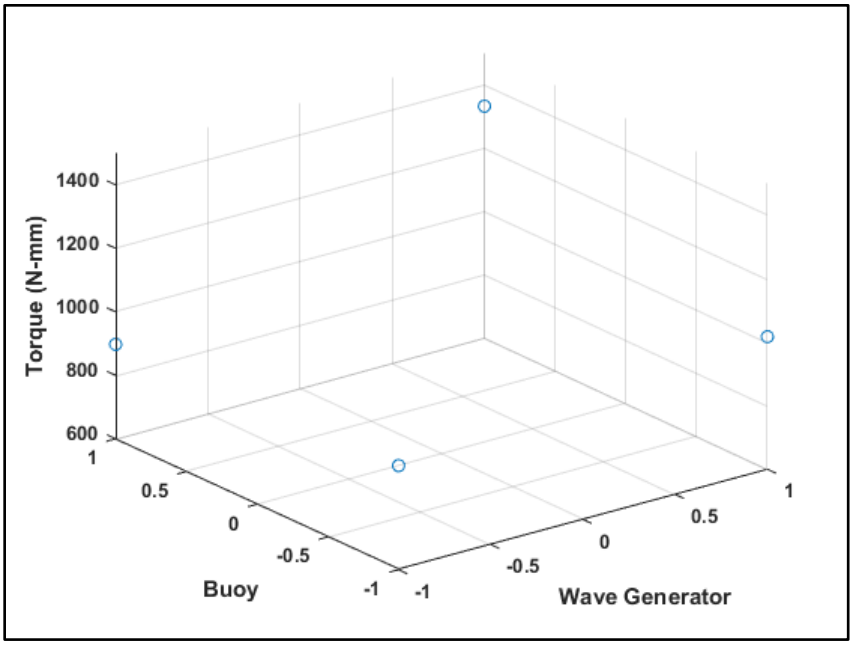

Figure B- 96 Buoy and Wave Generator Setting Combined Effect - Torque.